INAUGURAL-DISSERTATION

zur

Erlangung der Doktorwürde

der

Naturwissenschaftlich-Mathematischen Gesamtfakultät

der

Ruprecht-Karls-Universität

Heidelberg

Vorgelegt von:

Diplom-Biologe

Sven Wichert

aus Röbersdorf

Tag der mündlichen Prüfung:

Transcriptomic approaches in the brain at cell type resolution:

Analysis of neuron-glia interaction in

Plp1 and *Cnp1* null-mutant mice

Erstgutachter: Prof. Klaus-Armin Nave, PhD

Max-Planck-Institut für experimentelle Medizin, Göttingen

Zweitgutachter: Prof. Dr. Roland Eils

Theoretische Bioinformatik, Deutsches Krebs Forschungs Zentrum, Heidelberg

Declaration

Herewith I declare that I prepared the PhD Thesis entitled "Transcriptomic approaches in the brain at cell-type resolution: Analysis of neuron-glia interaction in *Plp1* and *Cnp1* null-mutant mice" on my own and with no other sources and aids than quoted.

Göttingen, 01. 11. 2009

Danksagungen:

Einen besonders großen Dank möchte ich Moritz aussprechen, der mich während der gesamten Zeit ungemein unterstützt, gefördert und gefordert hat. Zahlreiche, fruchtbare Diskussionen und Ideen führten auf den richtigen Weg zur Fertigstellung dieser Arbeit.

Bei Klaus möchte ich mich bedanken, dass ich in diesem breit und hochklassig aufgestellten Labor meine Promotion habe durchführen können. Darüber hinaus möchte ich mich für die Übernahme des Erstgutachtens bedanken.

Prof. Roland Eils danke ich für die Übernahme des Zweitgutachtens.

Ich möchte mich weiterhin bei Carolin, Anette und Uli für die erstklassige technische und experimentelle Untersützung bedanken.

Ebenso bei Gabi für ihre uneingeschränkte Hilfe bei administrativen und privaten Angelgenheiten über die letzten 4 Jahre.

Magda, Carolin, Anna, Lisa, Kathrin, Alexandra, Ali und Wilko als Mitglieder der Rossner-Gruppe sowie.

Tobi, Ben und Lisa gilt mein Dank für das Korrekturlesen dieser Arbeit.

Meinen Freunden Aiman, Max, Robert, Eva möchte ich für die tolle gemeinsame Zeit in Göttingen danken.

Ich möchte mich bei meiner Freundin Lina im besondernen bedanken, dass sie mich in besonders kritischen Zeiten bedingungslos unterstützt hat und stets aufzubauen vermochten. Ohne diesen privaten Halt wäre eine derartige Arbeit nicht möglich gewesen.

Ganz großen Dank an meine Eltern und meine gesamte Familie, die immer für mich da waren und mich in allem nur erdenklichen unterstützt haben.

DEDICATED

TO

CHRIS

TABLE OF CONTENT

I. List of figures

1   Zusammenfassung

Die Erstellung von Genexpressions-Profilen erlaubt profunde Einblicke in zellulärer Mechanismen unter physiologischen als auch pathologischen Bedingungen. Die Anwendung dieser Methode auf neurales Gewebe ist durch die enorme zelluläre Komplexität des Gehirns stark limitiert. Physiologisch relevante Veränderungen der Transkription in spezifischen Zellpopulationen können in komplexen Zellverbänden nicht detektiert werden. Daher ist die Aufreinigung einzelner Zelltypen aus Gewebsproben des zentralen Nervensystems (ZNS) somit ein hilfreicher Ansatz bei der Untersuchung des Expressionsprofils einzelner Zelltypen. Für die Umsetzung wurden in dieser Arbeit genetisch modifizierte Mausmodelle verwendet, die zelltyp-spezifisch Varianten des grün fluoreszierenden Proteins (GFP) exprimieren. Kombiniert mit speziellen Isolationstechniken, wie *fluorescence activated cell sorting* (FACS) oder *laser capture microdissection* (LCM), ist die Gewinnung intakter RNA aus unfixierten Zellen für die globale Transkriptionsanalyse einzelner Zelltypen möglich. In dieser Studie wurden FACS und LCM zur Isolation von definierte Neuronen und Gliazellen eingesetzt, um daraufhin Erkenntnisse über zelltyp-spezifische Genexpression zu gewinnen. Mittels FACS wurden Expressionsprofile von glialen Vorläuferzellen, Mikroglia und Oligodendrozyten erstellt und eine Transkriptom-Datenbank für gliale Zelltypen generiert. Ferner wurde mittels LCM das Expressionsprofil einzelner Projektionsneurone aus dem Kortex von *Cnp1* und *Plp1* mutanten Mäusen von frühen Krankheits- bis hin zu massiven pathologischen Stadien untersucht. Diese Mausmutanten entwickeln im adulten Tier axonale Degenerationen, wie sie in vielen neuro-degenerativen Erkrankungen, zum Beispiel Parkinson, Alzheimer oder Multipler Sklerose, beschrieben werden. Die Identifikation der molekularen Mechanismen, die mit diesen axonalen Degenerationen einhergehen, ist notwendig für die Entwicklung therapeutischer Ansätze. Für die Charakterisierung der Expressionsprofile der degenerierenden Projektionsneurone in diesen Mausmutanten, wurden zu vier Zeitpunkten während des adultem Stadiums Gewebsproben isoliert und analysiert. Mit Hilfe dieser konnte eine „Momentaufnahme" der Expressionsprofile von definierten neuronalen Subpopulation *in vivo ge*messen werden. Diese Studie liefert Auskunft über bekannte wie auch neue Kandidantengene und potentielle Mechanismen, die womöglich eine wichtige Rolle in der Verarbeitung und Kompensation von pathologischen Vorgängen neuro-degenerativer Erkrankungen spielen.

2   Summary

Global gene expression profiling is a powerful tool to obtain deep insights into physiological and pathological cellular mechanisms. The enormous cellular complexity of the mammalian brain, however, is a major obstacle for gene expression profiling. Physiologically relevant changes of transcription that occur in specific cell populations are likely to remain undetected in cellularly complex samples. The purification of single populations of neural cell types eliminates these difficulties. We have approached this problem in transgenic mice by labelling genetically-defined neural cell types that express variants of GFP. When combined with isolation techniques such as fluorescence activated cell sorting (FACS) or laser capture microdissection (LCM), the isolation of intact RNA from unfixed cells for global transcriptome analysis is possible.

In this study we applied FACS and LCM to isolate neurons and glia to gain insight into cell type specific gene expression. We profiled glial precursor cells, microglia and oligodendrocytes using FACS and generated a transcriptome database for glial cell types. LCM was used to study single isolated callosal projection neurons from the cortex of mouse models, which develop adult onset axonal degeneration a hallmark of many neurodegenerative diseases such as parkinson disease, Alzheimer disease and Multiple Sclerosis (MS). The identification of molecular mechanisms underlying axonal degeneration is critical to design rational therapies for neurodegenerative diseases. Therefore we profiled wild type controls, *Cnp1* and *Plp1* null mutant mice (myelin specific genes) at 4 different time points during adulthood. *Cnp1* and *Plp1* null mutants show axonal swellings and with age severe neurodegeneration, although CNS myelin seems ultra structural not affected.

In summary, we have shown the feasibility to "snapshot" gene expression profiles of genetically defined neuronal subtypes *in vivo* and to compare morphologically similar neurons at a given time in pathological conditions. We followed gene expression changes starting from early disease states until stages of severe pathological signs, focusing on cells known to be susceptible to a genetic predisposition. Our analysis revealed several known and novel candidate genes and mechanisms that likely play a role in the early adaptive responses of cortical projection neurons to cope with axonal stress.

3 Introduction

3.1 Cell type diversity in the brain

The mammalian central nervous system (CNS) comprises a large number of local and regional circuits that are formed by precise connections between neurons, which themselves are quite diverse from the perspective of morphology, physiological activity, and expression of specific neurotransmitters. The realization that cortical cell types are highly diverse was first made by early anatomists using Golgi staining to reveal axonal and dendritic morphology (S Ramon y Cajal, 1952). But neuronal populations comprise a minority in the CNS of higher vertebrates - approximately 90% of the human brain consists of glial cells populations such as astrocytes, oligodendrocytes, and microglia (F. He and Sun, 2007). All these different cell types are highly interconnected (Fig. 1).
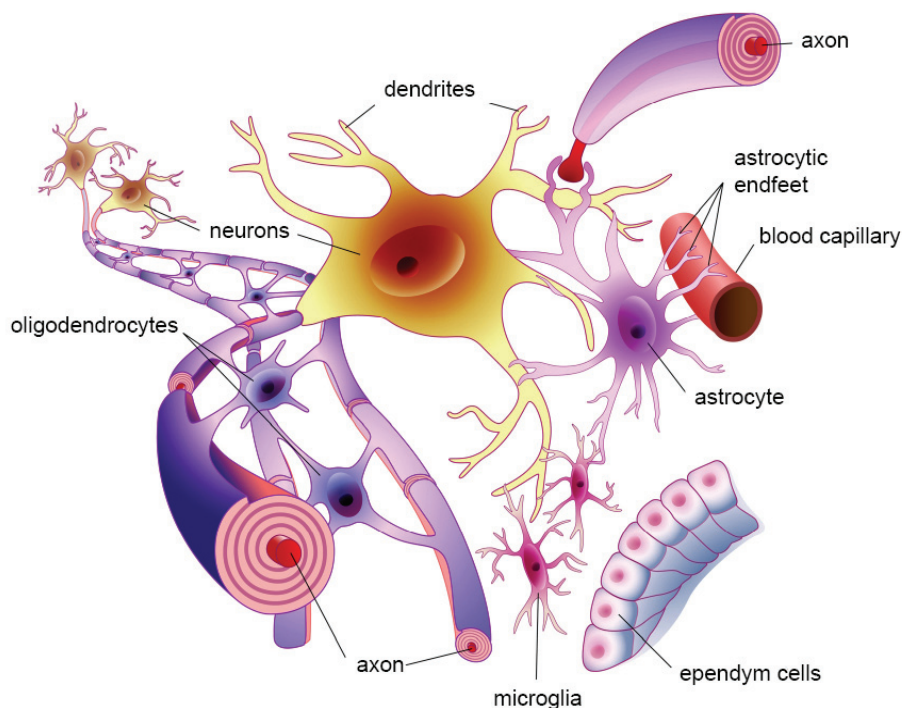
Fig. 1: Main cell types in the CNS
This diagram illustrates the relationships between the various CNS cell types. Depicted are connections formed between neurons, astrocytes, microglia, and myelinating oligodendrocytes as well as ependym cells and blood capillaries.

Therefore the complexity of neural networks in the CNS is enormous, resulting not only from the vast possible combinations and variations of cell-cell

interactions, such as inter-neuronal, neuron - glia or glia - glia contacts, but also owing to the diverse functions that neurons and glia serve themselves. The molecular nature of neuron–glia interactions that control and underlie development, function, and pathology of the mammalian brain remains among the greatest unsolved mysteries in neurobiology today.

3.1.1 History of neuroglia

Rudolf Virchow described in 1846 for the first time the brain connective tissue what he called 'nervenkit' or neuroglia (Virchow, 1856), which in his eyes was set against the concept of nervous elements:

> *'Hitherto, gentlemen, in considering the nervous system, I have only spoken of the really nervous parts of it. But if we would study the nervous system in its real relations in the body, it is extremely important to have a knowledge of that substance also which lies between the proper nervous parts, holds them together and gives the whole its form in a greater or less degree'*

During the second half of the 19th century many different forms of glial cells were described for instance by Otto Deiters, Jacob Henle, Camillo Golgi, and Gustav Retzius (Deiters, 1865; Henle and Merkel, 1869; Golgi, 1874; Retzius, 1894). In fact it was Camillo Golgi who described in 1871 a novel cell type in the CNS characterized by long, numerous, star-like processes (Golgi, 1874). In 1893, Michael von Lenhossék called this characteristic cell type 'astrocyte' (Lenhossék, 1895). At that time the concept that non-neuronal cell types are highly diverse was already established within field experts. 25 years later, Pio del Rio-Hortega identified microglia and oligodendrocytes as separate cell types (del Rio-Hortega, 1919). But it took 30 years more until myelin was described to be part of the Schwann cell (Geren, 1954). Ramon y Cajal once raised the question (S. R Ramon y Cajal, 1911):

'What is the function of glial cells in neural centers? The answer is still not known, and the problem is even more serious because it may remain unsolved for many years to come until physiologists find direct methods to attack it'

Until now, this question is still not entirely answered. Several concepts have been developed which appoint multiple roles to glial cells in brain function. Here we summarize briefly the basic concepts of the three non-neuronal cell types, namely astrocytes, oligodendrocytes, and microglia.

3.1.2   Astrocytes – function and physiological role

Astrocytes derive from neuroepithelial cells that form the ventricular zone; these progenitors give rise to astrocytes, neurons, and oligodendrocytes (Horner and Palmer, 2003). The mammalian CNS astrocytes are highly abundant and represent approximately 1/3 of the cells in the human brain (F. He and Sun, 2007). In the course of vertebrate evolution, there is evidence of a relative expansion of astrocytes in comparison to neurons, implying an evolutionary advantage of animals with a greater number of astrocytes (Nedergaard et al., 2003). In mammals astrocytes can be distinguished into two types: the protoplasmic and the fibrous. Protoplasmic astrocytes are found in the grey matter, have shorter and thicker processes and are mainly associated with synapses. Fibrous astrocytes, on the other hand, have long and thin processes, contain many filaments, and are mainly localized in the white matter. Both types of cells share similar functions, although they are morphologically and structurally different. Astrocytes are in direct contact with blood capillaries and play an important role in the metabolic supply of the CNS. Another major astrocytic function is the support of neuronal function by maintaining local ion concentrations, storing CNS glycogen, clearing neuronal waste, supplying neurotrophic factors and mediating the uptake of neurotransmitters (A. Nair et al., 2008) and (Dreyfus et al., 1999). However, another interesting role of astrocytes is their involvement in the CNS immune responses. Although their origin is not linked to the hematopoietic cells, they exhibit immune functions. They express toll-like receptors, act as antigen-

presenting cells and produce a variety of cytokines and chemokines. Astrocytes are also important for the signaling to the periphery as they secrete chemokines and cytokines and their end-feet contact the blood vessels (Dong and Benveniste, 2001). Activated astrocytes up-regulate their expression of GFAP in a process termed "astrogliosis", a term that has commonly been used as a marker for pathology in CNS diseases. The role of astrocytes in pathology can be dual. In multiple sclerosis (MS), astrocytes are responsible for the breakdown of the blood-brain barrier, the recruitment of T cells, along with the axonal damage and the oligodendrocytic death through the secretion of cytokines. On the other hand, astrocytes promote remyelination by helping to clear debris, secreting chemo-attractants for oligodendrocyte precursor cells (OPCs) and supporting the OPC survival, proliferation, and maturation (A. Williams et al., 2007). Astrocytes have both a beneficial and a detrimental role in the CNS after injury. They form a glial scar, which is thought to protect the fragile brain tissue from further destruction (Myer et al., 2006). On the other hand, the formation of a mechanically obstructive glial scar composed of astrocytes and connective tissue elements is partially responsible for the failure of neuronal regeneration within the CNS after injury (Fitch and Silver, 2008).

3.1.3   Oligodendrocytes – function and physiological role

Oligodendrocytes (from Greek, literally meaning cells with a few branches), or oligodendroglia (Greek, few tree glue), comprise a variety of neuroglia whose main function is the insulation of axons exclusively in the CNS of higher vertebrates (the same function is performed by Schwann cells in the peripheral nervous system). A single oligodendrocyte can extend its processes to 50 axons, wrapping approximately 1 mm of myelin sheath around each axon; Schwann cells can only wrap around 1 axon.

Oligodendroglia arises during development from OPCs, which can be identified by their expression of a number of antigens, including the ganglioside GD3 (Curtis et al., 1988; LeVine and J.E. Goldman, 1988; Hardy and Reynolds, 1991; Levine et al., 1993), the NG2 chondroitin sulfate proteoglycan (Levine et al.,

1993), and the platelet-derived growth factor receptor, alpha polypeptide (PDGFRA) (Pringle et al., 1992). In the mouse forebrain, the majority of oligodendroglial progenitors arises during late embryogenesis and early postnatal development from cells of the subventricular zones (SVZ) of the lateral ventricles. SVZ cells migrate away from germinal zones to populate both developing white and gray matter, where they differentiate and mature into myelin-forming oligodendroglia (Hardy and Reynolds, 1991; Levison and J.E. Goldman, 1993). However, it is not clear whether all oligodendroglial progenitors undergo this sequence of events. It has been suggested that some undergo apoptosis (B A Barres et al., 1992) and others fail to differentiate into mature oligodendroglia but persist as adult oligodendroglial progenitors (Wren et al., 1992).

As part of the nervous system, oligodendrocytes are closely related to nerve cells and, like all other glial cells, oligodendrocytes provide a supporting role for neurons which are introduced in more detail in section 3.2.1.

3.1.4   Microglia– function and physiological role

Microglial cells are considered as the immune cells of the CNS (Perry and S. Gordon, 1988; G W Kreutzberg, 1996). The origin of this cell type is not entirely clear to date. The current concept is that during embryonic development mesodermal glial cells invade the CNS parenchyma, followed by the second entrance of bone marrow-derived monocytes during the postnatal period (Rock et al., 2004; W.Y. Chan et al., 2007). Based on their morphology and status, microglia can be classified into two groups: the "resting" and the "activated" microglia. The "resting" microglia have a ramified morphology with many thin processes extending from the cell soma, while the "activated" ones have a round, amoeboid morphology. Activation of microglia is associated with cell transformation to phagocytes, capable of releasing potentially cytotoxic substances such as oxygen radicals, proteases, and proinflammatory cytokines (Colton and Gilbert, 1987; Banati et al., 1993). Recent studies have indicated that activation of microglia precedes or is concomitant with neuronal and glial

cell degeneration in neurologic disorders including Alzheimer's disease (P. L McGeer and E. G McGeer, 1995), Parkinson's disease (P L McGeer et al., 1993), multiple sclerosis (B\ö et al., 1994), and acquired immune deficiency syndrome dementia complex (Dickson et al., 1991; Gelman, 1993). The amoeboid phase is evident in early development during plasticity, while later on in adulthood microglia are in the "resting" mode. Under any kind of pathology, the microglia react and become "activated", not only by changing their morphology but also their metabolism, so that they can cope with the homeostatic changes (van Rossum and Uwe-Karsten Hanisch, 2004). The distinction of the microglial morphologies and the activating signals is highly complicated, as described in more detail in multiple excellent reviews (Streit et al., 1988; Barron, 1995; J. Gehrmann et al., 1995; Gonzalez-Scarano and Baltuch, 1999; Suzumura et al., 1991; U. K Hanisch and H. Kettenmann, 2007).

So far it is known that microglial activation is crucial for the involvement of the adaptive immune system, as microglia are the key components for the recruitment of neutrophils, leukocytes and macrophages (Aloisi, 2001). Nevertheless, microglial activation is a double-edged sword, as it is generally beneficial and acts in a protective way. But chronic microglial activation leads to neuronal damage and accounts for the injury observed in certain neurodegenerative diseases, such as Parkinson's disease and MS (Gao and Hong, 2008; Lassmann, 2008). The "resting" microglia were previously regarded as dormant cells. However, recent *in vivo* two-photon microscopy of transgenic mice expressing EGFP under the *Cx3cr1* promoter revealed that "resting" microglia have highly motile processes that roam the intercellular space, extending and retracting in a very dynamic fashion (Nimmerjahn et al., 2005; Davalos et al., 2005). Their somata remain stationary, while their processes constantly retract and rebuild, enabling the microglial surveillance of the brain parenchyma without perturbing the already existing glial-neuronal structures. Nonetheless, so far little is known about what controls and restricts this microglial activity in the healthy CNS.

3.1.5 Transcriptional profiling of specific CNS cell types

Given the advances in transcriptome analysis in the recent years, genome-wide gene expression profiling could provide a sound and unbiased method for neural cell type classification (Markram et al., 2004; Mott and Dingledine, 2003). This approach relies on the assumption that the overall function of a specific cell type within its context is highly correlated with its gene expression profile. DNA microarrays provide an ideal platform for such studies. To date, however, microarrays have not been effectively and systematically employed to address problems in cell type characterization. In the CNS, the majority of microarray experiments have been carried out on tissue homogenates, not allowing a precise distinction between cell types (Mirnics et al., 2000; Sandberg et al., 2000; Xinyu Zhao et al., 2001a; Zirlinger and D. Anderson, 2003).

There are two experimental problems that, if solved, would greatly accelerate progress in further characterization of cell types within the mammalian brain: First of all, the rapid and unambiguous identification of distinct cell types in the CNS without compromising RNA integrity; secondly, the isolation of the distinct cell types from the CNS in order to subject them to further analysis on their transcript or protein level while at the same time preserving RNA and / or protein integrity.

Over the last decade the number of available tools and methods to address these problems have radically advanced. Defining and identifying cell types was greatly improved by the availability of specific antibodies, but more importantly by genetic tools (Nolte et al., 2001; Jung et al., 2000; P.G. Hirrlinger et al., 2005; Rossner et al., 2006). Now cells can be distinguished for instance by known markers using immunocytochemical labeling, or by stereotaxic injection of fluorescent tracers into projection targets. Defined cell types or even subpopulations can be identified using fluorescent proteins, which expression are controlled by specific promoters or enhancers. Several studies have been carried out employing such labeling techniques (Z. Yang et al., 2005; Buchstaller et al., 2004; Colosimo et al., 2004; Rossner et al., 2006) to gain

insight into the genome-wide transcriptional profiles of specifically labeled cell types.

Data derived from DNA microarray studies in conjunction with several cell isolation techniques have lead to a better understanding of the generation and function of defined cell types in the CNS. The use of immunocytochemical labeling, isolation, and manual sorting of neuronal cells has lead to the identification of cell type-specific gene expression patterns for 12 different neuronal subtypes and the generation of a detailed taxonomic tree (Sugino et al., 2006). A different experimental approach characterized the specification and development of retrogradely labeled cortical projection neurons using fluorescence activated cell sorting (FACS) (Arlotta et al., 2005). In addition, striatal projection neuron subtypes were profiled with FACS (Lobo et al., 2006). Moreover, purified rat OPCs and premyelinating, postmitotic oligodendrocytes (OLs) have been profiled to reveal developmental gene expression changes during OL specification and differentiation (Nielsen et al., 2006; Dugas et al., 2006). A global and direct comparison between two major CNS neural cell types such as astrocytes and myelinating OLs has also been undertaken by Cahoy and colleagues (Cahoy et al., 2008). All approaches mentioned thus far are restricted to late embryonal or early postnatal development owing to the inability of the employed techniques to isolate the mentioned cell types due to their high fragility at later time points.

3.1.6 Laser capture microdissection; a tool for precise single cell isolation

Laser capture microdissection (LCM) allows precise separation of both single cells and small cell groups from a variety of tissues under direct microscopic observation. One of the major advantages of LCM is the fact that it can be combined with a variety of additional methodologies to further the isolation of distinct cells or groups of cells. LCM has been used in combination with tracers, reporter gene expression, with histological staining methods and with transgenically labeled cell types through the expression of fluorescent proteins.

However, the limiting factor of this approach is obtaining consistently high quality RNA from small amounts of starting material.

So far neurons have been a favored target for such investigations, both because of their clinical importance in neurodegenerative disorders such as Parkinson's disease and because they are readily labeled by antibodies to tyrosine hydroxylase (TH), the enzyme responsible of dopamine production. Two groups (Chung et al., 2005; Greene et al., 2005) compared dopaminergic neurons from neighboring midbrain regions, the ventral tegmental area (VTA) and the substantia nigra (SN), to identify genes contributing to the higher susceptibility of SN neurons to neurodegeneration in Parkinson's disease. All of these studies used antibody labeling or retrograde tracers to identify distinct cell populations. Drawbacks of these techniques are for example additional factors such as prolonged treatment in aqueous phase in the case of antibody labeling, which increases RNA degradation processes, or retrograde labeling interfering with the system under investigation. The use of cell type-specific transgenes allows the labeling of identical cells or cell populations with virtually no variance within a given mouse strain, thus increasing reproducibility of experimental data (Rossner et al., 2006). However, the choice of the proper reporter is crucial for successful labeling and subsequent LCM to achieve specificity. In a previous study we could demonstrate that the fluorescent signal of 'conventional' reporter mice harboring a *Thy1*-EYFP transgene construct, is lost during preparation, most likely because of rapid diffusion (**Fig. 2**). We could further show that nuclear targeting of enhanced yellow fluorescent protein (EYFPnuc) is sufficient to retain a strong and unambiguous signal after section preparation. In our generated mouse line, EYFPnuc expression is placed under transcriptional control of the *Thy1* promoter and labels predominantly cortical layer V callosal projection neurons (CPN) (Caroni, 1997).

The generated reporter mouse is thus suitable to transcriptionally profile a specific subpopulation of cortical neurons during development and aging. Furthermore, this tool could provide insight into transcriptional changes that occur during encephalopathies like MS.
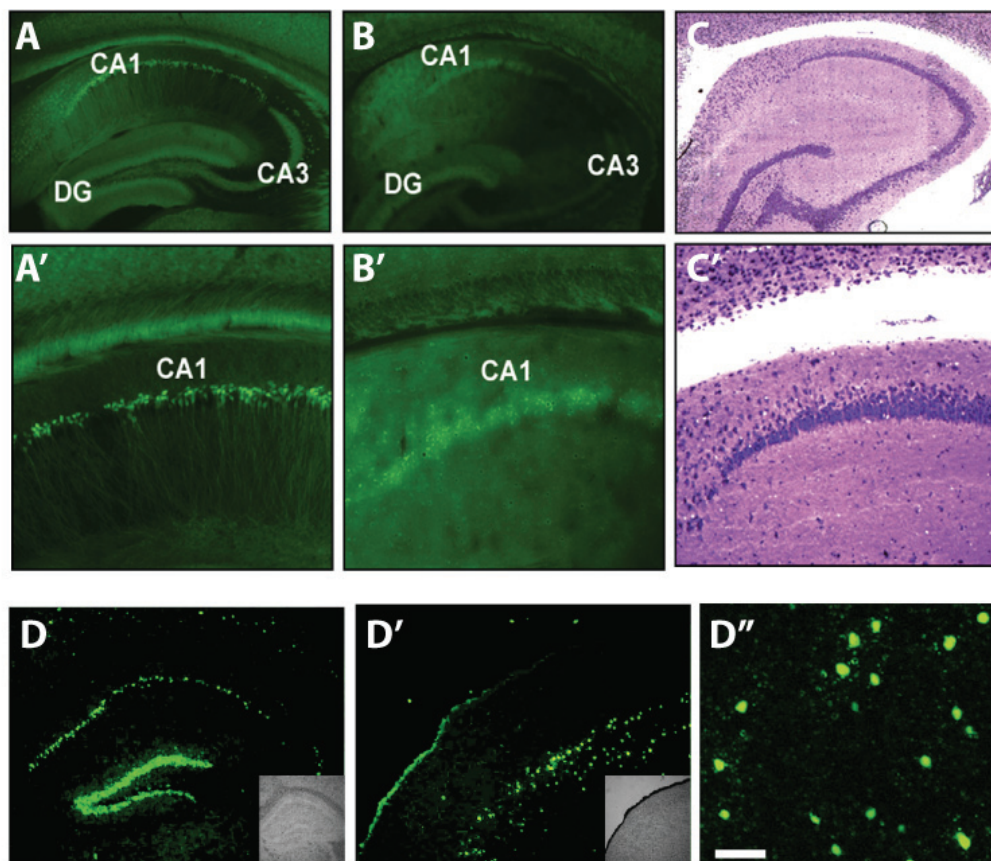
Fig. 2: Conventional GFP derivatives are not compatible with laser-directed micro-dissection. The cellular signal of a nuclear-targeted EYFP (EYFPnuc) is preserved in freeze-dried cryosections obtained from transgenic mice.
(A-C) The cellular resolution of EYFP expressed in transgenic mice is lost after cryosectioning. Sagittal sections of mouse brains from mice expressing cytoplasmic localized EYFP under the control of the *Thy-1* promoter were either fixed with 4% buffered PFA or immediately frozen on dry ice. (A, A') Vibratome sections obtained from PFA fixed tissue (30 μm) and (B, B') cryosections (15 μm; Cryo) from frozen tissue, were analyzed for EYFP fluorescence. After cryosectioning, the cellular resolution of the EYFP fluorescent signal is lost. The EYFP signal is retained but appears to be diffuse and faded. (C, C') Staining of the cryosection with thionin (Cryo) reveals that the cellular integrity of the tissue specimen is intact. (D-D'') Nuclear targeted fluorescent proteins appear to be promising candidates for a combined *in vivo* labeling and microdissection approach. In the hippocampus, EYFPnuc[+] nuclei can be detected in the granular cell layer (DG) and in the CA1 field of the pyramidal cell layer (CA1). In the CA3 field (CA3), fewer cells are EYFP positive. (D') Higher magnification of EYFP[+] nuclei in the somatosensory cortex. Scale bar, 50 μm. (D'') In the cortex, cells located in deeper layers show a nuclear EYFPnuc signal. The inset shows the morphology of the section at the level of the somatosensory cortex in bright field. Adapted from (Rossner et al., 2006)

11

3.2 Neuronal gene expression profiles of myelin mutant mice

So far only a few groups (Lu et al., 2004; Bernard et al., 2009; Chung et al., 2005) applied cell isolation techniques like LCM in combination with high throughput transcriptional profiling to investigate pathological changes in a specific cell population, which are mediated by dysfunction of a different but phenotypically unaffected cell type. Unraveling the transcriptional changes in these cells may help to identify disease-relevant mechanisms or transcriptional hallmarks. Once disease-relevant genes have been identified, treatments which more specifically interfere with the disease-causing mechanism could be developed. Established mouse models in which neurodegeneration (caused by axonal loss) is triggered by a dysfunction of oligodendrocytes are the *Cnp1 null* as well as *Plp1 null* mutants (Klugmann et al., 1997; Lappe-Siefke et al., 2003).

3.2.1 Mouse models of neurodegeneration

3.2.1.1 *Cnp1* null mice – a model of 'primary' axonal pathology

2', 3'-cyclic nucleotide 3'-phosphodiesterase (CNP) constitutes 4-5% of the total CNS myelin protein content and is expressed as the first of the major myelin-related proteins during brain development (Sprinkle et al., 1978). *Cnp1* expression is a marker of myelinating oligodendrocytes from early pre-myelinating stages till adulthood (P E Braun et al., 1988). In oligodendrocytes and their progenitors, *Cnp1* localizes to the cytoplasm (Nishizawa et al., 1985) or cytoplasm-containing uncompacted myelin regions such as the inner/outer mesaxon and paranodal loops (Kurihara and Tsukada, 1967; P E Braun et al., 1988). Outside the CNS, CNP is found in Schwann cells of the peripheral nervous system (PNS), in some immune cells (Sprinkle et al., 1985), photoreceptor cells of the retina (Giulian and Moore, 1980), and testis (Scherer et al., 1994).

CNP is an enzyme which was originally characterized by its ability to hydrolyze 2', 3'-cyclic nucleotides *in vitro*. CNP is found most abundantly in myelin of

oligodendrocytes in the CNS and to lesser extent in Schwann cells. The absence of a physiologically relevant substrate in myelinating oligodendrocytes or any other tissue indicates that catalytic activity is irrelevant for the role of CNP *in vivo*, therefore leaving the function of this enzyme unknown. Several, but rather divergent functions of CNP have been postulated in the literature. It was shown that CNP is involved in RNA metabolism (Heaton and Eckstein, 1996) supporting the rapid biogenesis of the myelin sheath (reviewed by (Sprinkle, 1989). Other studies demonstrated a direct interaction of CNP with mitochondria in bovine adrenal cell cultures (McFerran and Burgoyne, 1997). It was also reported that CNP acts as a microtubule-associated protein and promotes microtubule assembly (C Laezza et al., 1997; Maurizio Bifulco et al., 2002). The authors claim that phosphorylation of CNP interferes with its assembly-promoting activity, similar to the deletion of its carboxy terminus which leads to abnormal microtubule distribution within cells. Membrane localization of the protein and CNP-dependent microtubule organization suggest that CNP is a membrane-bound microtubule-associated protein that can link tubulin to membranes and may regulate cytoplasmic microtubule distribution.

In this context, it was rather unexpected that *Cnp1* deficient mice revealed no severe myelin phenotype. Cellular distribution of myelin proteins and myelin lipid content are not altered. Myelin spacing in the spinal cord and tubular networks within the oligodendrocytes also appeared to be unaffected by the loss of *Cnp1* (Lappe-Siefke et al., 2003). The mice also showed no morphological developmental delay till the age of 2.5 months, except for abnormal enlargement of the inner tongue processes of myelin, which occurs concomitantly to the earliest axonal defects within days of myelination onset (Edgar et al., 2009). It has been shown that the distribution of nodal sodium channels and paranodal adhesion proteins becomes disorganized with age in *Cnp1* deficient mice, suggesting a role of CNP in maintaining integrity of paranodes (Rasband et al., 2005).

Many mice unexpectedly develop ataxia and hind leg impairments at the age of 4 months, progressing until premature death between 9 and 15 months. This

phenotype was accompanied by axonal swellings at distal paranodal regions containing multivesicular bodies and cytoskeleton components and progressive axonal (but not neuronal) loss detected at the age of 7 months (Lappe-Siefke et al., 2003).

Axonal changes in the *Cnp1* knock-out mouse are characterized by focal accumulations of axonal organelles, being associated with impaired fast axonal transport and subsequent degeneration of the distal portions of long spinal axons.

Therefore, *Cnp1* null mutants serve in the present study as a model of 'primary' axonal loss, preceding the degeneration or retraction of myelin.

3.2.1.2 *Plp1 null* mice – a model of axonal loss with mild myelin disorder

Proteolipid protein (PLP) is the major CNS myelin protein, which is highly expressed in oligodendrocytes (I Griffiths, Klugmann, T. Anderson, D Yool, et al., 1998). The two protein isoforms PLP and DM20, originating from the *Plp1* gene, constitute together at least 50% of protein in CNS myelin (Lees MB and Brostoff SW, 1984). Unlike DM20, PLP expression is restricted to oligodendrocytes in the CNS (Braun, P.E., 1984).

The systemic consequences of mutations or absence of PLP/DM20 have been widely studied *in vivo*, giving important insight into the function of PLP. The natural mouse mutants *jimpy* (Dautigny et al., 1986; K A Nave et al., 1986) and the allelic *rumpshaker* mouse (Schneider et al., 1992) bear mutations in the *Plp1* gene and are models for the connate form of Pelizaeus-Merzbacher disease (PMD) and for hereditary spastic paraplegia 2 (SPG2) in humans, respectively. Dysmyelination and oligodendrocyte death are caused by the misfolded cytotoxic protein product in both the mouse models and the human patients (Skoff et al., 2004; I Griffiths, Klugmann, T. Anderson, Thomson, et al., 1998). In contrast are the *Plp1* null mutants not severely affected, with almost normal development of CNS white matter and no motor problems up to the age of 15 months (Boison et al., 1995; Rosenbluth et al., 1996; Klugmann et al.,

1997). Myelin synthesis appeared to be normal and oligodendrocytes were viable and differentiated. This suggested that PLP and DM20 are not crucial for myelin assembly. *Plp1*-deficient mice develop a late onset axonal pathology (I Griffiths, Klugmann, T. Anderson, D Yool, et al., 1998), showing accumulations of organelles at distal juxtaparanodal regions similar to *Cnp1* null mutants. Both models develop axonal pathologies upon oligodendroglial dysfunction, accompanied by impaired axonal transport and distal axonal degeneration. Mass spectrometry of *Plp1*-deficient myelin showed absence of Sirtuin-2 (*Sir2*), a NAD-depedent protein deacetylase that is under physiological conditions located to noncompacted myelin. These findings demonstrate a potential role of PLP in proper transport of cargo proteins into the myelin compartment, which could influence axon function (Werner et al., 2007).

Interestingly, axonal swellings in *Plp1* and *Cnp1* knock-out mice resemble those seen in other models for impairment of axonal transport such as paraplegin and spastin mutants (Edgar et al., 2004). Pathological analysis of myelin mutants indicates that oligodendrocytes modulate various processes within their myelinated axon beneath, including axonal transport (Witt and Scott T. Brady, 2000). Providing a basis for regulation of axonal transport by OLs, localized changes in kinase and phosphatase activities occur at nodal/paranodal regions of myelinated axons, precisely the site at which axonal organelles accumulate in *Plp1* knock-out mice. This suggests that localized deregulation of kinase/phosphatase activity and motor proteins might occur in the absence of various myelin-associated proteins. Such localized actions on motor proteins is supported by axonal transport impairment independent of changes in motor protein transcription (G Morfini et al., 2001; Gerardo Morfini et al., 2002; Gerardo Morfini et al., 2004). Another explanation for impaired axonal transport in myelin mutants are local energy deficiencies. This is consistent with axonal organelle accumulations observed in paraplegin-deficient mice, which are morphologically similar to those in myelin mutants (Gerardo A. Morfini et al., 2009).
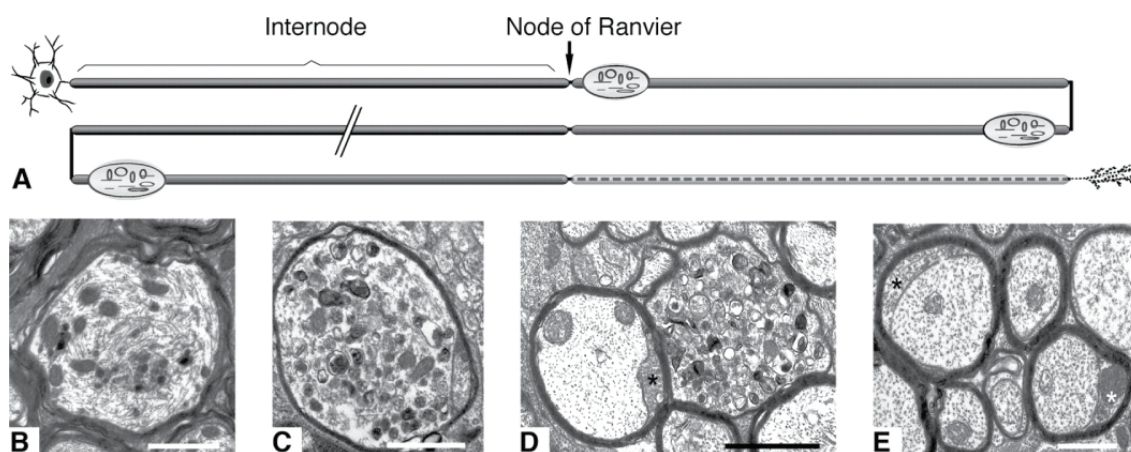
Fig. 3: Axonal transport abnormalities in myelin protein-deficient mice.
(A) Schematic summarizing the changes that occur in axons in the *Plp1 null* mouse model of spastic paraplegia type 2. Despite almost normal myelination, axonal organelles accumulate at the distal juxtaparanodal regions of myelinated axons, eventually causing localized swelling of the axon. Axonal swellings are not preferentially localized to proximal or distal portions of an axon, and it is likely (though not confirmed) that a single axon contains multiple swellings. The distal portions of the long axons of the spinal cord eventually degenerate (represented by the dashed line). (B–E) Electron micrographs of CNS fiber changes. Organelle accumulation and cytoskeletal disruption in a myelinated axon from a P120 Plp1 null mouse spinal cord (B). Morphologically similar organelle accumulations in the spinal cord (C) and optic nerve (D) of P120 *Cnp1* null mice. Swelling of the inner tongue process of the oligodendrocyte (asterisks in D and E) is a feature of the *Cnp1* null mouse. The swollen tongue appears not to compress the axon but seems to be accommodated by expansion of the compact myelin sheath, as illustrated in these P120 optic nerve fibers. Scale bars: B, C, 2 μm; D, E, 1 μm. Figure from (Gerardo A. Morfini et al., 2009)

Dysfunction and degeneration of different neuronal populations are features of adult-onset neurodegenerative diseases (AONDs) (Bossy-Wetzel et al., 2004; Mattson and Magnus, 2006). Despite their heterogeneous etiology, AONDs share several characteristics: they are progressive and their clinical phenotype results from an age-dependent decline in neuronal function that is initially associated with loss of synaptic activity rather than neuronal cell death, a late event in the disease process. *Cnp1* and *Plp1* null mutant mice reflect these disease hallmarks and can therefore be considered as model systems to study AONDs (Gerardo A. Morfini et al., 2009).

It has thus far not been investigated how neurons, which develop age-dependent axonal pathologies, react to the lack of glial support on a transcriptional level. Neurons deprived of oligodendroglial support may change their gene expression pattern in order to adapt to primary disease causing

16

changes. We addressed this question by expression profiling of a specific neuronal subpopulation in the cortex of *Cnp1* and *Plp1 null* mutant mice. We therefore crossbred myelin mutants with the *Thy1*-EYFPnuc reporter mouse line (described in section …) and subjected *Plp1*-/Y, *Cnp1*-/-, and wild-type controls to LCM.

18

4   Objectives

The main aims of the study were:

(i) Characterization of reference transcriptional profiles of the main glial cell populations (Microglia, Astroglia and Oligodendroglia) from acutely isolated, FACS purified cells.

(ii) Generation of transcriptional profiles of a cortical projection neurons and white matter tracts in mouse models, which show axonal degeneration caused by a dysfunction of oligodendrocytes.

(iii) Generation of a model of the diseased transcriptional network underlying early adaptive events of axonal degeneration.

5 Materials and Methods

5.1   Materials

5.1.1   Laboratory supplies and equipment.

5.1.1.1   Equipment

Picodrop Spectrophotometer	Picodrop Limited
Agilent 2100 Bioanalyzer	Agilent Biotechnologies
7500 Fast Real-time PCR System	Applied Biosystems
Light Cycler 480	Roche
Biophotometer	Eppendorf
Heraeus Biofuge Fresco	DJB Labcare
Centrifuge 5810R	Eppendorf
Thermocycler T3	Biometra
Thermocycler TGradient	Biometra
Electrophoresis power supply	Pharmacia LKB
UV Gel Documentation System	iNTAS
Thermomixer comfort	Eppendorf
Arium 611 Water Purification System	Sartorius
Leica DM IRBE inverted microscope	Leica
Veritas Microdissection Instrument	Molecular Devices
Cryotome CM3000	Leica
EpMotion pipette robot	Eppendorf
Hybridization Oven 645	Affymetrix
Fluidics Station 450	Affymetrix
Scanner 3000 7G	Affymterix

5.1.1.2   Software

Windows XP Professional	Microsoft
OSX	Apple
Microsoft Office 2003	Microsoft
Acrobat Reader Professional 8.0	Adobe
Endnote X2	Thomson Research Soft
Creative Suite CS3	Adobe
Lasergene 7.0.0	DNA Star Inc.
Vector NTI Advance 10	Invitrogen
MicroWin 2000	Berthold Technologies
R.2.6 (statistical computing environment)	http://cran.r-project.org/
Bioconductor Packages	http://www.bioconductor.org/

Partek Genomics Suite 6.4	Partek
GSEA 2.0	Broad Institute of MIT
visANT	http://visant.bu.edu
GenePattern 2.0	Broad Institute of MIT
Tinn-R	SourceForge
ImageJ v1.41	http://rsbweb.nih.gov/ij/index.html
qBase v1.3.5	http://medgen.ugent.be/qbase/
Gene chip operating software	Affymetrix

Bioconductor packages

bridge	affxparser	goTools	mouse4302cdf
Biostrings	ade4	graph	mouse4302probe
biomaRt	ABarray	GraphAlignment	mouse430a2.db
bioDist	DBI	graphics	mouse430a2cdf
biocViews	EMV	GSEABase	mouse430a2probe
base	exonmap	gtools	multtest
ArrayTools	feature	Heatplus	oligo
AnnotationDbi	fields	KEGG.db	pdInfoBuilder
annotate	gcrma	keggorth	plier
AnnBuilder	gdata	limma	R2HTML
annaffy	genefilter	maanova	RankProd
affyQCReport	GeneMeta	made4	RColorBrewer
affyio	geneplotter	makecdfenv	RMySQL
affydata	geneRecommender	makePlatformDesign	siggenes
affycoretools	GeneSelector	marray	simpleaffy
AffyCompatible	GEOmetadb	maSigPro	
affycomp	GEOquery	MASS	
affy	GOstats	mouse4302.db	

5.1.1.3 Plasticware

General laboratory materials from Eppendorf, Falcon, Gilson and ABgene were used for molecular biology applications. For cell culture applications plastic wear from Falcon and Nunc was used.

Kits:

QIAprep Spin Miniprep Kit	Qiagen
QIAquick Gel Extraction Kit	Qiagen
QIAfilter Midi und Maxi Kit	Qiagen
T7 Megascript Kit	Ambion
Transcriptor High fidelity cDNA Synthesis Kit	Roche
cDNA Pre Amplication Kit	Roche
SuperScript III First Strand Synthesis Kit	Invitrogen

RNeasy Mini Kit	Qiagen
RNeasy Micro Kit	Qiagen
RNase-Free DNase Set	Qiagen
Deoxynucleoside Triphosphate Set	Roche
WT-Ovation Pico System	Nugen
FL-Ovation cDNA Biotin Module	Nugen
WT-Ovation Exon Module	Nugen
GeneChip WT sense Target Labeling Kit	Affymetrix

5.1.1.4 Reagents

General reagents

General chemicals from Sigma-Aldrich or MERK were used unless stated otherwise.

Agarose	Applichem
Agar	BD
GeneRuler 1 kb DNA ladder	Fermentas
GeneRuler 100 bp DNA ladder	Fermentas
6x DNA Loading Dye	Fermentas
Power SYBR Green PCR Master Mix	Applied Biosystems
Trizol reagent	Invitrogen
Acetonitryl	J.T.Baker
Fomamide	Sigma-Aldrich
SSPE buffer (20x)	AppliChem
Salmon Sperm DNA	Sigma-Aldrich
Yeast tRNA	Sigma-Aldrich
SSPE buffer (20x)	AppliChem
Universal probe library (Mouse)	Roche

Enzymes

Restriction enzymes	New England Biolabs
REDTaq DNA polymerase	Sigma-Aldrich
Taq polymerase	Roche
T4 DNA ligase	Promega
Superscript III Reverse Transcriptase	Invitrogen
Power SYBR green PCR master mix	Applied Biosystems
TaqMan PCR master mix	Applied Biosystems

5.1.1.5 Microarrays

Mouse430A 2.0	Affymetrix
Mouse Exon 1.0 ST	Affymetrix

5.1.1.6 Molecular biology buffers

dNTP-stock solutions (100 mM)

25 mM each dATP, dCTP, dGTP, dTTP (Boehringer, Mannheim)

Ethidiumbromide

1-1.5 µg/ml for agarose gels in 1x TAE

TAE (50x, 1000ml)

2 M Tris-Acetate, pH 8.0

50 mM EDTA

57.1 ml Glacial acetic acid

Add dH$_2$O up to 1000ml

TE (1x)

10 mM Tris-HCl, pH 8.0

1 mM EDTA

Modified Gitschier buffer (MGB, 10x)

6.7 ml 1 M Tris-HCl (pH 8.8)

1.66 ml 1 M (NH$_4$)$_2$SO$_4$

650 µl 1 M MgCl$_2$

Add dH$_2$O up to 10 ml

MGB buffer (1x, working solution)

1 ml 10x MGB

100 µl β-Mercaptoethanol

500 µl 10 % Triton X-100

8.4 ml dH$_2$O

5.1.1.7 Protein biochemistry buffers

Lysis buffers

Lysis buffer I (for brain)

50 mM Tris-HCl, pH 7.5

150 mM NaCl

1 mM EDTA

25

1 % Triton X-100

1 mM PMSF (add before use)

1 tablet Complete Mini protease inhibitor (Roche)/ 10 ml of lysis buffer

* protease inhibitors are added freshly to the lysis buffer before use

5.1.1.8   Protein purification buffers

Wash buffer I (WB I)

10 mM Tris, pH 7.5

150 mM NaCl

0.05 % Tween-20

10 mM EDTA

Adjust pH to 7.5

Wash buffer II (WB II)

50 mM Tris, pH 7.5

Elution buffer I (EB I)

0.1 M Glycine, pH 3.0

Elution buffer II (EB II)

0.1 M Glycine, pH 2.5

Neutralization buffer (NB)

1 M Tris, pH 8.0

5.1.1.9   SDS PAGE and Western Blotting

Separating SDS gel (12 %, 4 gels, 1.5 mm thickness)

13 ml dH$_2$O

15 ml 30 % Acrylamide (BioRad, 29.1)

9.4 ml 1.5 M Tris-HCl (pH 8.8)

370 µl 10 % SDS

125 µl 10 % APS (Ammonium persulfate)

30 µl TEMED (BioRad)

Stacking SDS gel (4 gels)

6.1 ml dH$_2$O

1.3 ml 30 % Acrylamide (BioRad, 29.1)

2.5 ml 0.5 M Tris-HCl (pH 6.8)

100 µl 10 % SDS

50 µl 10 % APS (Ammonium persulfate)

10 µl TEMED

SDS running buffer (Laemmli buffer, 1x)

25 mM Tris-HCl

192 mM Glycine

1 % (w/v) SDS

SDS sample buffer (6x)

7 ml 0.5M Tris-HCl buffer (pH 6.8)

3 ml Glycerol (30 % final concentration)

1 g SDS

1.2 ml 1 % Bromophenol blue

0.2 - 2 % β-Mercaptoethanol (add fresh)

Transfer buffer (1x)

48 mM Tris base

39 mM Glycine

10-20 % Methanol

Blocking Buffer

5 % non-fat dry milk powder in TBS or PBS (1x)

Western blot stripping buffer

0.2 M Glycine-HCl, pH 2.5

0.1 % Tween-20

Coomassie blue (Staining solution)

2 g Coomassie brilliant blue (R-250)

1 l Methanol

200 ml Acetic acid

800 ml dH$_2$O

Stir overnight and filter through Whatmann paper.

Destaining solution

50 ml Methanol

10 ml Acetic acid

40 ml dH$_2$O

Tris buffered saline (TBS, 20x)

1 M Tris base

3 M NaCl

Adjust pH 7.4 (with HCl)

TBS with Tween-20 (TBST, 1x)

50 mM Tris-HCl (pH 7.4-7.6)

150 mM NaCl

0.05 % - 0.15 % Tween-20

5.1.1.10 DNA and Protein markers

GeneRuler 1 kb DNA ladder (Fermentas)

GeneRuler 100 bp DNA ladder (Fermentas)

Precision Plus prestained protein standard (BioRad)

5.1.1.11 Immunocytochemistry buffers

Phosphate buffered saline (PBS) (1x cell culture, 1000 ml)

136 mM NaCl

2.6 mM KCl

10 mM Na$_2$HPO$_4$ x2 H$_2$O

1.4 mM KH$_2$PO$_4$

Set pH to 7.2 with 10 N NaOH

Add dH$_2$O up to 1000 ml

4 % Paraformaldehyde in PBS/TBS

100 ml 0.2 M NaH$_2$PO$_4$ (Sodiumdihydrogenphosphate)

400 ml 0.2 M Na_2HPO_4 (di-Sodiumhydrogenphosphate)

108 ml 37 % Formalin

392 ml dH_2O

Filtered with a 500 ml Nalgene sterile filter unit

Blocking Buffer

2 % BSA (Fraction V)

2 % Goat serum

0.02 % Biotin

0.1 % Porcine skin gelatine

0.01 % Saponin

Dissolved in TBS or PBS

Mounting Agent

Aqua polymount (Polysciences)

5.1.1.12 Immunohistochemistry buffers

Phosphate buffer (stock solution)

0.2 M NaH_2PO_4

0.2 M Na_2HPO_4

Phosphate buffer (working solution, pH 7.4)

20 ml 0.2 M NaH_2PO_4

80 ml 0.2 M Na_2HPO_4

100 ml dH_2O

Bovine Serum Albumin (PBS/BSA)

20 ml 0.2 M NaH_2PO_4

80 ml 0.2 M Na_2HPO_4

1.8 g NaCl

1 g BSA

100 ml dH_2O

Citrate Buffer (stock solution)*

0.1 M Citric acid ($C_6H_8O_7*H_2O$)

0.1 M Sodium citrate ($C_6H_5O_7Na_3*_2H_2O$)

*Stored at 4°C

*Citrate Buffer (working solution, 0.01 M, pH 6.0)**

9 ml 0.1 M Citric acid ($C_6H_8O_7*H_2O$)

41 ml 0.1 M Sodium citrate ($C_6H_5O_7Na_3*_2H_2O$)

450 ml dH_2O

*Always freshly prepared

*Tris Buffer (stock solution)**

0.5 M Tris base

Adjust pH 7.6 with HCl

*Store at 4°C

*Tris Buffer (working solution)**

100 ml 0.5M Tris base (pH 7.6)

9 g NaCl

Add up to 1000 ml with dH_2O

*Always freshly prepared

Blocking buffer (2 % milk powder in Tris Buffer)

20 g of non-fat milk powder

Add up to 1000 ml with Tris buffer

5.1.1.13 Histological stains and reagents

Mayer's Haematoxylin solution

1 g Haematoxylin (Merck) was dissolved in 1000 ml dH_2O and 0.2 g sodium iodate and 50g potassium aluminium sulphate ($K_2Al_2(SO_4)_4*24H_2O$) was added under constant shaking. Finally, 50 g chloralhydrate and 1 g citric acid were added and the solution was filtered before use.

Eosin solution

Stock solution (10x)

10 g of Eosin were dissolved in 100 ml of dH_2O and left to mature.

<u>Working solution</u>

2.5 ml stock solution

250 ml dH$_2$O

12 drops glacial acetic

Scott's solution

2 g KHCO$_3$ (potassiumhydrogencarbonate)

20 g MgSO$_4$ (magnesium sulphate)

Add up to 1000 ml with dH$_2$O

Thionin solution

Stock 1.3% thionin:

13 gm Thionin

1000 ml dH$_2$O

Stir and heat gently for 1 hour. Filter the solution after the dye has dissolved. Store in a stoppered bottle.

Buffers:

1. 1 M Acetic Acid (HAc):

58.5 ml glacial acetic acid

dilute to 1 liter with distilled water

2. 1 M Sodium Hydroxide (NaOH):

50 gm sodium hydroxide pellets

dissolve to 1 liter with distilled water

Working Stains (1%):

80.0 ml 1M HAc

14.4 ml 1M NaOH

305.6 ml Thionin stock

HCl- Alcohol

1.25 ml HCl

350 ml Ethanol

150 ml dH$_2$O

Staining solution

Eosin solution

0.1 g Eosin was dissolved in 100 ml dH$_2$O and 0.1 g methylene blue in 100 ml dH$_2$O. The two solutions were mixed and left for 3-4 days to mature. The solutions were filtered through Whatmann paper, let to dry over night and then dissolved in 10 ml pure methanol. The solution was stored at 4°C.

Staining solution

Dissolve 1 g of Luxol blue (1B, MBS from Chroma) in 1000 ml 96 % ethanol while stirring and warming. Let the solution cool down at room temperature and filter though Whatmann paper. Before use, for every 100 ml of staining solution add 50 µl of concentrated acetic acid (CH$_3$COOH).

'Nuclear fast red' solution

Dissolve 0.2 g of 'nuclear fast red' in 200 ml of boiling 5% aluminium sulfate solution and boil for an additional 5-10 min. Let it cool down at room temperature and filter with Whatmann paper.

5.1.1.14 Mouse lines

CNP null mutants (Lappe-Siefke et al., 2003)

PLP null mutants (Klugmann et al., 1997)

Thy1-EYFPnuc (Rossner et al., 2006)

hGFAP-EGFP (Nolte et al., 2001)

CX3CR1-EGFP (Jung et al., 2000)

PLP-DsRed (P.G. Hirrlinger et al., 2005)

5.1.1.15 Oligonucleotides

Oligonucleotides were synthesized in the Max Planck Institute of Experimental

Medicine.

Genotyping primers for various mouse lines

Thy-1 EYFPnuc	Forward:	Forward: CGGCTACGGCCTGCAGTGCT,
	Reverse:	Reverse: GGCGGATCTTGAAGTTCACCTTGATG.
	Amplification product: 200 bp	
Cnp1	puro3:	CATAGCCTGAAGAACGAGA
	Forward:	GATGGGGCTTACTCTTGC
	Reverse:	GCCTTCAAACTGTCCATCTC
	Amplification product: 600 bp for mutant and 900 bp for wild-type	
Plp1	Forward:	GGAGAGGAGGAGGGAAACGAG
	Reverse:	TCTGTTTTGCGGCTGACTTTG
	Neo:	TTGGCGGCGAATGGGCTGAC
	Amplification product: 300 bp for mutant and 150 bp for wild-type	

Quantitative real-time PCR primers

Actb	Forward:		ACGGCCAGGTCATCACTATTG
	Reverse:		AGGAAGGCTGGAAAAGAGCC
	Hydrolysis	Probe	CAACGAGCGGTTCCGATGCCC

Atp5b	Forward:		GGCACAATGCAGGAAAGG
	Reverse:		TCAGCAGGCACATAGATAGCC
	Hydrolysis	Probe	CCAAGGGTGGGAAAATCGGACTCTTTG

Med1 (var1)	Forward:	ACGAGGGACGAGGAAGTTG
	Reverse:	TCTGGTTAAATTTTGCATGGAG
	UPL probe:	#79 (cat. no. 04689020001)

Rock2	Forward:	AGTCCCTGGGTAGTTCAGCTC
	Reverse:	GCCTGGCATGTACTCCATC
	UPL probe:	#98 (cat. no. 04692152001)

Pttg1	Forward:	GAAAAGTTCTTCCCTTTCAATCC
	Reverse:	TTCATTCAGGGTCATGAGAGG
	UPL probe:	#7 (cat. no. 04685059001)

Krt12	Forward:	GCGACGGTTTTGACGAGA
	Reverse:	TTTTTCGAGTTTTATTTGGGTCTT
	UPL probe:	#94 (cat. no. 04692110001)

Antibodies

Primary antibodies directed against

Antibody Species Company Dilution Purpose

GFAP Mouse Novocastra 1:200, IHC

CC1 (APC) Mouse Calbiochem 1:50, IHC

IBA1 Rabbit Wako 1:200, IHC

NeuN Mouse Chemicon 1:500, IHC

5.2 Methods

5.2.1 Animals

All experiments were performed in accordance with the federal law and on approval of the animal care committee of the Bezirksregierung Braunschweig, Germany. Mice were housed under a 12 h light/dark cycle (lights on at 5:00 A.M.) with food and drinking water available ad libitum.

5.2.2 Tissue preparation for time course study

EYFPnuc under *Thy-1* promoter expressing transgenic mice were generated by Moritz Rossner at the ZMBH in Heidelberg (Rossner et al., 2006); referred to as TYNC. *Cnp1* null mouse line (*Cnp1-/-*) was generated by Corinna Lappe-Siefke at the Department of Neurogenetics, Max Planck for Experimental Medicine, Goettingen (Lappe-Siefke et al., 2003). The hemizygous *Plp1*-knockout mice (*Plp1-/*Y) were generated by Matthias Klugmann at ZMBH, University of Heidelberg (Klugmann et al., 1997). TYNC mice were crossed with WT, *Cnp1* null and *Plp1* null mice to generate following genotypes:

WT (controls)	TYNC +/-, *Cnp1* +/+, *Plp1* +/y
Cnp-/-	TYNC +/-, *Cnp1* -/-, *Plp1* +/y
Plp -/y	TYNC +/-, *Cnp1* +/+, *Plp1* -/y

For this study 1, 3, 6 and 12 month old male *Cnp1-/-*, *Plp1-/*Y and age-matched control mice (n = 3/genotype) were sacrificed by cervical dislocation. To reduce biological variation, all mice were processed between 9 and 10 h after light onset. Brains were removed from the skull and bisected along the midline using a razorblade. One half was frozen on dry ice, sealed with parafilm and stored at –80°C until further use and the other half was post immersion fixed in 4% paraformaldehyd (PFA) for 48 hours and paraffin embedded (**Fig. 4**).
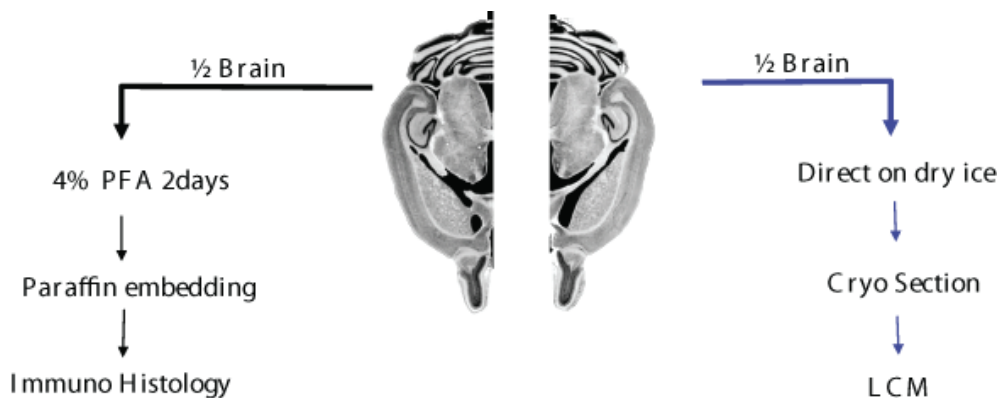
Fig. 4: Mouse brain preparation scheme
Scheme depicts procedure for tissue sampling. For immunohistochemical analysis (left panel) and for laser capture microdissection (right panel).

5.2.3 Preparation of mouse genomic DNA for genotyping

For the preparation of mouse genomic DNA for genotyping, 2-3 mm of the tail were cut and placed in microcentrifuge tubes. 180 µl of 1x MGB and 20 µl of proteinase K (10 mg/ml) were added to each tube and incubated at 55ºC overnight with vigorous shaking. Once the tails were dissolved, proteinase K was heat-inactivated by incubating the DNA lysate at 95ºC for 10 min. Then, the DNA lysate was centrifuged at 13.000g for 1 min to pellet all the undigested material and the supernatant was collected in fresh tubes. 1-2 µl of this diluted DNA preparation was used for genotyping PCR amplification.

5.2.4   Genotyping polymerase chain reaction (PCR)

PCR-Mix:

	TYNC	*Cnp1-/-*	*Plp1-/Y*
DNA	1	1	1
Fwd Primer	0,2	0,5	0,5
Rev Primer1	0,2	0,5	0,5
Rev Primer2		1	0,5
NTP	2	2	2
Buffer (5x)	4	4	4
DMSO	1	1	1
Go Taq	0,2	0,2	0,2
H$_2$O	11,4	9,8	10,3
Program	#1	#2	#1

PCR program #1:

95°C	3´	
56°C	30´´	
72°C	1´	36x
95°C	30´´	
56°C	1´	
72°C	10´	
4°C	Pause	

PCR program #2:

95°C	3´	
50°C	30´´	
72°C	90´´	36x
95°C	30´´	
50°C	1´	
72°C	10´	
4°C	Pause	

5.2.5   Preparation of CNS cryosections for LCM

Serial coronal brain sections at the level of the striatum (bregma 1 mm to 0.5 mm), were prepared using a cryostat (Leica) at −18°C and were mounted on Starfrost glass slides (Sigma Aldrich) for single cell isolation (8 µm thick sections) and for micro region isolation (20 µm thick sections) on PEN-membrane slides (Molecular Devices). Once the first section had been mounted, the slide was kept inside the cryochamber (-18°C)

35

while the next section was cut. Eight to twelve sections were mounted in this way on each slide. Cutting and mounting was performed as quickly as possible to ensure that all sections adhered properly to the membrane. Two slides were prepared at a time and processed in parallel. After sectioning, the slides were stored on dry ice until dehydration and staining.

Sections mounted on PEN slides (for micro region isolation) were stained prior to dehydration. Slides were fixed in 70% EtOH for 30 sec, rehydrated in H_2O for 10 sec stained in 2% thionin staining solution (Sigma) washed two times in fresh H_2O. For dehydration sections were subsequently fixed in 70% EtOH for 30 sec, followed by a dehydration series in 95% EtOH for 30 sec, two times 'freshly' pured 100% EtOH for one min. and two times Xylene for two min. After dehydration slides were air dried, transported and kept in a box with desiccant. Sections for single cell isolation were only subjected to dehydration procedure. We used only precooled RNAse free plasticware and solutions;

5.2.6   Laser capture microdissection

The EYFP$^+$ cells were microdissected from the motor and somatosensory cortex from 10 slides in total; we used the HS Transfer Caps (Molecular Devices) to capture between 100 and 300 neurons per cap, for a total sample size between 700 and 800 microdissected neurons. The corresponding CC-WM microregions were microdissected from 10 adjacent slides and were also pooled. For the microdissection, we used the Arcturus Veritas microdissection system with fluorescence package (Molecular Devices). The isolation of EYFP$^+$ cells was done by identifying single bright fluorescent cells in the fluorescence mode. Cells were only collected if no adjacent nuclei were detected in close proximity. Successful cutting and collection steps were subsequently validated in bright-field and fluorescent mode on the quality control slot of the device. Microdissected samples were lysed in 100 µl of RNA lysis buffer (Qiagen, Hilden, Germany) byvigorous vortexing for 30 sec and stored at -80°C until further use. All procedures were done under RNAse-free conditions.

5.2.7   Fluorescent-activated cell sorting (FACS)

To increase purity of microglia, oligodendrocytes and glial precursors cells, cells were sorted using transgenic animals that express fluorescent proteins under cell type specific promoters. More specific, heterozygous *Cx3cr1*-EGFP, *Plp*-DsRed and hGFAP-EGFP mice were used for FACS. The forebrain was isolated by removal of the olfactory lobes, cerebellum, and midbrain/hindbrain structures by crude dissection, and the tissue was diced with a curved-blade surgical scalpel. To isolate cerebral cortical gray matter cells the brain was sliced in 2-3 mm coronal sections and the cerebral cortex was carefully dissected away from the ventral white matter tracks. This tissue was enzymatically dissociated to make a suspension of single cells, essentially as described by (Giulian and Baker, 1986). Cortex samples were incubated with 2 ml HBSS (containing Mg^{2+}), 1 ml trypsin and 1 ml 0.05% DNase at 37°C for 10 min. The cell suspension was then triturated with a 10 ml pipette and incubated at 37°C for another 10 min. The same step was repeated with a 5 ml pipette and a glass Pasteur pipette. The cell suspension was then centrifuged for 10 min at 800 rpm and the cell pellet was resuspended with 3 ml Mg^{2+}-containing HBSS. After filtration through a nylon 40 µm cell filter (BD Falcon), the cell suspension was incubated with 80 µl of PI (stock 1 mg/ml, Sigma) and 4 µl Hoechst (stock 5 mg/ml, Sigma) at 37°C for 20-30 min. Propidium iodide (PI) intercalates into double-stranded nucleic acids; it is excluded by

36

viable cells but can penetrate the cell membranes of dying or dead cells. Hoechst 33342 is also a non-toxic membrane-permeable dye that intercalates in the DNA and is used to stain living cells. 5 ml of HBSS were then added and the pellet resuspended in 10 ml of glial culture medium. The cell suspension was kept on ice until it could be sorted in a BD FACSAria™ cell sorter with the right filters and based on the manufacturer's instructions (BD Biosciences).

5.2.8 RNA isolation and quantification

5.2.8.1 RNA purification (100ng–5µg)

'RNeasy mini preps' (Qiagen) were used to purify the total RNA from e.g. FACS-sorted microglia, glial precursor cells and oligodendroytes as well as for brain lysates. Total RNA was purified following the manufacturer's instructions. In brief, cells or tissue were lysed in RLT buffer and kept at -20°C until further use. The samples were thawed quickly by incubating them at 37°C in a water bath and further homogenized by vigorous vortexing for 1 min. 100% EtOH was added to provide the appropriate binding conditions, and the homogenates were applied to RNeasy mini columns where the total RNA binds to the membrane and the contaminants are efficiently washed away. The RNAs were eluted from the column with 100 µl of RNase-free ddH$_2$O.

5.2.8.2 Small scale RNA purification (500pg-100ng)

For isolation of minute amounts of total RNA (100pg - 100ng) the RNeasy micro kit (Qiagen) was used according to manufacturer's instructions. Same modifications as for standard RNA purification were applied (Section 5.2.8.1).

5.2.8.3 Precipitation of RNA

2 µl of Pelletpaint (Calbiochem) carrier were added to 100 µl of RNA. Pelletpaint builds a meshlike matrix which pulls precipitated RNA down and facilitates later visualization of pellet. After vigorous vortexing for 20 sec, 50 µl of 7.5 M NH$_4$Ac were added, vigorous vortexed for 20 sec and 360µl of 100 % EtOH was added to the RNA mixture. The RNA solution was centrifuged for 30 min at maximum speed with a table micro centrifuge at 4°C. The supernatant was discarded, the pellet was washed with 300 µl of 70% ethanol centrifuged at full speed for 10 min, supernatant discarded the pellet was left to air dry at RT. X µl of RNase-free ddH$_2$O was added to the pellet and put on ice for a further 15 min to dissolve.

5.2.8.4 Quantification of RNA

Quality and concentration of RNA were examined with the Nano labchip and the Bioanalyzer2000 (Agilent). Quantity and purity was also determined using a Picodrop Spectrophotometer (Picrodrop Limited).

5.2.9   cDNA synthesis

5.2.9.1   Standard protocol for 30 ng – 2 µg total RNA

cDNA synthesis is based on the characteristic feature of eukaryotic messenger RNAs to harbour the defined polyadenylated tail on the 3' end. First-strand cDNA was synthesized for quantitative real-time PCR (QRT-PCR). Total RNA was mixed with 2 µl of random nonamer (200 pmol/µl) and 2 µl of oligo-dT (0,5 pmol/µl) primers. The mixture was heated to 70°C for 5 min and then incubated on ice for 2 min. 4 µl of 5x First-Strand buffer, 2 µl of 0.1 M DTT and 1 µl of 10 mM dNTPs were added to the mixture and the final volume was adjusted with dH_2O to 19 µl. Finally 1 µl of SuperScript™ III RT (200 units/µl) was added to complete the synthesis reaction mixture. This mixture was incubated in the thermocycler at 25°C for 10 min, then 50°C for 30 min, 55°C for 30 min. Finally the reaction was terminated by heating to 70°C for 15 min and further incubation on ice. The cDNA was used later as a template for amplification in PCR.

5.2.9.2   Pre amplification protocol for 0,5 ng - 30 ng total RNA

For minute amounts of RNA amplfication step is mandatory prior to perform QRT-PCR. Therefore cDNA synthesis was performed with a linear PCR amplification step. We used the Pre-Amplification kit (Roche) for amplification. Amplified cDNA yield was between 1 – 3 µg for LCM samples. The protocol supplied by manufacturer was exactly followed.

5.2.10 Quantitative real-time PCR for mRNA expression

5.2.10.1 SYBR green Assays

For each SYBR green assay, 5 µl of SYBR green master mix, 1 pmol of each forward and reverse primer pair, 1 µl of dH_2O and 4 µl of cDNA mixture were mixed in a 96-well plate. Real-time PCR was carried out using SYBR Green Master Mix according to the manufacturer's instructions.

5.2.10.2 Hydrolysis Probe Assays

For hydrolysis probe assays the same protocol as for SYBR green assays was followed with the exceptions of using Taqman chemistry instead of SYBR green and addition of 1 pmol of assay specific hydrolysis probe. Probes from the Universal Probe Library (Roche), were used for most assays.

QRT-PCR was performed using either the 7500 fast real-time PCR system (Applied Biosystems) or the Light Cycler 480 (Roche). The PCR reaction was carried out for 40 cycles in the following temperature conditions: ten sec at 95ºC, 25 sec at 60ºC and 35 sec at 72ºC. The data acquisition was done at 72ºC. Relative expression analysis was calculated with ddCT method (Pfaffl, 2001) and was performed using the excel-based QRT-PCR analysis macro qBase (Hellemans et al., 2007). The results are depicted as bar graphs of normalized relative values with lowest value standardized to 1. Error bars represent standard deviation (SD).

5.2.11 Amplification for microarray hybridization

3' Expression arrays

Total RNA of pooled single cells or micro-regions was resuspended with pretested T7-tagged dT21V oligonucleotides. Two-round T7-RNA polymerase-mediated linear amplification was performed according to optimized protocols for low-input RNA amounts (see Small Sample Target Labeling Assay Version II; Affymetrix). Biotin-labeled second-round aRNA was generated with a NTP-mix containing Biotin-11-CTP and Biotin-16-UTP (PerkinElmer, Boston, MA) (2 mM f.c.). Biotin-labeled amplified RNA (aRNA) size distribution and quantity was analyzed with the Agilent 2100 Bioanalyser using the RNA 6000 Nano LabChip kit (Agilent Technologies, Boeblingen, Germany). Samples with lower size compressed RNA products were discarded.

Whole transcript (WT) Exon / Gene microarrays

Total RNA (0.5 ng – 10 ng) was amplified using the WT-Ovation Pico RNA Amplification System V1 (Catalog # 3300–12; NuGen) and labeling with FL-Ovation cDNA Biotin Module V2 (Catalog #4200–12; NuGen) according to the protocol provided by the supplier.

5.2.12 Microarray hybridization.

3' Expression arrays

At least 5 µg of labeled cRNA was fragmented by heating the sample to 95°C for 35 min in a volume of 20 µl containing 40 mM Tris acetate, pH 8.1, 100 mM KOAc, and 30 mM MgOAc. Fragmentation was checked by alkaline agarose electrophoresis. Hybridization, washing, staining, and scanning were performed under standard conditions as described by the manufacturer. Mouse430A 2.0 genechips were used that contain over 22,600 probe sets representing transcripts and variants from over 14,000 well-characterized mouse genes.

Whole transcript (WT) Exon / Gene microarrays

At least 10 µg of labeled cDNA was hybridized to WT microarrays. Design of WT microarrays are listed in Table 1. Hybridization, washing, staining, and scanning were performed under standard conditions as described by the manufacturer.

Table 1: Summary of WT microarray design

	HuGene 1.0ST	MoGene 1.0ST	MoExon 1.0ST
Number of Probes	764'885	770'317	1.4 million (core)
	-	-	2 million (extended)
	-	-	2,1 million (full)
Number of Probe sets	28'869	33'252	54'675
Number of Probe sets	27'901	27'547	28'206
Number of Probe sets	206'728	208'644	219'230

5.2.13 Microarray data analysis

5.2.13.1 Analysis for 3' expression microarrays

Microarray raw data (.cel files) were exported using Gene chip operating software (gcos) (Affymetrix). Normalization and higher-level analysis were done in R environment employing affy, simpleaffy, limma and several other packages downloaded from Bioconductor (detailed list see section 5.1.1.2). Data normalization, filtering and determination of significance cut-offs were performed following rigorous standards, optimized to achieve a minimum of false positive discoveries. Briefly, normalization was carried out using the Robust Multichip Average (RMA) model implemented in the R package *Affy*, using default settings. The normalized microarray data was quality controlled (box-plot analysis, principal component analysis, and Spearman correlation tree) which led to the exclusion of two microarrays. The remaining data were re-normalized, log transformed and filtered based on

1) Absolute expression values, meaning probe sets were rejected where absolute signal intensity were below 100

2) Fold change (FC); probesets with a FC higher than 1.5 were included in further analysis for single gene analysis. A FC threshold of 1.3 was applied for further pathway level analysis using gene set enrichment analysis (GSEA; www.broadinstitute.org/gsea/).

K-mean Clustering

For K-means clustering we identified significant genes by 2-way ANOVA (phenotype over time, P-val < 0.001, average expression > 2 * SD). Expression values of filtered genes were transformed in order to evaluate the overall expression profiles regardless of fold change and absolute expression. We defined the arithmetic mean of each gene over all samples as 0 and the SD was set to 1. K-means clustering was performed to obtain 9 clusters using default settings in R ('stats' package).

Network integration and visualization

We used the Gene Ontology (GO) (http://www.geneontology.org/) and Kyoto Encyclopedia of Genes and Genomes KEGG databases (http://www.genome.jp/kegg/pathway.html) to functionally annotate the gene cluster that were obtained by K-means clustering. We used the Visual Analysis Tool for Biological Networks and Pathways (VISant, version 3.68) http://visant.bu.edu/) to integrate and visualize selected gene set clusters of CPNs from *Cnp1* null mice. We used the VISant-database predictome of protein linked interactions to connect nodes based on published interactions (referred to as 'edges' and drawn as straight and undirected lines between respective nodes). We used the information available for the human protein collection (containing > 90.000 entries compared to the mouse collection with only roughly 6,000 entries) that has been extracted from several large-scale experimental and literature extracted databases (see http://visant.bu.edu/ for interaction statistics and methods selected).

5.2.13.2 Analysis for whole transcript (WT) microarrays

All array data obtained from WT platforms were analyzed with Partek Genomic Suite v6.4 (www.partek.com). Data was pre-processed, which included probe level RMA background correction, quantile normalization across all arrays, and Log_2 transformation followed by median polish to summarize probes to obtain the overall score for each probe set. The data were filtered based on the expression values of each probe set within the replicate set for each sample; if the expression value of a probe set was below 3.5 (log_2 value) in all samples, the probe set was removed from the analysis. In order to identify probe sets that were significantly different between samples A and B, a one-way anova statistical test was performed on normalized and filtered probe set level intensities between each group to generate p-value and fold change values. Exon level analysis was performed with the 'exonmap' package in R using default settings.

5.2.14 Protein biochemical methods

5.2.14.1 Lysis of brains

Wild-type and mutant mice were sacrificed by spinal cord dislocation and decapitated. The brains were removed and immediately put on a precooled brainslicer. Brains were coronally cut in 500μm sections. Sections from Bregma -1 mm to +1 mm were washed with PBS and further macrodissected with precooled spates. Somatosensory- and motor cortex (Cx), white matter tracts (WM) and hippocampus were isolated, frozen on dry ice and stored at -80°C. Micro-regions were thawed in 1ml PBS and homogenized using an Ultraturrax (T8) on highest settings (20-30s). 600 μl brain lysate were removed and combined with 1 ml RLT buffer for further RNA isolation. For protein isolation 600 μl of 2x Ripabuffer was added to the remaining brain lysate and further subjected to the tissue homogenizer for two times 20 sec on ice. Protein samples were incubated for 20-30 min on ice, the insoluble cellular debris were pelleted by centrifugation at 2000 rpm at 4°C for 10 min and the supernatant was used for further analysis or stored at -70°C.

5.2.14.2 Quantification of protein concentration by Lowry assay

The protein concentrations were determined using the Bio-Rad DC Protein Assay kit according to the manufacturer's 'microplate assay' protocol. The working principle of the kit is similar to the Lowry assay (LOWRY et al., 1951). The absorbance was measured at 650 nm in a Mithras (Berthold) multiplate reader. The assay is based on the reaction of proteins with an alkaline copper tertrate solution and folin reagent, which leads to the loss of 1, 2, or 3 oxygen atoms, producing one or several reduced species that have a characteristic blue colour with maximum absorbance at 750 nm. The colour development is primarily due to the amino acids tyrosine and tryptophan, and, to a lesser extent, cystine, cysteine and histidine (LOWRY et al., 1951).

5.2.14.3 SDS polyacrylamide gel electrophoresis

The proteins were separated using the discontinuous SDS polyacrylamide gel electrophoresis (SDS-PAGE) described by Laemmli (Laemmli, 1970). The glass plates and the 1 mm spacers were assembled according to the Bio-Rad instructions. We used commercial twelve % separating gel solution of acrylamide. The chamber and the gels were assembled based on the manufacturer's protocol. The protein lysates were diluted in 6x SDS sample buffer containing one % β-mercaptoethanol and heated for five min to 90°C. five µl of pre-stained Precision-plus (BioRad) was loaded on a well as a molecular weight standard. The gels were run at 10 mA/gel of constant current. After the bromophenol blue tracking dye entered the separating gel, the power was increased to 15 mA / gel. The electrophoresis was terminated once the bromophenol blue had reached the lower end of the gel. The gel was removed and preceded for Coomassie staining or protein blotting.

5.2.14.4 Coomassie staining

The gels were fixed for 15 min in 25 % isopropanol / 10 % acetic acid and then briefly washed with dH_2O. After incubation in the coomassie blue staining buffer overnight, the gels were incubated with the destaining solution and scanned with an UMAX Astra47000 scanner.

5.2.14.5 Western blotting (WB)

Electrophoretic transfer

Proteins were transferred from the SDS-gel onto a PVDF membrane (Amersham/Millipore, pore size 0.45 µm) by electrophoresis, as originally described with modification (Towbin et al., 1979). PVDF membranes were activated for 30 sec in 100 % methanol and further incubated in transfer buffer for 15 min. The gels, the Whatmannpaper and the blotting pads were pre-soaked in transfer buffer for 15-30 min and further assembled according to the manufacturer's protocol. Proteins were transferred at a constant voltage of 38 V and a maximum current of 275 mA for a 1.5 mm gel and for 1.5-2 hrs at room temperature.

Immunological detection of proteins on PVDF membranes

After electrophoretic transfer, the membranes were blocked for 1 hr at room temperature in blocking buffer (five % non-fat dry milk in TBS). The primary antibody diluted in blocking buffer was applied overnight at 4°C with constant gentle shaking.

After three times ten min. washes in TBST (0.05 % Tween-20 in TBS), HRP-conjugated secondary antibodies were applied for at least 1 hr in blocking buffer, followed by three times ten min. washes with TBST. The membranes were washed once with TBS before being exposed using the Enhanced Chemiluminescence Detection kit (PerkinElmer) according to the manufacturer's instructions (Western Lightning™, Western Blot Chemiluminescence Reagent Plus, PerkinElmer Life Sciences, Inc.). ECL photographic film (Hyperfilm™, Amersham Biosciences) was used to expose the membranes. The time of exposure varied depending on the signal intensity. To reprobe the same membrane with a second antibody, the membrane was incubated with stripping buffer for 1 hr at 60°C with rigorous shaking. After one wash with TBST, the membrane was incubated in blocking buffer for 30 min before probing with the second primary antibody.

5.2.15 Histology and immunohistochemistry

5.2.15.1 Perfusion and fixation of mouse tissue

The mice were deeply anaesthetized by injecting 2.5 % avertin (0.017 ml per g of mouse body weight) intraperitoneally. After anaesthesia, the mice were washed with 70 % ethanol in the stomach and the skin was removed from the ventral side. A transversal cut was made just below the diaphragm and the abdomen were slowly opened until the heart was visible. A new needle (27 gage) was inserted into the left ventricle and, immediately after starting the perfusion, a small incision was made in the right auricle to allow the blood to flow out of the body. Perfusion was carried out with HBSS and changed from HBBS to fixative (4 % PFA in PB for paraffin embedded tissue. The perfusion was carried out with 30-50 ml of fixation solution. The brain and the spinal cord were removed carefully and collected into vials with cold perfusion buffer. The tissue samples were stored in 4 % PFA overnight at 4°C and then in 1 % PFA until further use.

5.2.15.2 Paraplast impregnation and embedding of the tissue

After post-fixation, the tissue was washed 3-4 times with PBS. The brains were cut into halfes and were transferred into plastic chambers for dehydration and paraplast impregnation. The following steps were carried out before tissue embedding: 50 % ethanol for 1 hr, twice in 70 % ethanol for 2 hrs, twice in 96 % ethanol for 1 hr and twice in 100 % ethanol for 1 hr each. Then, the 100 % ethanol was replaced by isopropanol for 1 hr, twice in xylene for 2 hrs and the tissues were impregnated with paraplast at 60ºC for 2 hrs. Finally, the tissue was embedded in molten paraplast and left to harden.

5.2.15.3 Haematoxylin-Eosin (HE) staining

5-7 µm thick sections were cut from the paraffinized block using a microtome. The sections were floated on a warm water bath (42°C), placed on positively charged glass slides and then dried overnight at 37°C. The sections were then incubated at 60°C for 10 min before being deparaffinized and rehydrated in the following steps: twice in xylol and once in xylol/isopropanol (1:1) for 10 min, 100 %- 90 %- 70 %- 50 % alcohol for 5 min and finally dH$_2$O. The sections were incubated with 0.1 % haematoxylin for 5 min staining the basic cell nuclear compartment blue. Following a wash with dH$_2$O, the sections were dipped in HCl-alcohol solution once for 5-10 sec and then in Scott's

solution for 5 min. They were briefly rinsed with dH_2O, counterstained with 0.1 % eosin for 3-5 min and then rinsed with dH2O. Sections were dehydrated by incubating them in an increasing alcohol concentration (50 %, 70 %, 90 %, and 100 %) for 2 min, then in xylol/isopropanol (1:1) and twice in xylol for 5 min. Finally, they were mounted with 'Eukitt' (Kindler GmbH).

5.2.15.4 DAB-based immunodetection on paraffin sections

The sections were processed as described in section 5.2.15.1 until rehydration. The sections were then incubated for 5 min in citrate buffer before being 'cooked' for 10 min in boiling citrate buffer (at 650 watts in microwave oven). After this, the sections were left in the citrate buffer for about 20 min to cool down and subsequently rinsed in Tris buffer/ 2 % milk for 5 min. Endogenous peroxidases were inactivated by incubating the sections with 100 µl of 3 % hydrogen peroxide for 5 min. Next, the sections were incubated with 100 µl of goat-serum diluted in PBS/BSA (1:5) for 20 min at room temperature before proceeding with the 100 µl of the primary antibody diluted in PBS/BSA. After an overnight incubation at 4°C, the sections were washed with Tris buffer/ 2 % milk and incubated with 100 µl of bridging antibody, i.e. biotinylated secondary antibody (Dako) for 10 min. They were then rinsed with Tris buffer/ 2 % milk and probed with 100 µl of tertiary complex, i.e. Horseradish Peroxidase streptavidin complex (Dako), by incubating the sections for 10 min. They were then rinsed with the Tris buffer and incubated with 100 µl of DAB for 10 min. Finally, the sections were rinsed twice with dH_2O for 5 min each and counterstained for 30 sec with haematoxylin following the steps until mounting (section 5.2.15.3). The enzymatic reaction between the HRP and DAB yielded a very a stable brown precipitate that was visualized under the microscope (section 5.2.15.5)

5.2.15.5 Light and Fluorescent Microscopy

The light and fluorescent microscopic observation was performed with an oil immersion 100x, 63x and 40x lenses and air 20x lenses (Leica, DMRXA) in the different experiments and the microscope was equipped with a ProgResC14 camera system (Jenoptic, Jena, Germany). The images were digitalized, analyzed and processed using Image J software (http://rsbweb.nih.gov/ij) and Photoshop creative suite 3 (Adope).

5.2.15.6 Image analysis and counting software

Aquisition of immunostainings were digitalized using a 20x Nikon objective integrated in the Veritas microdissection instrument. Veritas operating software automatically composes overview images of the region of interest resulting in high resolution image composites, which we used for cell quantification. For DAB and thionin stained sections we used bright field for image acquisition and in the case of EYFPnuc positive cell counting we took advantage of the fluorescence mode using the EGFP filter set of Veritas (exitation 503–548 nm, emission 565–585 nm). Composite images were processed using a in-house programmed macro in ImageJ, which is a open source image processing and analysis tool programmed in Java (http://rsweb.nih.gov/ij/).

45

6   Results

6.1 Exon-level expression profiling of different glial populations

6.1.1 Purification of different glial cell types in the central nervous system

6.1.1.1 FACS sorting of hGFAP-EGFP$^+$ glial precursor cells

To purify glial precursor cells (GPCs), we took advantage of a transgenic line of mice that expresses EGFP driven by the human glial fibrillary acidic protein (hGFAP) promoter (Nolte et al., 2001), a well-established glial cell marker. We employed FACS to enrich the EGFP$^+$ cells to 99% purity. We purified cortical hGFAP-EGFP$^+$ cells at P6 where hGFAP-driven EGFP expression labels two populations of astrolgia (i) protoplasmic mature astrocytes and (ii) glial precursor cells (GPCs). Therefore a heterogeneous cell population is labeled with EGFP at P6, comprising differentiating glial progenitor cells in distinct stages including mature astrocytes, as shown in Fig. 5 A, A'.

6.1.1.2 FACS sorting of *Cx3cr1*-EGFP$^+$ microglia

MG were purified through the use of a knock-in mouse line where EGFP was placed via homologous recombination in the Cx3cr1 locus (Jung et al., 2000). Thus EGFP expression is under transcriptional control of the endogenous Cx3cr1 promoter a well-established microglia cell marker (Fig. 5 B, B'). We FACS-purified the EGFP+ MG at P10 from cortex to yield >99% pure MG. The high purity of MG was confirmed by examining the expression levels of genes, which are exclusively expressed in MG samples. Our results confirmed the presence of well-established MG markers, which are shown in Fig. 7 C.

6.1.1.3 FACS sorting of *Plp1*-EGFP$^+$ oligodendrocytes

To purify oligodendrocytes (OLs) we took advantage of a transgenic mouse line that expresses DsRed under control of the *Plp1* promoter, which labels oligodendrocytes (P.G. Hirrlinger et al., 2005) (Fig. 5 C, C'). We subjected cortical cells of these mice at P16 to FACS to yield >99% pure OLs. The high

purity of OL was confirmed by examining the expression levels of genes, which are exclusively expressed in OL and also include published OL markers Fig. 7 C.
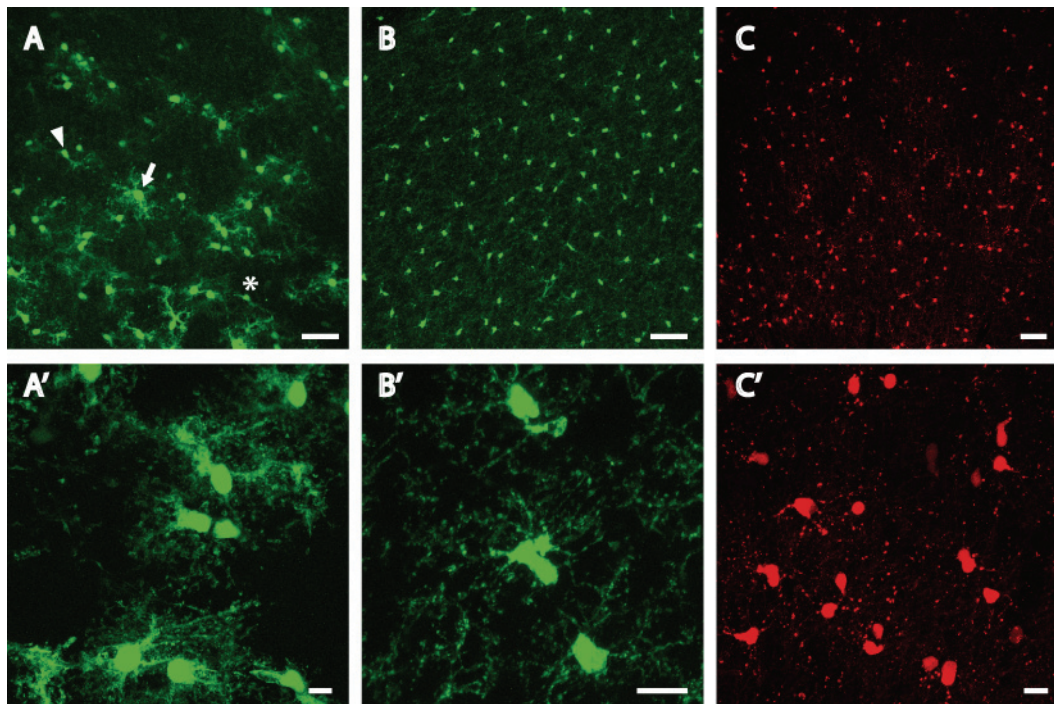
Fig. 5: Transgenic mouse tools for cell type identification and purification via FACS
Cell type-specific expression of fluorescent proteins in the brain of transgenic mice. (A) hGFAP-driven expression of EGFP highlights glial precursor cells (GPC) at P6 in cortex. The labeled cell population is highly heterogeneous including early (asterisk) and late (arrowhead) precursor cells as well as mature protoplasmic astrocytes (arrow; scale bar = 50μm). (A') Typical arborization of mature astrocytes (scale bar = 10μm). (B) The Cx3cr1 promoter induces strong expression of EGFP in the major MG cell population in cortex at P10 (scale bar = 50μm). (B') Typical non-activated MG (scale bar = 10μm). (C) DsRed expression, driven by the *Plp1* promoter stains somata of OLs (P16; scale bar = 50μm). (C') Punctate staining in oligodendroglia processes due to clustering effects of DsRed in compacted myelin (scale bar = 10μm).

6.1.2 Microarray quality controls

Total RNA prepared from purified cell types was used to generate labeled cDNA with a one-step linear random-primed amplification protocol to amplify all RNAs. This labeled cDNA was hybridized to Affymetrix Mouse Exon 1.0 ST Arrays. We performed data analyses using the exonmap package (Okoniewski et al., 2007) and Partek Genomic Suite. Fig. 6 depicts a summary of quality controls (QC) of the microarray performance. To exclude an overall shift in signal intensities, we checked signal distribution by using a histogram as well as box plots serving as indicators for general shifts in hybridization performance (Fig. 6 A, B).

Unsupervised hierarchical clustering using all data points revealed small, but evident differences between GPCs and oligodendrocytes as well as higher differences of OL and GPCs to MG (Fig. 2 C). These finding were further supported by principal component analysis (PCA) which illustrates the principal components of all 7 samples from the surveyed cell types. PCA showed that replicate samples group together and different cell types are clearly separated from each other, with a distinct separation of MG samples from OL and GPCs (Fig. 6 D).
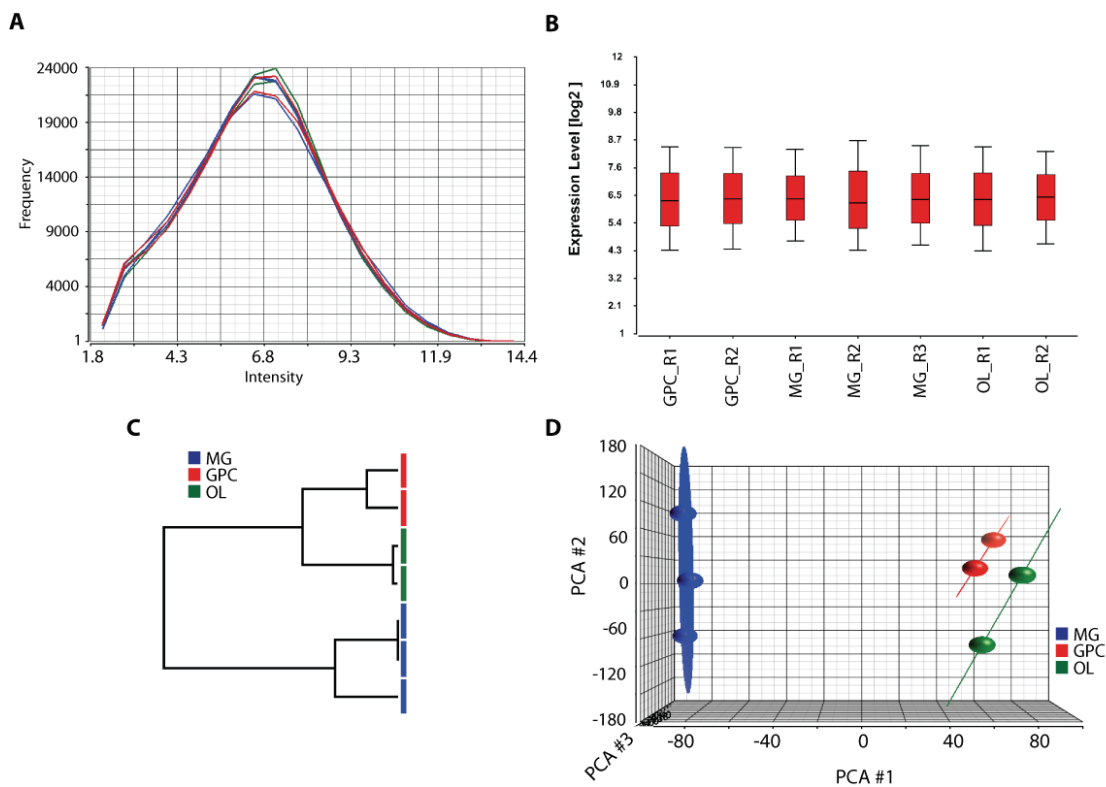
Fig. 6: Quality control parameters of microarray data from purified glial cell types
(A) Signal distribution of raw microarray data before normalization, depicted as histogram (signal intensity on the x-axis, frequency on the y-axis). (B) Box plots of normalized data from all microarrays (normalized by Robust Multichip Average (RMA) method) show a homogenous intensity distribution. (C) Hierarchical clustering of microarray data derived from highly purified CNS cell types revealed three distinct clusters representing GPCs, MG, and OLs. The similarity of gene expression between different samples is represented by horizontal distances on each branch of the dendrogram. Biological replicates show the highest degree of correlation, represented by short horizontal distances. (D) Principal component analysis (PCA) revealed high correlation of biological replicates and a closer relation of OL to GPCs.

Considering the highly specialized functions of MG and OLs, the differences in their gene expression profiles were anticipated underscoring the different

developmental origin of each cell type. However, it is not known how expression profiles of GPCs relate to expression profiles of mature OLs or MG.

6.1.3 Cell type specific expressed genes

To assess cellular identity of sorted cell types, we identified genes which were exclusively expressed in each cell type. We thus applied stringent filter criteria to our microarray data and identified genes expressed in a cell type-specific fashion as illustrated in Fig. 7 A. Examination of top ranking genes exclusively expressed in hGFAP-EGFP$^+$ cells showed an enrichment of genes previously shown to be expressed in glial precursor cells such as radial-glia, Ng2$^+$, oligodendrocyte progenitor cells (OPCs) and astrocytes (AG). GPC marker genes included Tenascin-C (*Tnc*) (S. Bartsch et al., 1992; Yuasa, 2001) and platelet derived growth factor receptor, alpha polypeptide (Pdgfra) (Fig. 7 B). Genes exclusively expressed in *Cx3cr1*-EGFP$^+$ cells showed high enrichment in known markers for MG shown in Fig. 7 such as chemokine (C-C motif) ligand 3 (*Ccl3*), complement component 3a receptor 1 (*C3ar1*) (C.B. Martin et al., 2007), prostaglandin D2 synthase 2, hematopoietic (*Ptgds2*) (Mohri et al., 2007), colony stimulating factor 1 receptor (*Csf1r*) (Pollard, 1997). Top ranked genes for *Plp1*-DsRed$^+$ cells included various marker genes specific for oligodendrocytes: myelin-associated oligodendrocyte basic protein (*Mobp*), myelin oligodendrocyte glycoprotein (*Mog*) (Y. Yamamoto et al., 1994), myelin and lymphocyte protein (*Mal*) and extracellular lysophospholipase D (*Enpp2*) (Cahoy et al., 2008) illustrated in Fig. 7 D. Our unsupervised expression analysis thus was able to detect known and well-described marker genes for each examined cell type. Furthermore, could we detect several genes, which were not previously published as exclusively expressed in the cell types under investigation.
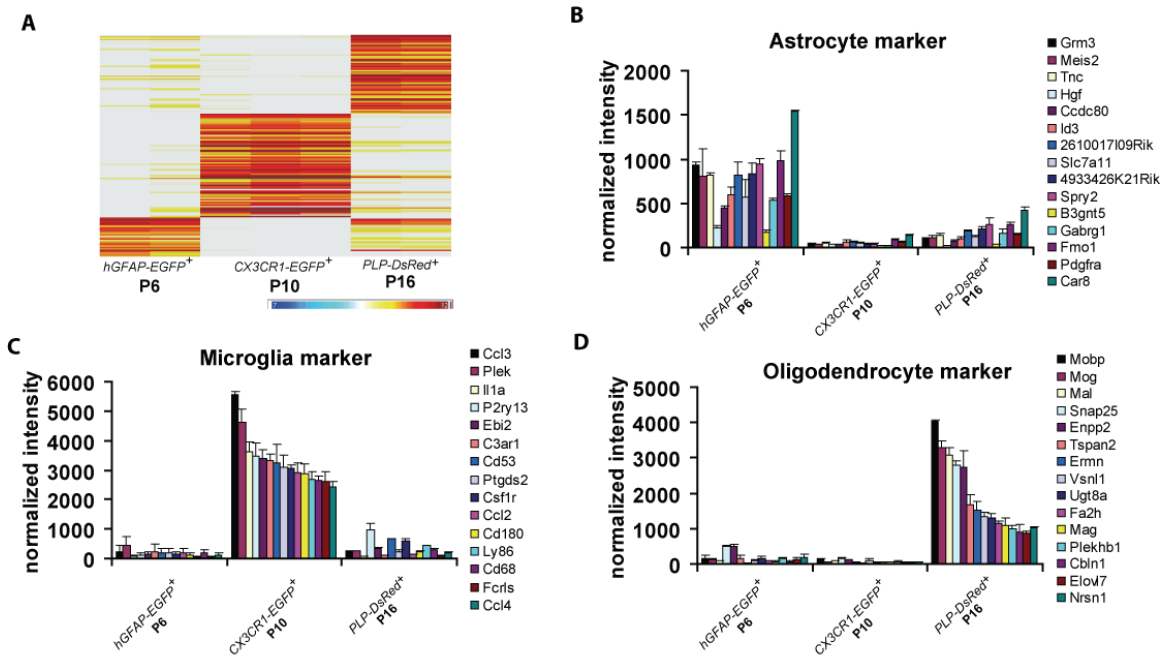
Fig. 7: Genes strongly enriched in isolated cell types.
(A) Heatmap of 158 genes which showed highly significant exclusive expression in the cell types indicated. Selection criteria for hGFAP-EGFP+ cells: one-way ANOVA FDR < 0,01 and fold change > 7, resulting in 30 genes; for Cx3cr1-EGFP+ cells: one-way ANOVA FDR < 0,0001 and fold change > 10, resulting in 88 genes; and for Plp1-DsRed+ cells: one-way ANOVA FDR < 0,01 and fold change > 8, resulting in 40 genes. Expression levels of top ranking genes, which showed high enrichment in hGFAP-EGFP+ cells (B), in Cx3cr1-EGFP+ cells (C), and in Plp-DsRed+ cells (D). The y-axis represents normalized intensities determined by RMA normalization. Error bars represent standard deviation (SD).

6.1.4 Classification of FACS-purified cell populations based on marker gene expression

To further classify the identity of cells, which were positive for EGFP under transcriptional control of the hGFAP promoter at P6, we looked for mRNA expression levels of published cell type-specific marker genes. Known marker genes for GPCs such as *Pdgfra* , *Gfap*, and epidermal growth factor receptor (*Egfr*), revealed robust expression in GPCs (Fig. 4 A). Interestingly, we found markers such as chondroitin sulfate proteoglycan 4 (*Cspg4*/*Ng2*) and SRY-box containing gene 10 (*Sox10*) as being expressed at very low levels in GPCs. Astroglial and glial precursor markers were not detected in MG samples, whereas OL data revealed low expression of all markers (Fig. 8 A). Transcript data for selected glutamate transporters *Glast* and *Glt-1* show significant expression in GPCs and OLs, but not in MG, similar to the AMPA receptor

subunit *Gria2* (Fig. 8 B). We detected a very low expression of glutamate receptor, ionotropic, NMDA1 (*Grin1*) exclusively in OL. Unexpectedly, we identified several neuronal markers expressed in GPCs and OL, including neural cell adhesion molecule 1 (*Ncam1*), doublecortin (*Dcx*), and neurofilament, medium polypeptide (*Nefm*) (Fig. 8 C). Expression of additional neuronal marker genes such as cholinergic receptor, nicotinic, alpha polypeptide 3 (*Chrna3*), enolase 2 (*Eno2*), neural PAS domain protein 1 (*Npas1*), and cholinergic receptor, nicotinic, alpha polypeptide 5 (*Chrna5*) (Cahoy et al., 2008), was virtually absent in all samples.
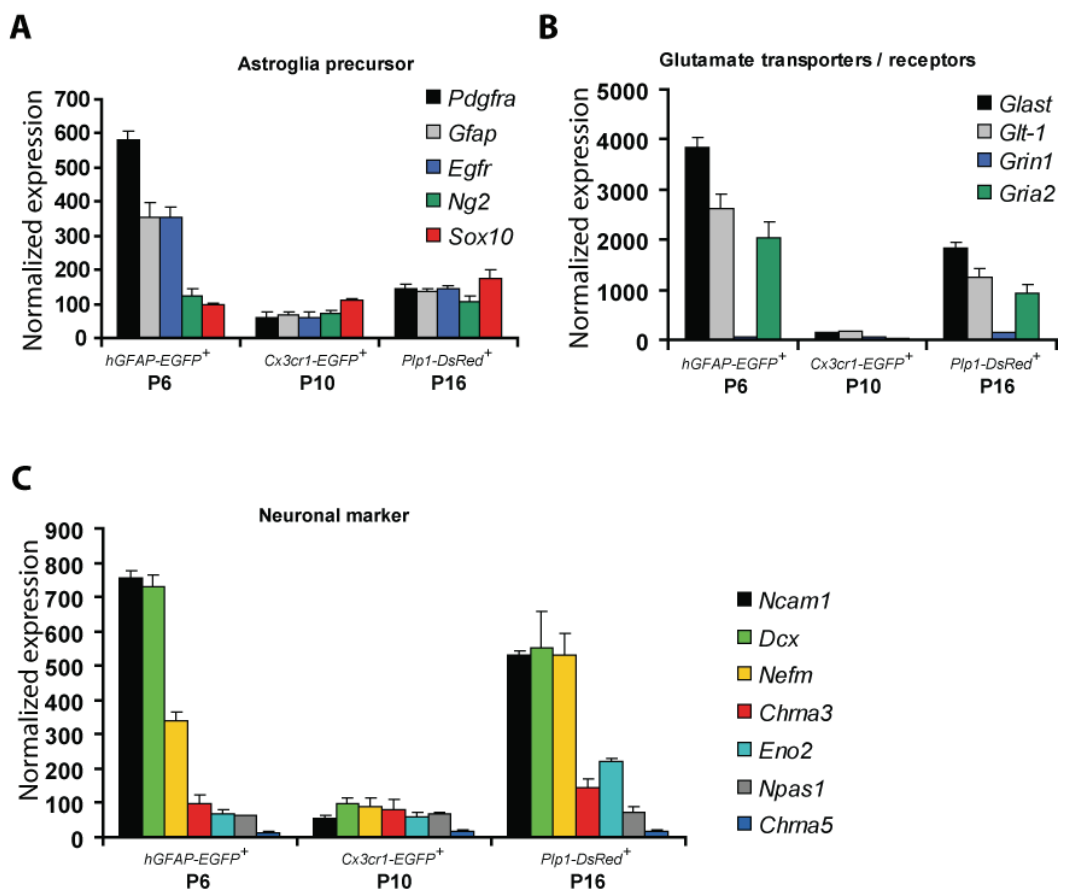
Fig. 8: Classification of FACS-purified cell populations based on marker gene expression.
Expression levels of marker genes in FACS-purified cell populations for (A) glial precursors, (B) Glutamate transporters/receptors, and (C) neurons . The y-axis represents the level of normalized gene expression. Error bars represent SD; n = 2 (GPC, OL) and n = 3 (MG).

6.1.5 Cell type-specific alternative splicing events

To estimate the degree of alternative splicing events that occur in GPCs, OLs and MG, the data was subjected to exon level analysis. A one-way ANOVA test was applied to identify cell type-specific alternative splicing events. The exon level analysis was performed using the exonmap package in R (Okoniewski et al., 2007). Out of > 28,000 genes we identified 2478 transcripts supported by microarray data as being alternatively spliced between different cell types, with significant p-values in the one-way ANOVA test (p-val < 0.0001). In Table 2 are the top ranking 50 genes listed (genes ranked according to their ANOVA p-value).

Table 2: Putative cell type specific alternative spliced genes

Symbol	Description	Symbol	Description
Ryr2	ryanodine receptor 2, cardiac	Inpp5d	inositol polyphosphate-5-phosphatase D
Stab1	stabilin 1	Atp13a4	ATPase type 13A4
Lrp1b	low density lipoprotein-related protein 1B	Arhgap9	Rho GTPase activating protein 9
Bcan	brevican	Npr2	natriuretic peptide receptor 2
Cspg5	chondroitin sulfate proteoglycan 5	Ntrk3	neurotrophic tyrosine kinase, receptor, type 3
Grin2c	glutamate receptor, ionotropic, NMDA2C (epsilon 3)	Syne1	synaptic nuclear envelope 1
Acsl6	acyl-CoA synthetase long-chain family member 6	Nwd1	NACHT and WD repeat domain containing 1
Plcb4	phospholipase C, beta 4	Myo1f	myosin IF
Fusip1	FUS interacting protein (serine-arginine rich) 1	Fgfr3	fibroblast growth factor receptor 3
Itgam	integrin alpha M	Synj2	synaptojanin 2
Pfkm	phosphofructokinase-1	Ttll11	tubulin tyrosine ligase-like 1
Dtna	dystrobrevin alpha	Col2a1	collagen, type II, alpha 1
Fgfr2	fibroblast growth factor receptor 2	Vegfa	vascular endothelial growth factor A
Dmd	dystrophin, muscular dystrophy	Gsn	gelsolin
Jarid1d	jumonji, AT rich interactive domain 1D (Rbp2 like)	Pde3b	phosphodiesterase 3B, cGMP-inhibited
Ptpro	protein tyrosine phosphatase, receptor type, O	Atp2b3	ATPase, Ca++ transporting, plasma membrane 3
Dock3	dedicator of cyto-kinesis 3	Ptprc	protein tyrosine phosphatase, receptor type, C
Myo10	Myosin 10	Plat	plasminogen activator, tissue
Mlxipl	MLX interacting protein-like	Bai1	brain-specific angiogenesis inhibitor 1
Sytl2	synaptotagmin-like 2	Atp1a2	ATPase, Na+/K+ transporting, alpha 2 polypeptide
Dnm1	dynamin 1	Acsbg1	acyl-CoA synthetase bubblegum family member 1
Sgk1	serum glucocorticoid regulated kinase 1	Polr3h	polymerase (RNA) III (DNA directed) polypeptide H
Ltbp1	latent transforming growth factor binding protein 1	Tmem87a	transmembrane protein 87A
Egr1	early growth response 1	Dgkb	diacylglycerol kinase, beta
Mlc1	megalencephalic leukoencephalopathy	Abca9	ATP-binding cassette, sub-family A (ABC1), 9
Ptprt	protein tyrosine phosphatase, receptor type, T	Myo7a	myosin VIIa
Ngef	neuronal guanine nucleotide exchange factor	Pcdha4	protocadherin alpha 4

Five examples for genes that show significant evidence for alternative splicing were chosen for detailed illustration in Fig. 9 and Fig. 10. Exon level expression profiles of plasminogen activator, tissue (*Plat*), which is a serine protease involved in extracellular metabolism (Endo et al., 1999), as one of the

candidates is depicted in Fig. 9 A. Profiles show high expression of *Plat* in OLs and GPCs in most of the probesets except for a region spanning four exons where we observed a much lower expression (indicated by a black circle). Fig. 9 B depicts the expression profile of phosphofructokinase-1 (*Pfkm*), one of the key enzymes that catalyze glycolysis. Transcripts of *Pfkm* exhibit cell type specific isoforms, which are not annotated in Ensembl (Fig. 9 B). Another interesting candidate is Myosin 10 (*Myo10*), of which 4 isoforms are annotated in Ensembl. In the CNS, both full-length *Myo10* and a shorter form of *Myo10* that lacks a myosin head domain, are expressed. The 'headless' *Myo10* variant is unable to function as a molecular motor, but is otherwise identical to the full-length transcript. All isoforms are expressed in neurons, such as Purkinje cells, as well as non-neuronal cells, such as astrocytes and ependymal cells (Sousa et al., 2006). Expression profiles indicate a higher expression level of the short isoforms in GPCs (Fig. 9 C). Expression profiles for full-length *Myo10* revealed several exons, which are potentially alternatively spliced between different cell types.
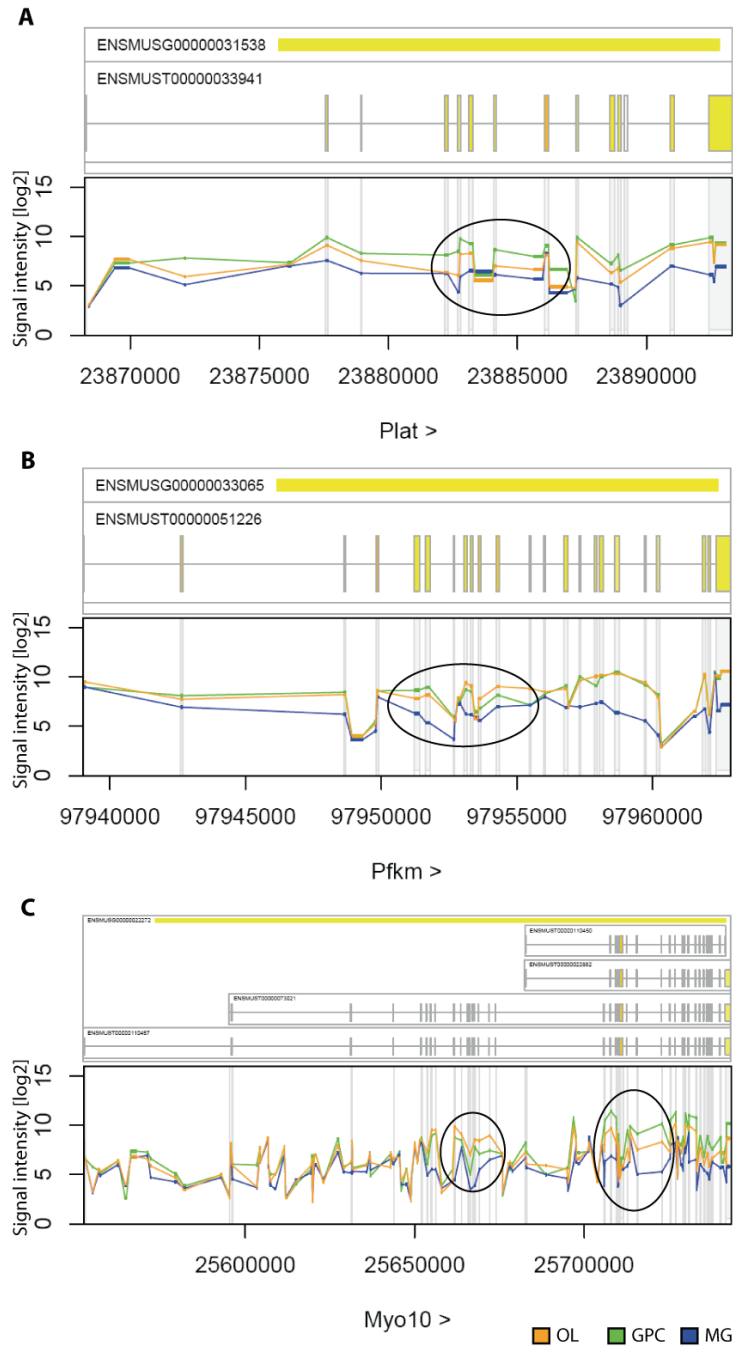
Fig. 9: Cell type-specific alternative splicing events.
Expression levels in each of the exon probesets across the entire length of transcripts from different cell types under investigation are shown. Blue profiles represent the mean signal intensity in the three replicates of microglia (MG) samples, green profiles plot the mean signal intensity in the two arrays derived from glial precursors cells (GPC), and the orange graphs depict the mean signal intensity in the two arrays probed with oligodendroglial (OL) samples. Ensembl-annotated splice variants of each gene are illustrated in the upper panels. Exonic regions are illustrated as grey bars in the lower panels. Black circles indicate hot spots for putative alternative splicing events. '>' or '<' (next to gene name) indicates direction of transcription. (A) Plasminogen activator, tissue (*Plat*) is potentially alternatively spliced in GPC and OL and not expressed in MG. (B) Phosphofructokinase-1 (*Pfkm*) expression profiles show high levels for OL and GPC, which deviate in exons located in the middle of the gene. (C) Expression profiles of

54

Myosin 10 (*Myo10*), for which 4 transcripts are annotated in Ensembl, show specific expression of short variants in GPC. Additional splice variants are detected in exons coding for the full-length version (right circle).

Expression profiles of tubulin tyrosine ligase-like 1 (*Ttll1*), which catalyzes the addition of tyrosine to the C-terminal glutamate of α-tubulin, exhibit high correlation between GPC and OL, in contrast to MG (Fig. 10 A). Some exons in the MG samples show very low expression in comparison to OL and GPC samples. As an example for potential exon skipping, we found polymerase (RNA) III (DNA directed) polypeptide H (*Polr3h*) shown in Fig. 10 B. Exon three shows high expression only in GPC samples, whereas its expression dropped to background levels in MG and OL.
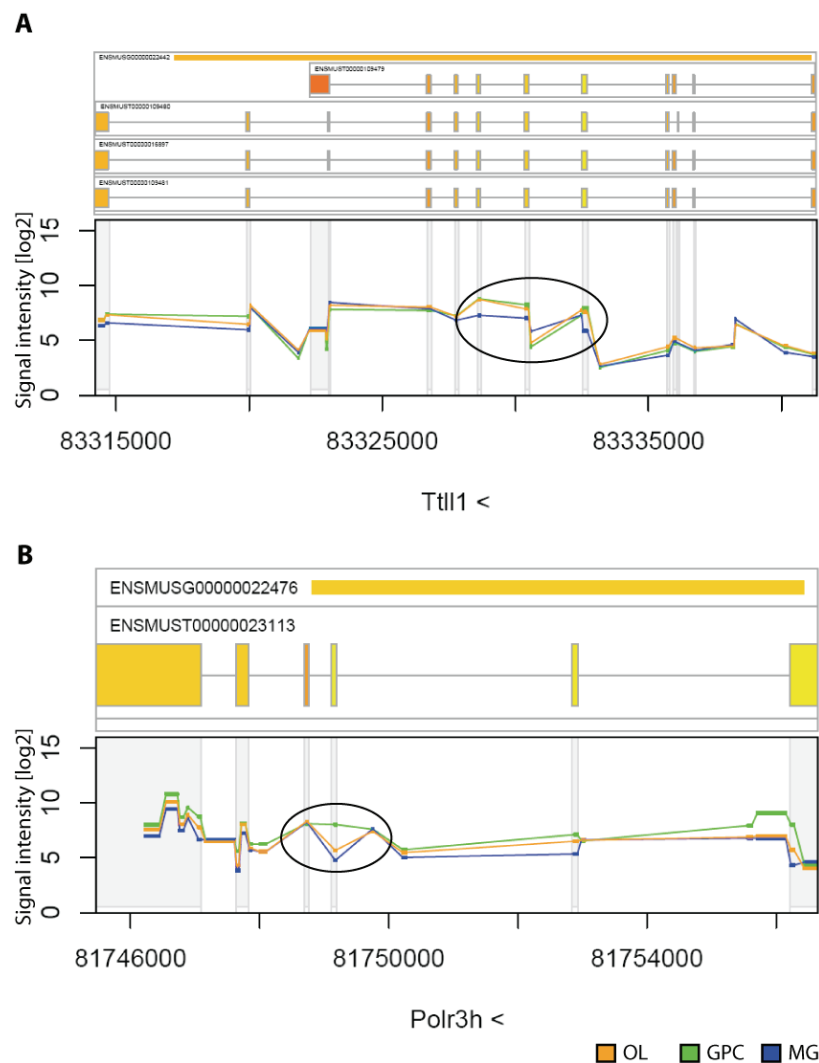
Fig. 10: Putative cell type-specific exon skipping events
Expression levels in each of the exon probesets across the entire length of transcripts from different cell types under investigation are shown. Blue profiles represent the mean

signal intensity in the three replicates of microglia (MG) samples, green profiles plot the mean signal intensity in the two arrays derived from glial precursors cells (GPC), and the orange graphs depict the mean signal intensity in the two arrays probed with oligodendroglial (OL) samples. Ensembl-annotated splice variants of each gene are illustrated in the upper panels. Exonic regions are illustrated as grey bars in lower panels. Black circles indicate hot spots for putative alternative splicing events. '>' or '<' (next to gene name) indicates direction of transcription. (A) Tubulin tyrosine ligase-like 1 (*Ttll1*) exhibited significant lower expression for three adjacent exons in MG samples. (B) Polymerase (RNA) III (DNA directed) polypeptide H (*Polr3h*) shows closely related expression profiles for all cell types under investigation, except for exon three which is exclusively expressed by GPC.

Genes which are down regulated in mutants may reflect disease relevant pathways which are shut . They are probably involved in oligodenglial axonal support and could therefore serve as surrogate marker for potential drug targets

6.2 Transcriptional and histological analysis of specific neurons and white matter tracts in *Cnp1* and *Plp1* deficient mice over time

Previous studies have shown that the myelin protein composition as well as its ultra-structure is not dramatically changed in mice lacking CNP and PLP (Klugmann et al., 1997; Lappe-Siefke et al., 2003). Although oligodendrocytes are depleted of highly abundant myelin proteins, *Cnp1* and *Plp1* null mice exhibit no sign of dysmyelination, and show no obvious developmental delay. However, myelinated neurons of *Cnp1* as well as *Plp1 null* mutant mice develop axonal swellings, leading to axonal degeneration in the mature animal. The underlying molecular mechanism of which has not been identified so far. We speculate that oligodendrocytes not only ensheathe axons for the purpose of saltatory nerve conduction, but also provide trophic support to the axon. Thus far, the nature of this glial support function is poorly understood. To characterize the impact on cellular composition in the brain caused directly or indirectly by loss of *Cnp1* and *Plp1*, we studied the inflammatory responses as well as overall glial and neuronal cell numbers. We aimed to characterize the response of several cell types in the motor cortex as well as in the corresponding white matter tracts at different time points during progression of the phenotype. For our analyses we chose animals of 1, 3, 6, and 12 months of age. Per time point we used three, sex (male) and age matched, biological replicates. Sample from each time point were subjected to immunohistochemical (IHC) staining, RNA expression analysis and biochemical experiments to validate and correlate our findings with different methods.

6.2.1 Consequences of *Cnp1* and *Plp1* deficiency on cellular composition in primary motor cortex and corpus callosum

Due to the exclusive expression of *Cnp1* and *Plp1* in OL we examined whether the overall number of OLs is altered over time in the respective null mutant mice. We took advantage of cell type specific marker protein expression to quantify cell type abundance. First, we quantified the overall number of

oligodendrocytes in primary motor cortex (Cx) and white matter tracts of the corpus callosum (WM) at 1, 3, 6, and 12 months of age. An anti-CC1 antibody raised against the adenomatous polyposis coli (APC) protein, which is a well-characterized marker for oligodendrocytes, was used for labeling and subsequent quantification (Bhat et al., 1996), see Fig. 11 A, B. Quantification of CC1$^+$ cell bodies revealed no significant difference in oligodendrocyte numbers between wild-type (WT), *Cnp1* and *Plp1* mutants in Cx and in WM, as shown in Fig. 11 B. Due to unspecific binding of CC1 antibody at least on paraffin sections of aged mouse brains, we could not reliably quantify CC1 IHC stainings of 12 months old animals (Fig. 11 A, B, right panel). Based on our data we conclude that the number of oligodendrocytes remains unchanged until the age of 6 months.
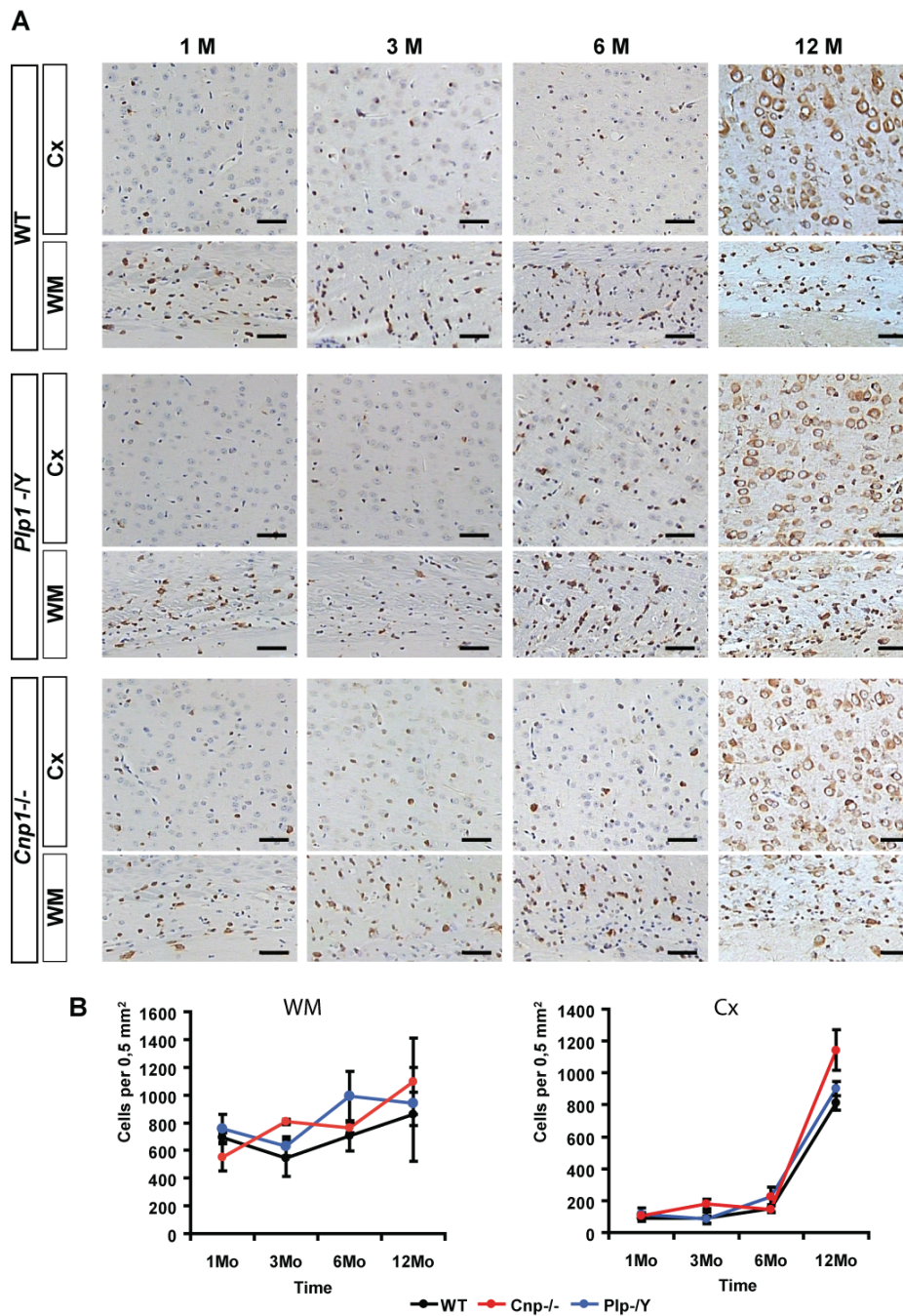
Fig. 11: *Cnp1* and *Plp1* **mutant mice reveal no change in oligodendrocyte number in WM and Cx.**
(A) Representative photomicrographs of CC1 IHC in mouse brain. Brains from all time points were post-fixed in 4% PFA, and near-midsagittal sections were subjected to immunostaining. Images of CC1 (brown) immunostaining and DAPI (blue) counterstaining were captured digitally. Scale bar = 50 µm. (B) Total numbers of CC1+ cells in Cx and WM per 0.5 mm^2, error bars indicate standard deviation (SD). Quantification was done in a semi-automated manner using a self developed ImageJ macro, and were based on CC1$^+$ cell bodies. Total numbers of CC1$^+$ cells were unchanged over all time points in all genotypes. High values at the 12 months time point in Cx are due to unspecific binding of CC1 antibody in aged brains.

Previous studies on *Cnp1* mutants showed extensive accumulation of amyloid precursor protein (APP) in axons of WM appearing at 1 month progressing up to 6 months of age. Moreover, the overall number of axons is decreased in WM at 6 months old mice (Burzyńska, 2007). These findings prompt the question whether neuronal cell bodies in the Cx of *Cnp1* mutant mice are also decreased. We used the NeuN (Neuronal Nuclei) antibody, which labels most neuronal cell types throughout the nervous system of mice (including cerebellum, cerebral cortex, hippocampus, thalamus, spinal cord, and neurons in the peripheral nervous system including dorsal root ganglia, sympathetic chain ganglia, and enteric ganglia). NeuN staining shown in Fig. 12 A exhibit normal distribution and morphology of neurons in Cx compared to WT. Quantification showed no significant changes in neuronal numbers over time (Fig. 12 B). NeuN$^+$ cell bodies were counted within an area of 0,5 mm^2 from three sections, derived from three animals per genotype at 1, 3, 6, and 12 months of age.

In addition to the APP$^+$ axonal swellings other well described hallmarks of neuronal degeneration such as increased astrogliosis (accumulation of Gfap$^+$ astrocytes) and microglyosis (activation and invasion of Iba1$^+$ microglia) were found. Immunostaining for ionized Ca^{2+}-binding adaptor 1 (Iba1), which is expressed selectively in microglia/macrophages and is a Ca^{2+}-binding peptide produced by activated monocytes and microglial cells, is shown in Fig. 13 A. Alterations in overall numbers of Iba1$^+$ cells reflect the extend of activation, invasion or proliferation of microglia in central nervous system (CNS). Quantification of Iba1$^+$ cells shown in Fig. 13 B, revealed a significant increase of microglia in WM at several time points in *Cnp1* and *Plp1* mutants. Microglial activation was found to peak at 1 and 12 months of age in *Cnp1* mutants and at 6 months of age for *Plp1* mutants.
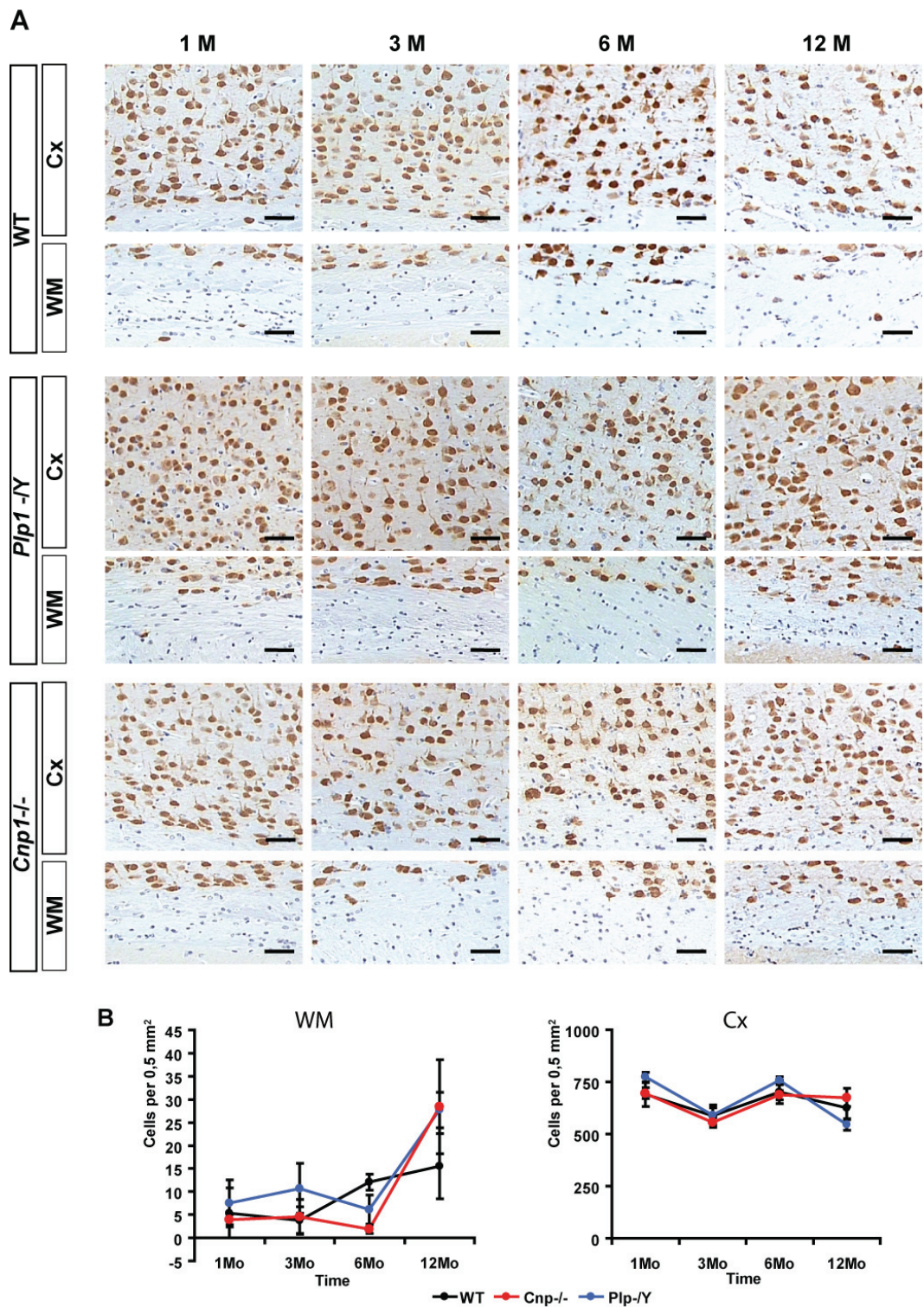
Fig. 12: Neuronal cell numbers are unchanged in Cx and WM
(A) Representative photomicrographs of NeuN immunostaining in mouse brain. Brains from all time points were post-fixed in 4% PFA, and near-midsagittal sections were subjected to immunostaining. Images of NeuN (brown) immunostaining and DAPI (blue) counterstaining were captured digitally. Scale bar = 50 μm. (B) NeuN^{+} cells in Cx and WM per 0,5 mm^2. The total number of NeuN^{+} cells was unchanged over all time points in all genotypes.
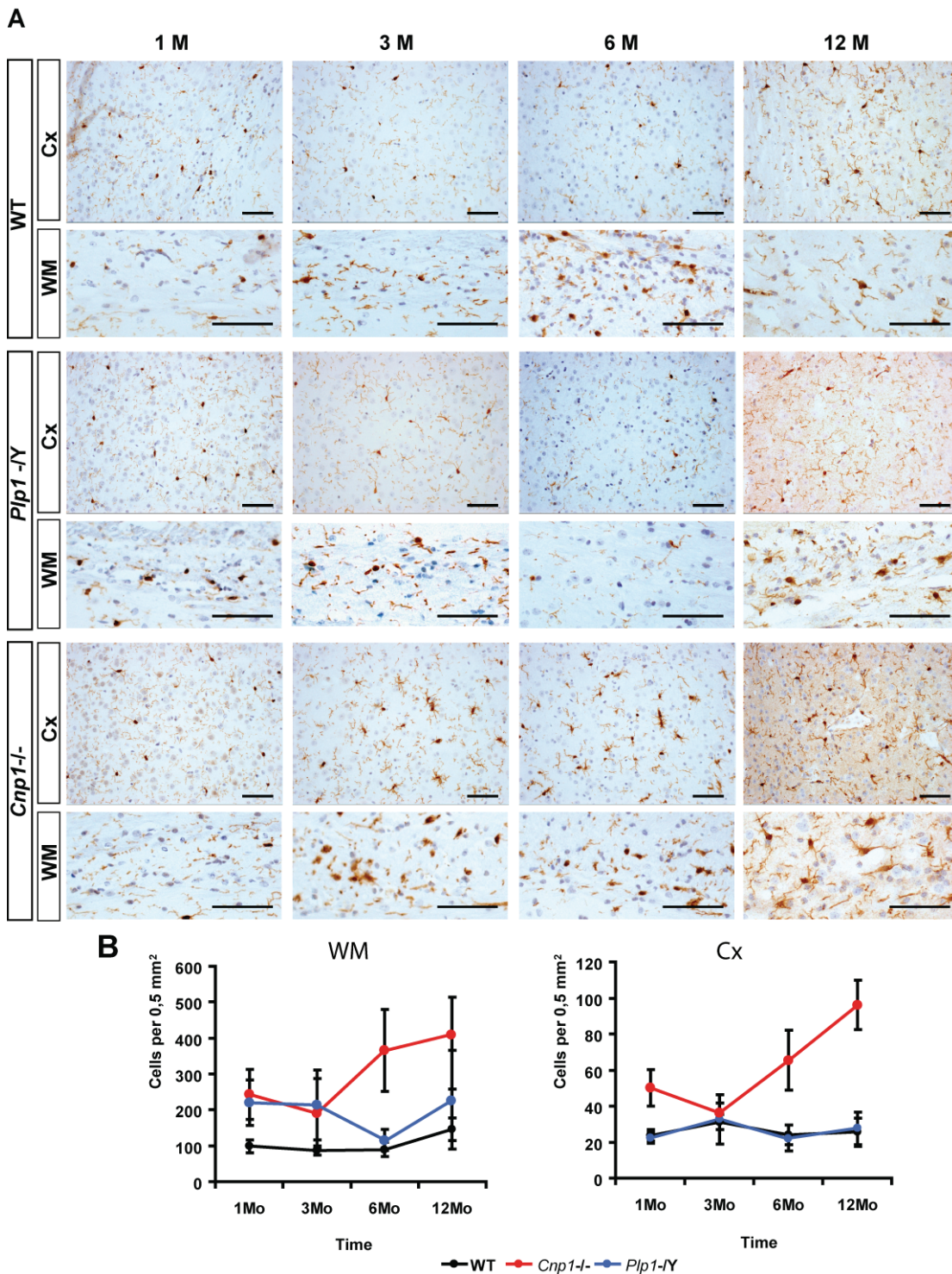
Fig. 13: Microglial cell numbers increased in Cx and WM over time in myelin mutant mice

(A) Representative photomicrographs of IBA1 immunostaining in mouse brain. Brains from all time points were post-fixed in 4% PFA, and near-midsagittal sections were subjected to immunostaining. Images of IBA1 (brown) immunostaining and blue DAPI counterstaining were captured digitally. Scale bar = 100 μm. (B) IBA1^{+} cells in Cx and WM per 0,5 mm[2]. Quantification was done in a semi-automated manner using an in-house developed ImageJ macro. Total number of IBA1^{+} cells were increased in WM of mutants at all time points.

62

Another histological indication for ongoing inflammatory processes within the CNS is reflected by an increase in astrocyte activation, which can be detected by α-GFAP IHC. Under control conditions astrocytes were present at low level throughout the brain parenchyma, both in WM and Cx. Morphologically, resting astrocytes are characterized by numerous thin fibrillary processes, forming a net-like pattern. Identification and quantitation of astrocytes is challenging due to their great abundance and numerous processes formed by this cell type. In addition, classification, as done for MG, of astrocytes was not possible due to high intra-region variability of the degree of reactive gliosis. We therefore quantified astrogliosis using the area (in percent), which is covered by GFAP staining in defined regions within Cx and WM (Fig. 14A). Quantification in WM revealed, similar to the results for microglia, an increased staining for GFAP in *Cnp1* mutants at 1, 3, and 6 months which was finally adapted at 12 months by increased staining also in WT and *Plp1* mutant mice. Both WT and *Plp1* mutant samples show a progressive increase in GFAP staining over time (Fig. 14B). Cx was not affected at 1 and 3 months by astrogliosis, but dramatically developed in *Cnp1* mutants at 6 and 12 months of age. Expression patterns for WT and *Plp1* mutants were very similar at all time points in Cx.
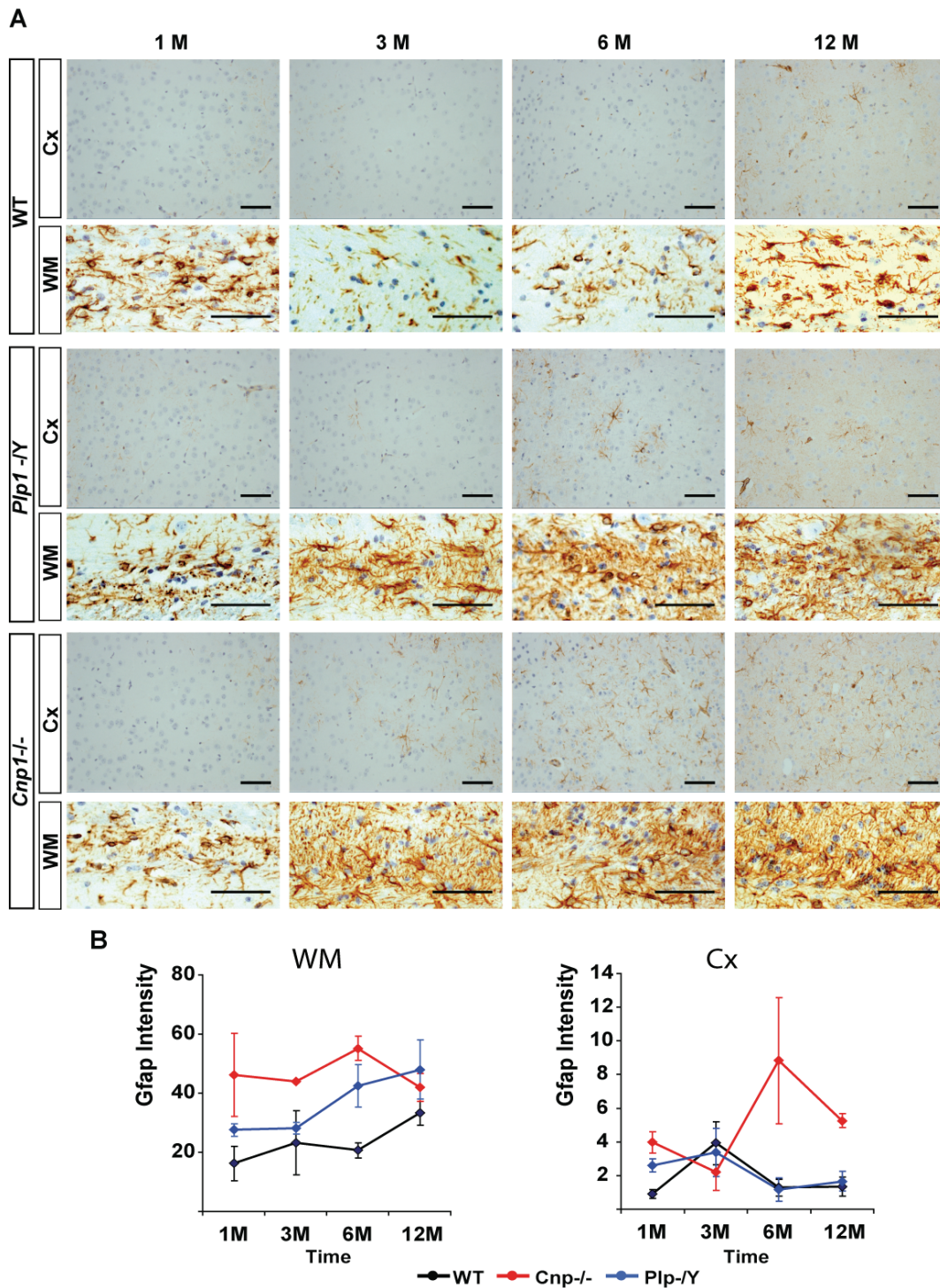
Fig. 14: Increased activation and invasion of GFAP+ astrocytes in Cx and WM in myelin mutants over time

(A) Representative photomicrographs of GFAP immunostaining in mouse brain. Brains from all time points were post-fixed in 4% PFA, and near-midsagittal sections were subjected to immunostaining. Images of GFAP (brown) immunostaining and DAPI (blue) counterstaining were captured digitally. Scale bar = 100 μm. (B) Percentage of GFAP signal in Cx and WM. Quantification was done in a semi-automated manner using an in-house developed ImageJ macro. There is more GFAP signal detected in Cx of Cnp null mice at 6 months and 12 months of age, in WM more GFAP is observed at 1, 3, and 6 months of age compared to WT controls.

In summary, oligodendrocytes appear normal in morphology and number in Cx and WM. Similar results were obtained for NeuN staining, which labels neurons. Hallmarks of microgliosis as well as astrogliosis were present for *Cnp1* and *Plp1* mutant mice. WM regions were more severely affected than Cx. *Cnp1* mice furthermore showed an earlier and more severe progression of astro- and microgliosis compared to *Plp1* mutant mice, which is in agreement with previously published data (Klugmann et al., 1997; Lappe-Siefke et al., 2003).

Table 3: Summary of histological observations in WM and Cx of WT controls, *Cnp1-/-* and *Plp1-*/Y

		1M Cx	1M WM	3M Cx	3M WM	6M Cx	6M WM	12M Cx	12M WM
CC1	WT	-	-	-	-	-	-	**NA**	
	Cnp1-/-	-	-	-	-	-	-		
	Plp1-/Y	-	-	-	-	-	-		
NeuN	WT	-	-	-	-	-	-	-	-
	Cnp1-/-	-	-	-	-	-	-	-	+
	Plp1-/Y	-	-	-	-	-	-	-	+
IBA1	WT	-	-	-	-	-	-	-	-
	Cnp1-/-	+	+	-	+	-	++	+++	++
	Plp1-/Y	-	+	-	+	+	++	-	+
GFAP	WT	-	-	+	+	-	+	-	++
	Cnp1-/-	+	++	+	++	+++	++	++	++
	Plp1-/Y	+	+	+	+	-	++	-	++

6.2.2 Impact of the loss of Cnp1 on distinct neuronal cell type populations

Previous observations from a pilot study, where we isolated cerebellar Purkinje cells (PC) employing laser capture microdissection, indicated a substantial loss of PC in *Cnp1* mutant mice. This is in contrast to the results of NeuN staining in cerbral cortex, where we could not verify this finding for cortical neurons. It is possible that only a specific group of cortical neurons is affected by the loss of *Cnp1*, which could be masked by quantifying all neurons. We therefore subjected callosal projection neurons in the Cx of TYNC mice to a more detailed histological analysis. This particular mouse line expresses a nuclear variant of

EYFP (EYFPnuc) under transcriptional control of the *Thy1* promoter (Rossner et al., 2006) predominantly in CPNs. To examine the impact of *Cnp1* and *Plp1* loss on neuronal survival, we compared total number of CPN and PC present at 3 months and 12 months of age in the Cnp null mutant mice versus WT controls.

For quantification of cerebellar PC we used a thionine staining, which labels cell bodies (Fig. 15 A). PC were identified based on their characteristic location, morphology and size (Fig. 15 B). We counted the total number of PC in lobe five and six in three animals per genotype, by quantifying 10 sections per animal in 3 and 12 months old mice. Analysis revealed no significant difference at 3 months but a significant reduction to 25% of WT levels in *Cnp1* mutants at 12 months (Pval < 0.001, students T-test), illustrated in Fig. 15 C. For quantification of EYFPnuc⁺ CPN we took 8µm coronal cryosections (Fig. 15 E) of three animals per genotype and analyzed ten sections per animal. Quantification was performed with an automated cell recognition ImageJ macro, which detects EYFPnuc⁺ cells in a predefined cortical region (Fig. 15 D). Analysis revealed no significant difference between WT and Cnp1-/- at 3 and 12 months of age shown in Fig. 15 E.
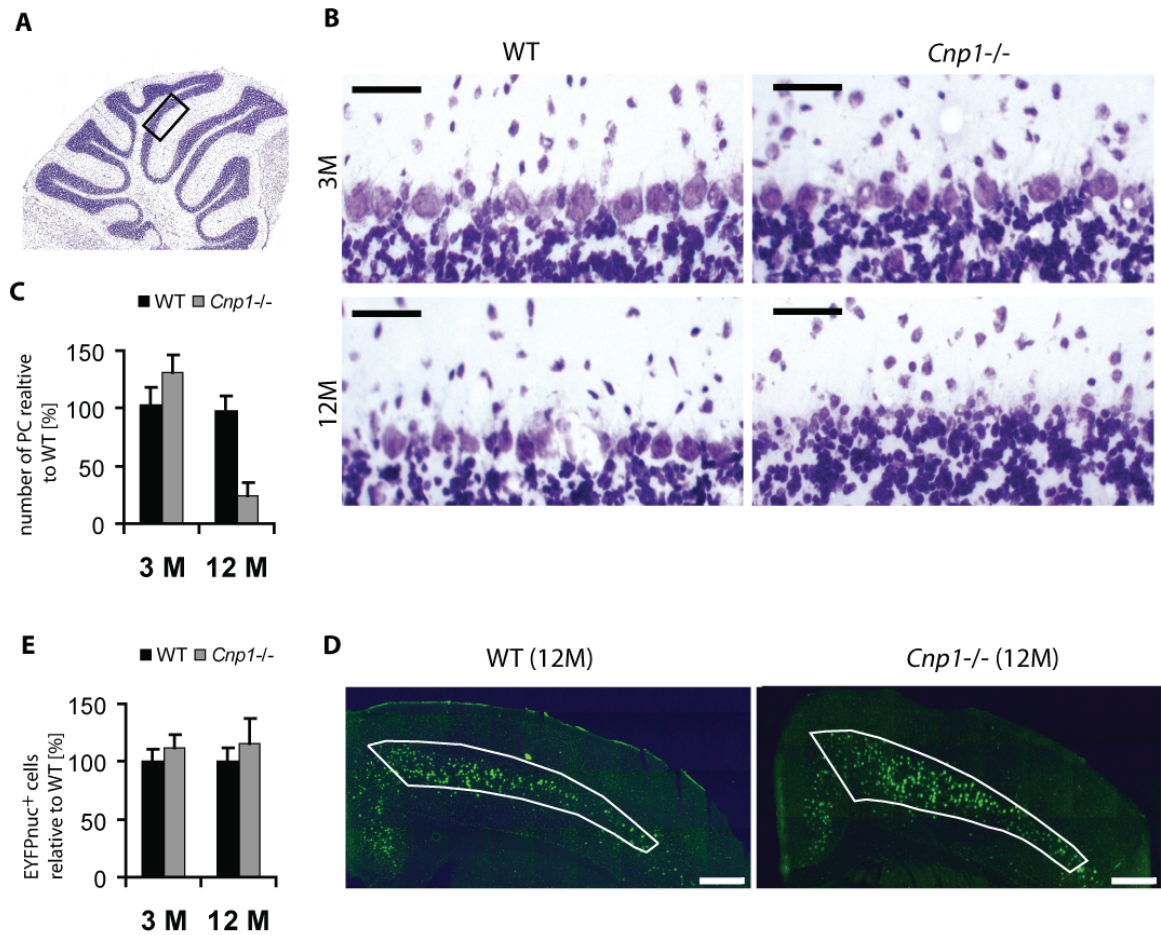
Fig. 15: Lack of *Cnp1* causes substantial loss of Purkine cells
Histological analysis of the cerebellar and cerebral cortex of wild-type and *Cnp1* null mutant mice. (A) Sagital cryosection of wild-type (WT) cerebellum stained with thionine; scale bar = 500 μm. The inset represents the region of images shown in higher magnification (B). The left panel shows cerebellar cortical sections with an intact Purkinje cell layer of 3 to 12 months old WT mice; scale bar = 50μm. Cnp1 mutant mice show progressive Purkinje cell loss from 3 to 12 months. (C) Average number of Purkinje cells per lobes 5+6 at 3 and 12 months of age. (D) Coronal cryosection of cerebral cortex of wild-type and Cnp1 mutant mice. CPN express transgenic EYFPnuc in motor and somatosensory cortex, scale bar = 50 μm. (E) Quantification of total EYFPnuc+ cells in wild-type and Cnp1 mutant mice shows no significant change in 12 months old mice. Values are relative to wild-type levels in percent.

6.2.3 Isolation of CPN and WM by LCM

Applying high throughput techniques like DNA microarrays in the CNS is still challenging due to the presence of multiple different cell types. In order to get reliable and reproducible results it is mandatory to reduce the cellular complexity as much as possible, and to perform the analysis with a defined cell population. The use of LCM has proven especially helpful in isolating specific neuronal population from Cx (Rossner et al, 2006).

We used 8μm coronal cryosections for single cell isolation. Coronal cryosections were prepared from primary medial motor cortex (bregma +1 to +0.5, Fig. 16 A). EYFPnuc-expressing CPN were identified using the fluorescence mode of the Veritas microdissection instrument (Molecular Devices), shown in Fig. 16 B. EYFP$^+$ CPN were collected from primary motor cortex and the somatosensory cortex (target area highlighted in yellow). Single CPN are depicted in Fig. 16 prior to LCM (C), following LCM (D) and isolated on the capture cap (E). We collected 600 -700 CPN for each animal. One aim of our study was to generate gene expression profiles of neurons, which are deprived of oligodendroglial support. In this context it is also of interest as to know, how OLs react upon loss of *Cnp1* or *Plp1* on the level of transcription. Isolation of OLs in adult CNS was at least for us impossible because of lack of proper mouse tools, which allow LCM-compatible OL identification. Additionally are cellular dimensions of oligodendrocytes below the size threshold of our microdissection device.

However, to obtain expression profiles of adult oligodenrocytes, we decided to isolate the corpus callosum, a WM region enriched for oligodendrocytes. WM micro-regions were isolated from the same coronal plane depicted in green box in Fig. 16 A. Fig. 16 F-H shows the corresponding procedure for WM before and after LCM, and the captured area on the cap. WM micro-regions were isolated from 15 cryosections (20 μm thick), which were previously mounted on PEN membrane-framed slides. For single cell isolation we employed the capture modus using only IR laser to attach neurons to the capture cap. Micro-regions were isolated using the UV laser (UV-power set to 4 mW), attachment to the cap was done with the IR laser (power = 75 %; pulseduration = 2000 - 5000 μsec). Immediately after LCM, single cells and micro-regions were lysed in RLT buffer (Qiagen). Total RNA amounts derived from LCM samples were in the range of 500 pg for CPN and 1-5 ng for WM micro-regions per sample. RNA integrity could not be evaluated since the RNA yield was below the detection limit. RNA was subjected to a T7-based two-round amplification protocol prior to microarray hybridization. RNA amplification yielded between 11.2 - 22.4 μg for CPN and 31.3 - 45.3 μg for WM samples. The fragment size of amplified

RNA was determined by electrophoretic separation on an Agilent RNA Bio-Lab-chip, shown in Fig. 16 I. Antisense RNA abundance (fluorescence) is graphed as a function of RNA fragment size. The mRNA profiles demonstrate a significant population of fragments in the 200-1,200 nt size range and serves therefore as a measure of successful amplification.
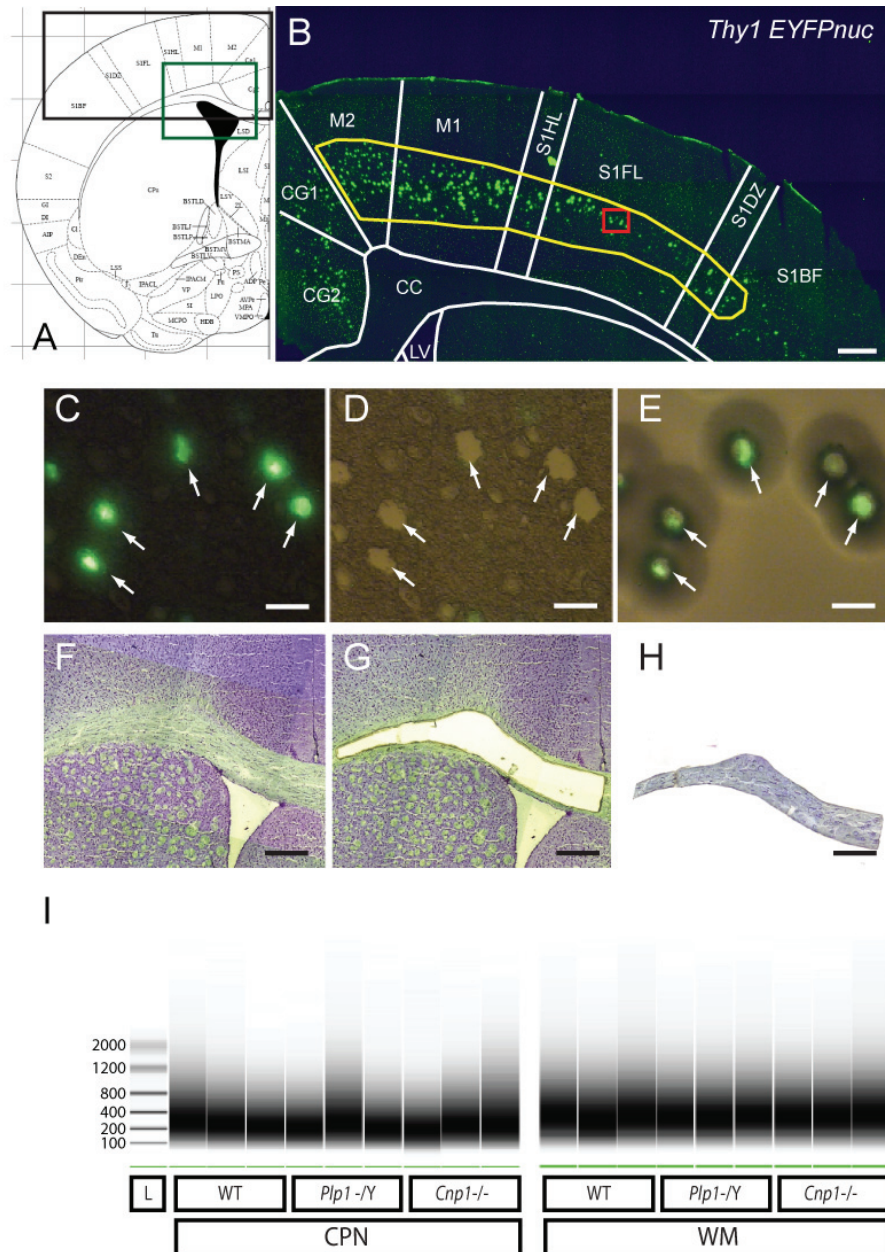
Fig. 16: Fluorescence-directed laser microdissection enables the isolation of RNA derived from neuronal cell types with high precision.
(A) Anatomical structure of the coronal mouse brain (adapted from Paxinos mouse brain atlas (Paxinos and Franklin, 2004)). The black rectangular represents the area of fluorescent micrograph for single cell isolation (mirrored in (B)); the green box represents the area for WM micro-region isolation (F-H). (B) Fluorescent micrograph was taken from a 6 months old WT brain. For better orientation, the boundaries of the corpus

callosum (WM) and of the lateral ventricle (LV) were marked in the fluorescent picture. In Cx, at the level of the primary motor and somatosensory areas, mainly cells of the deeper layers are EYFPnuc+ (layer V and few cells in layer VI). In the upper layers II, III, and IV, a low number of dispersed cells were EYFPnuc positive, usually with a weaker signal intensity. Samples isolated with laser microdissection were chosen from the primary motor and somatosensory cortex (yellow area); 20x magnification; scale bar = 200 μm. (C-E) Fluorescence-directed laser microdissection of single EYFPnuc[+] CPN. In the fluorescent mode, single cells were identified and attached via Laser Capture to a HS capture cap; only strongly EYFPnuc-expressing cells in the plane of section were chosen for isolation. The infrared (IR) laser settings were chosen to cover the nucleus as precisely as possible using a 60x objective. Cells with other nuclei in close proximity were not isolated. Depicted are five nuclei (arrows) at a distance where contamination was considered to be low. Successful capture was controlled in the bright field and fluorescent mode on the tissue section (D) and on the HS cap (E); 60x magnification; scale bar = 20 μm. (F-H) LCM of WM micro-regions was performed on 20 μm thionine-stained adjacent cryosections, which were mounted on PEN membrane slides. (F) Section prior to LCM; (G) section post LCM; (H) cap after LCM. LCM was performed with a combination of laser capture and UV-directed microdissection. WM was collected from 12 sections; 20x magnification; scale bar = 100 μm. (I) Aliquots of each amplified RNA were separated by capillary electrophoresis (Agilent Bioanalyzer, together with the RNA 6000 Series II Nano Kit), along with RNA ladder (L; Ambion). Shown are aRNAs after two rounds of linear amplification from all samples derived from the 3 months time point.

6.2.4 Microarray quality controls

Our approach to restrict cellular complexity using LCM comprises a major experimental challenge. LCM on brain samples is a technically highly demanding method, which is not *per se* compatible with microarray technology due to extremely low RNA yield. We therefore introduced quality controls on several levels, addressing the following questions:

- How large is the variation between samples after 2 round amplification?

- How preserved is RNA integrity after LCM?

- Are correlation co efficiencies of biological replicates higher than between non replicates?

Evaluation of microarray performance was assessed via standard microarray quality control parameters shown in Fig. 17. Box plots in Fig. 17 A depict signal distributions of raw data (upper panel) and normalized data (lower panel) and show comparable distributions for all microarrays analyzed in this study. In order to exclude factors which may bias the analysis, we evaluated also the extend of RNA degradation for each sample. For this purpose we generated a

RNA degradation plot seen in Fig. 17 B. All probes are ordered according to their relative position in the coding transcript (from 5'- to 3'-end). Arithmetic mean intensity for every position results in a specific slope for each microarray, which reflects the degree of RNA degradation. The results show similar slopes for all microarrays. Thus, we could exclude a bias originating from different RNA degradation rates in samples during LCM.
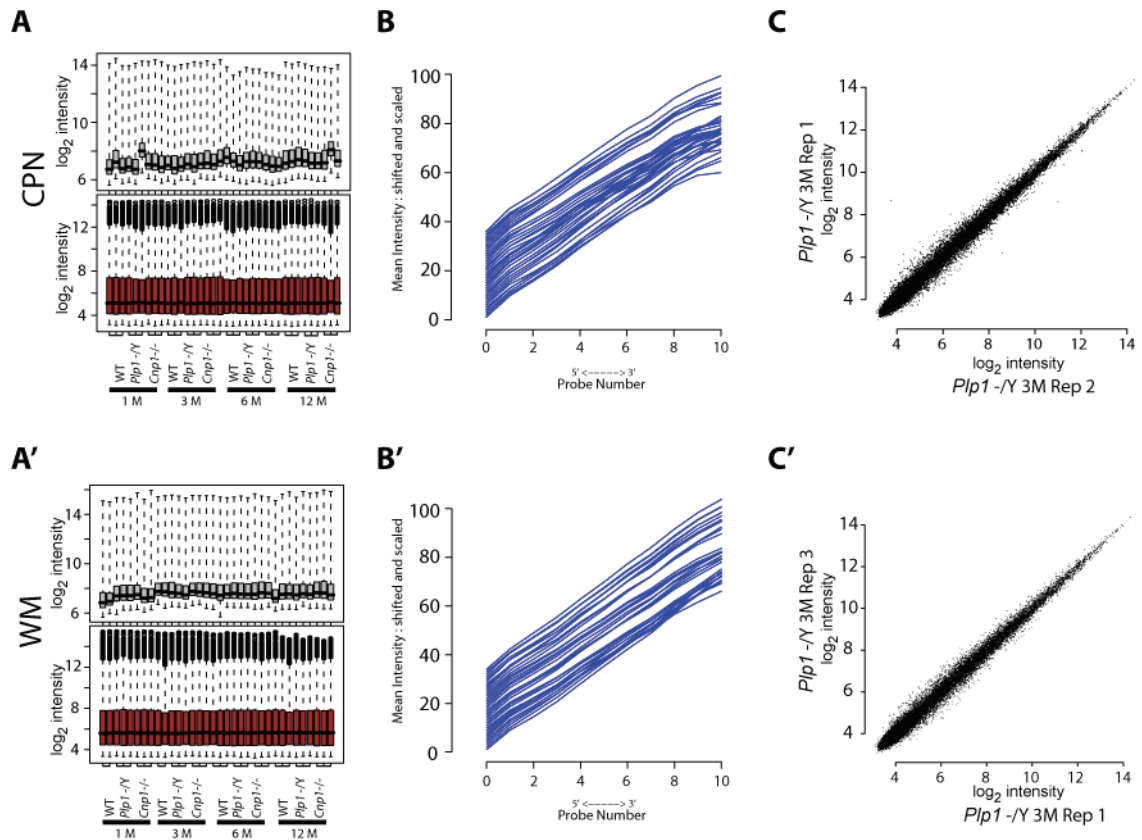
Fig. 17: Quality controls of microarray data obtained with LCM-derived RNA
(A) Box plots of raw data from all microarrays (upper panel) and after RMA normalization (lower panel) show a homogenous intensity distribution. After normalization all microarrays have the same signal intensity distribution. (B) RNA degradation plot. Within each probe set, probes are numbered directionally from the 5'- to the 3'-end. Probe intensities are averaged by probe number, across all genes. All traces show the same slope indicating a similar RNA degradation degree for all samples. (C) Representative scatter plots of biological replicates show a high correlation coefficient, which was between 0,97 and 0,99 for all replicates.

Correlation coefficients of biological replicates were within 0.97 and 0.99, representative scatter plots of biological replicates are shown in Fig. 17 C. Affymetrix quality controls are listed in Table 4 and further support the high performance of our LCM-based microarray analysis. In summary, all quality

controls met stringent criteria and indicate that our generated microarray data is highly consistent between biological replicates, confirming the viability of the dataset.

Table 4: Standard Affymetrix quality control parameters

Sample	Age	Back-ground	Present Calls[%]
WT R1	1M	59	48
WT R2	1M	78	53
WT R3	1M	64	40
Plpy/- R1	1M	70	49
Plpy/- R2	1M	50	47
Plpy/- R3	1M	112	45
Cnp-/- R1	1M	76	50
Cnp-/- R2	1M	72	49
Cnp-/- R3	1M	64	50
WT R1	3M	76	47
WT R2	3M	59	51
WT R3	3M	69	46
Plpy/- R1	3M	78	50
Plpy/- R2	3M	64	51
Plpy/- R3	3M	78	50
Cnp-/- R1	3M	76	52
Cnp-/- R2	3M	76	51
Cnp-/- R3	3M	89	53
WT R1	6M	79	46
WT R2	6M	75	44
WT R3	6M	65	47
Plpy/- R1	6M	65	46
Plpy/- R2	6M	70	48
Plpy/- R3	6M	68	47
Cnp-/- R1	6M	66	48
Cnp-/- R2	6M	60	48
Cnp-/- R3	6M	64	46
WT R1	12M	72	51
WT R2	12M	78	52
WT R3	12M	81	52
Plpy/- R1	12M	80	50
Plpy/- R2	12M	75	52
Plpy/- R3	12M	74	52
Cnp-/- R1	12M	70	51
Cnp-/- R2	12M	115	45
Cnp-/- R3	12M	102	51

6.2.5 Marker gene expression exhibit high cell type specificity

Gene expression analysis in the CNS is generally complicated by the coexistence of many different cell types, resulting in high background noise and the inability to detect small differences in cell type specific gene expression. The purification of single populations of cortical projection neurons should overcome these limitations and allow us to generate expression profiles of defined neuronal populations.

To assess the degree of purification obtained by our LCM procedure, we first assessed the expression of known cell type markers illustrated in Fig. 18. Depicted are arithmetic means of normalized intensities derived from three biological replicates including standard deviation. In Fig. 18 A we examined the expression of *Cnp1* and *Plp1* in WT vs. null mutants animals, which serves also as a direct validation of proper sampling. These genes are only expressed by myelinating cells and are therefore well accepted oligodendrocytic markers. Transcription levels of *Cnp1* and *Plp1* were very high in wild-type WM samples whereas null mutants showed no signal for their corresponding knock-out gene (upper panel). Expression of *Cnp1* and *Plp1* were 1000 fold decreased in CPN to very low signal intensities.

The expression of neuronal markers like Enolase 2 (*Eno2*) or Thymus cell antigen 1, theta (*Thy1*, shown in Fig. 18 B) are absent in WM but show very high expression in all CPN samples. *Eno2* showed a slight increase of expression over time in all genotypes whereas *Thy1* expression remained constant over time. From the IHC results (Fig. 3 and 4) where we detected higher expression of astrocytic and microglial markers especially in WM samples of *Cnp1* and *Plp1* mutant mice, we expected that this should be also reflected on the level of transcription. Fig. 18 C (left panel) depicts mRNA expression profiles of *Gfap*, a known marker for activated astrocytes. Profiles exhibit a constant low expression in WT samples at all time points, whereas in *Plp1* and *Cnp1* mutants the expression increased significant over time starting at 3 months. In the CPN samples, *Gfap* expression could not be detected. To check on the transcriptional level whether the overall numbers of astrocytes changed, regardless of their physiological status, we evaluated *S100b* expression (Fig. 18 C, right panel). In WM samples, we could not detect significant changes of *S100b* expression between genotypes. Unexpectedly, we also observed a robust mRNA expression profile of S100b in CPN, exhibiting a similar pattern for all genotypes investigated. Gene expression analysis of microglia markers Mac-2 and Iba1 (Fig. 18 D, upper panel) revealed the same results as for Gfap with very weak expression in WT samples and an increasing expression over time in

Cnp1 and *Plp1* mutant mice in WM. CPN showed no signal for microglial markers (Fig. 18 D, lower panel).
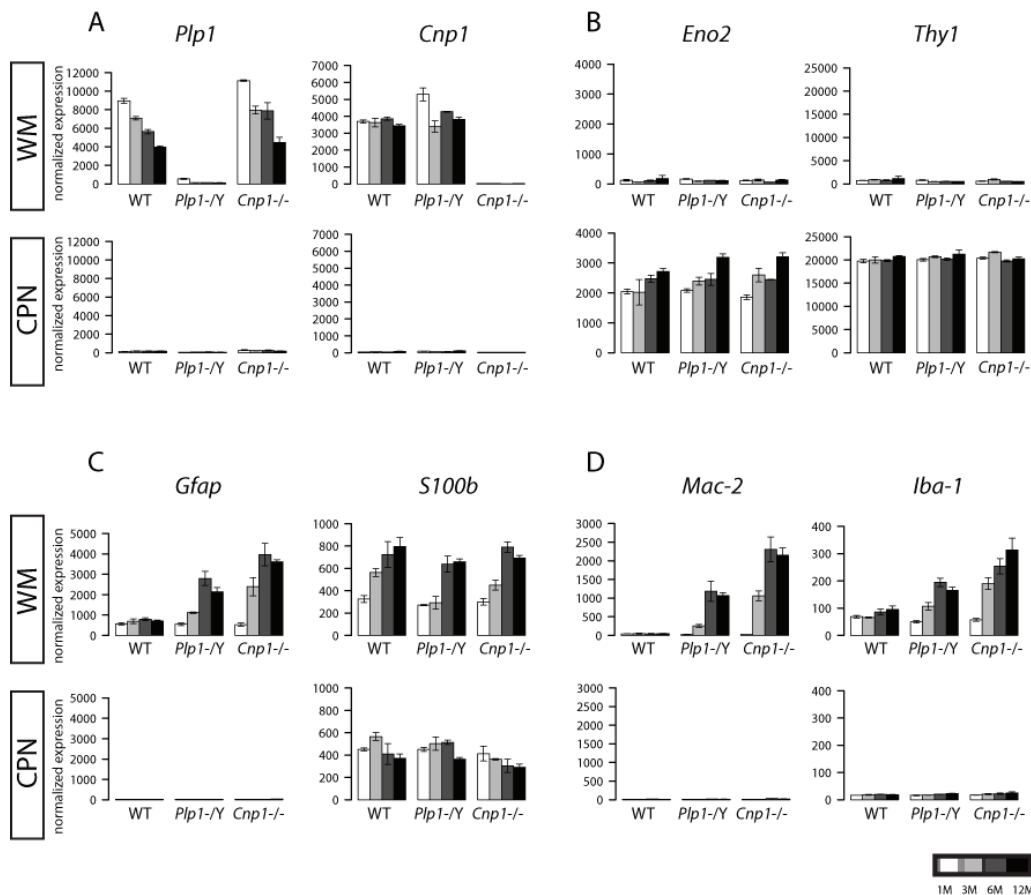
Fig. 18: Validation of LCM isolation precision based on cell type specific marker gene expression.
(A) mRNA levels of the oligodendrocyte-specific marker genes *Plp1* and *Cnp1* are highly enriched in WM versus CPN samples in wild-type animals. In mutant animals the mRNA signal is completely absent. (B) Neuronal markers *Thy1* and *Eno2* are highly expressed in neuronal samples and show very weak expression in WM samples. (C) *Gfap* expression as a marker for activated astrocytes shows age-dependent up-regulation in *Plp1* and *Cnp1* mutant mice, whereas in WT controls *Gfap* expression stays constant at low levels during aging. *Gfap* signal could not be detected in neuronal samples. *S100b*, another accepted marker for astrocytes, is robustly expressed in CPN as well, and its expression levels do not change over time in all studied genotypes. (D) As markers for microglia, *Iba1* and *Mac-2* were used. *Iba1* is supposed to stain all microglia and *Mac-2* only activated microglia. According to the expression data, the number as well as the activation status is increased in WM over time in myelin mutants. Bar plots represent arithmetic means (n = 3), error bars indicate SD.

6.2.6 Loss of *Cnp1* and *Plp1* mediates substantial gene expression changes in CPN and WM

Cnp1 and *Plp1* knock-out animals develop an axonal pathology albeit these proteins are predominantly expressed in oligodendrocytes. It is not known so

far whether a dysfunction of oligodendrocytes can mediate transcriptional changes in myelinated neurons. We identified a significant amount of differentially expressed genes in CPN and in WM of *Cnp1* and *Plp1* mutant mice. To identify these genes we performed pair-wise comparisons as well as two-way ANOVA tests. The analysis revealed a large number of significantly differentially expressed genes (adj. p-val. < 0.001, Benjamin Hochberg correction), which were in CPN at least 1.8-fold up- or down-regulated in *Cnp1* mutants. Surprisingly, we found only a modest number of differentially regulated genes in *Plp1* null mutants in CPN over time, as illustrated in Fig. 19 A (left panel). We detected more down-regulated genes in *Cnp* null in contrast to *Plp* null samples in neurons, where no trend towards up- or down-regulation is obvious. The analysis of WM samples (Fig. 19 A, right panel) revealed differential expression of >2000 genes in both mutants during the time course. In WM dramatic changes in differential expression can be observed already at 1 month of age in *Cnp1* mutant mice, which even increased at later time points and remained constantly high. Similarly as for CPN a strong tendency towards gene down-regulation can be observed. In contrast to the *Cnp1* mutant animals, *Plp1* null samples show a different pattern in WM over time. The number of affected genes remains rather constant, with a slight peak at the 3 months time point, and the total number of differentially expressed genes is smaller compared to *Cnp1* mutant mice (Fig. 19 A, lower right panel). In contrast to the analysis of neurons, *Plp1* profiles in WM show a slight trend to more down-regulated genes.

In CPN samples of Plp and Cnp mutants 104 and 412 genes were differentially expressed, respectively. Of these genes, 40 showed altered gene expression in both mutants (Fig. 19 B, upper left panel), covering 40% of deregulated genes in *Plp1* mutants. In WM samples of *Plp1* and *Cnp1* deficient mice were 1204 and 1364 genes significantly deregulated, respectively. 657 genes were commonly affected in *Plp1* and *Cnp1* mutants, representing an proportion of ~50% of the genes found in both mouse models (Fig. 19 B, upper right panel).

Direct comparison of deregulated genes in CPN (598 genes) versus WM (2110 genes) revealed 180 overlapping genes (Fig. 19 B, lower panel).

In summary, loss of *Cnp1* leads to more dramatic changes in gene expression over time compared to the *Plp1* mutants. The affected genes are predominantly down-regulated in *Cnp1* mutant samples, while such tendency is hardly detected in the *Plp1* mutant mice. However, a significant overlap of dysregulated / deregulated genes between *Cnp1* and *Plp1* knock-out animals can be observed, as well as a number of genes deregulated both in neurons and WM.
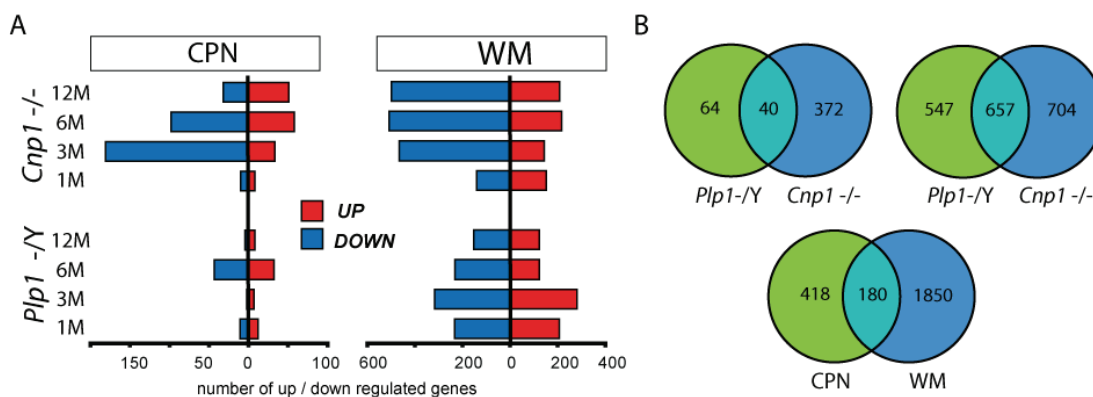
Fig. 19: Distinct gene expression responses in CPN and WM of *Cnp1* versus *Plp1* mutants.

(A) Total numbers of up- and down-regulated genes at each time point are shown; gene selection criteria were as follows: adj. p.val < 0.001, fold change (FC) > 1.8. Up-regulated genes are plotted as red bars and down-regulated genes as blue bars. The number of deregulated genes in neurons is substantially higher in the more severely affected *Cnp1* mutants when compared to *Plp1* mutants. The difference in numbers of deregulated genes in WM samples are less pronounced between the genotypes.

(B) Venn diagrams illustrating a high extend of commonly deregulated genes between *Plp1* and *Cnp1* mutant mice in CPN (upper left panel) and WM (upper right panel). Comparison of differentially regulated genes in neurons versus WM reveals a large overlap (lower panel).

6.2.7 Gene set enrichment analysis

To obtain a global view of deregulated genes, that, for example, belong to a certain molecular pathway, we employed Gene Set Enrichment Analysis (GSEA) to examine changes in *a priori* defined gene sets. GSEA is a computational method that determines whether a defined set of genes shows statistically significant, concordant differences between two biological states, e.g.

phenotypes (Mootha et al., 2003; Subramanian et al., 2005). GSEA was performed with 5214 gene sets obtained from Molecular Signature Database (MSigDB) at the Broad Institute (http://www.broadinstitute.org/gsea/). An example of a gene set with significantly enriched genes affected by loss of *Plp1* is illustrated in Fig. 20 A and B. It depicts a typical enrichment score curve for the gene set "COMPLEMENTKEGG" which is defined by genes involved in the classical complement cascade annotated by KEGG (Kanehisa et al., 2008). We used "Signal-to-Noise ratio" (SNR) statistics to rank the genes according to their correlation with either WT (red) or *Plp1*-/Y (blue) samples. In Fig. 20 A , the graph shows enrichment towards the WT samples, implying that a loss of Plp leads to a down-regulation of the complement cascade in CPN at the age of 3 months. In WM samples (Fig. 20 B), genes involved in the classical complement cascade appear unaffected by the loss of *Plp1*. A summary of selected gene sets, which were significantly enriched in *Cnp1* and *Plp1* mutant mice are depicted as a heat map in Fig. 20 C. Similar patterns of gene set shifts were observed in both mutants in CPN and WM. The only exception for WM samples are genes involved in cholesterol biosynthesis, which exhibit a shift to down-regulation in *Plp1* mutants at all time points examined, whereas *Cnp1* mutants display slight up-regulation at all time points.
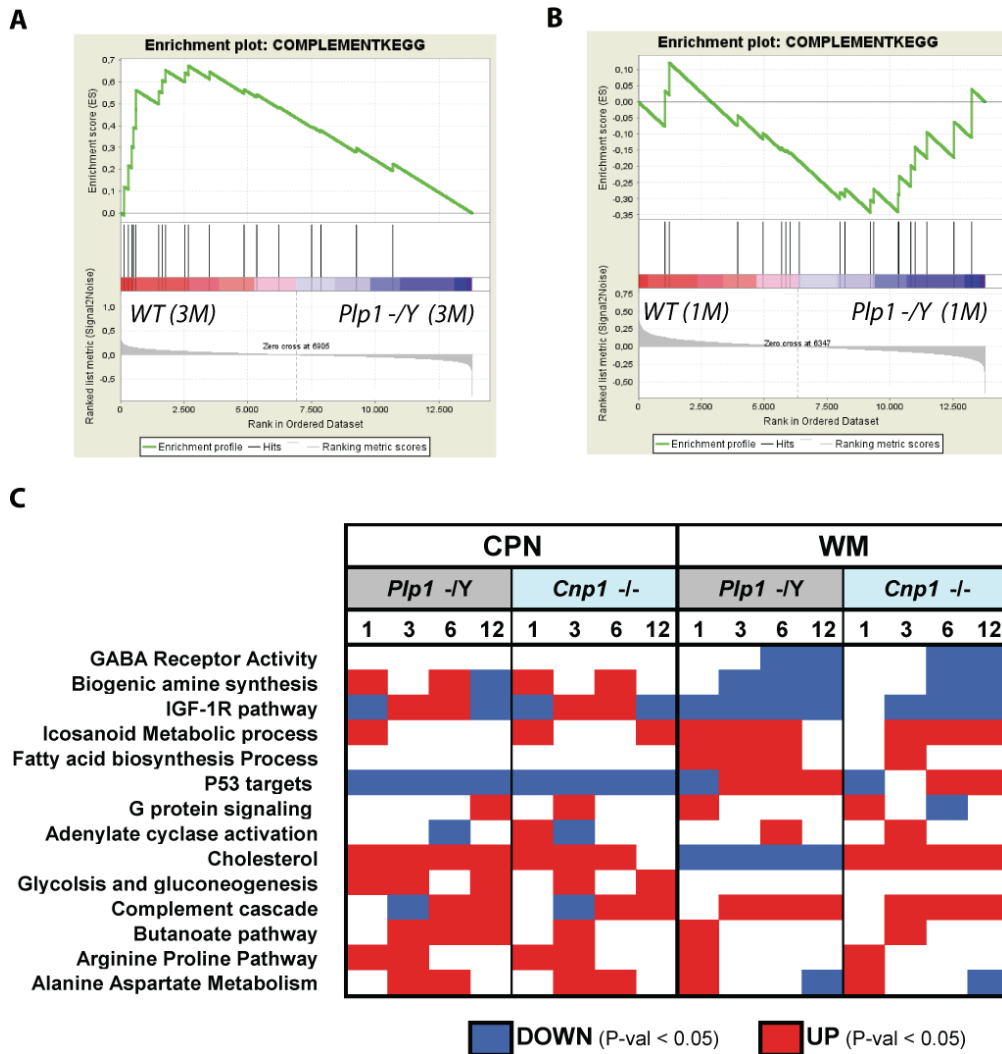
Fig. 20: GSEA Enrichment Score curves
Gene set enrichment analysis (GSEA) was performed with 5214 different gene sets obtained from Molecular Signature Database (MSigDB) at the Broad Institute (MIT). "Signal-to-Noise ratio" (SNR) statistics were used to rank genes according to their correlation with either wild-type samples (red) or Plp -/Y (blue). The graph on the bottom of each panel represents the ranked, ordered, non-redundant list of genes. Genes on the far left (red) show a higher correlation with wild-type samples, whereas genes on the far right (blue) correlated the most with Plp1-/Y samples. On each panel, the vertical black lines indicate the position of each of the genes of the studied gene set in the ordered, non-redundant data set. The green curve corresponds to the ES (enrichment score) curve, which is the running sum of the weighted enrichment score obtained from GSEA software. (A) shows that genes belonging to the complement gene set (includes 19 genes) correlate with three months old WM samples from wild-type (WT) mice and not Plp1-/Y mice; the high significance of the enrichment in WT is expressed in the values of ES = 0,67 and NOM p-val = 0,002. (B) No significant changes in the enrichment of the complement gene set in any of the genotypes at one months time point (ES = -0,34, NOM p-val = 0,629). (C) Summary of selected gene sets over all time points in callosal projection neurons (CPN) and corpus callosum white matter (WM). Up-regulated gene sets and down regulated gene sets with a NOM p-val > 0,05 are indicated in red and green, respectively.

78

6.2.8 Differentially expressed genes in CPN can be separated into three main groups

The aim of our study was to elucidate neuronal responses triggered by the loss of major myelin proteins. We therefore focused on the CPN dataset and in particular on the *Cnp1* mutants, because they develop a more severe pathology, which is already detectable at 1 month of age. We used a two-way ANOVA analysis to identify differentially expressed genes in CPN of *Cnp1* and *Plp1* mutants. For every single probe set, the effects of genotype (WT, *Cnp1-/-* and *Plp1-/Y*), age (1, 3, 6, and 12 months), and the interaction between genotype and age were evaluated. We chose differentially regulated genes with a p-value < 0.001 for the interaction and an average expression of at least two standard deviations above background for further cluster analysis. In *Cnp1* mutants, 666 genes fulfilled the criteria, and in *Plp1* mutants 161 genes. Detailed characterization of deregulated genes was done by partitioning clustering in order to group genes according their expression profiles over the time course of the experiment. To improve partitioning clustering, all significantly regulated genes were scaled to mean = 0 and standard deviation = 1. By transforming the selected genes, the influence of differences in expression levels or fold changes were minimized. For unsupervised partitioning clustering, the K-means method was employed to group selected genes based on their expression profiles into 9 clusters. Repeated clustering resulted in 3 classes of clusters as depicted in Fig. 21 :

- Cluster group one includes genes, which are up- or down-regulated in mutants at all time points (Fig. 21 A).

- Cluster group two showed differential expression only at the 3 months time point (Fig. 21 B)

- Cluster group three contains genes, which exhibit expression changes starting at the 6 months time point (Fig. 21 C).

K-mean clustering was independently performed for genes differentially regulated in *Cnp1* and *Plp1* mutant CPN. Selected members of each cluster are listed in Appendix A, Appendix B and **Appendix C**.
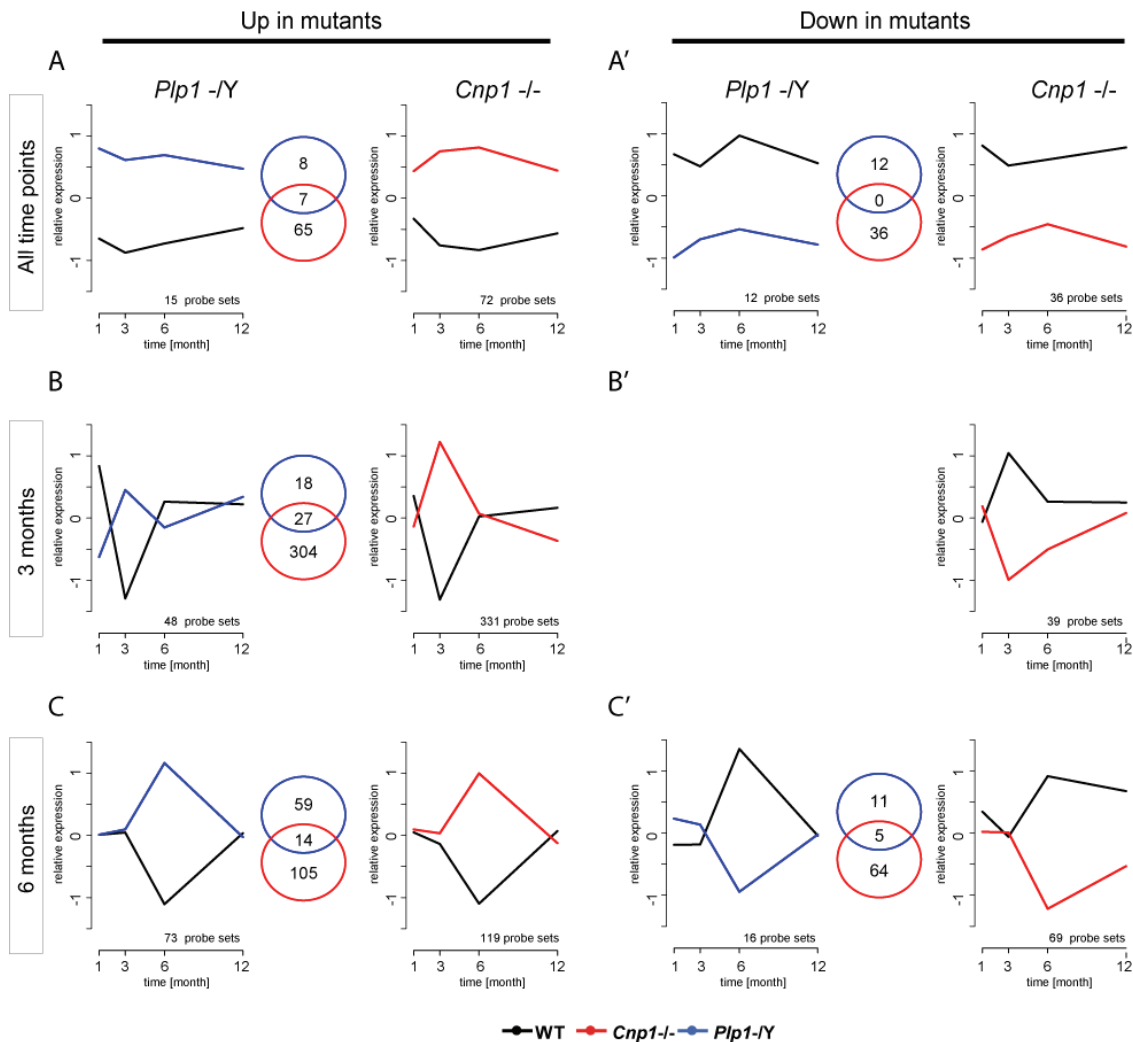
Fig. 21: K-means clustering of affected genes into similar profiles
K-mean clustering separated 2-way ANOVA significant genes (p val < 0.001, average expression > 2 * SD) into 6 clusters. The diagrams of clusters A to C show transformed and called expression values (y-axis) obtained by microarray analysis for each time point (x-axis). Each group is represented by a prototypical expression profile. For each group the corresponding graph is drawn for *Plp1*-/Y (blue) and *Cnp1*-/- (red) mutants both for up-regulated (A, B, C) and for down-regulated in the knock-outs (A', B', C'). Adjacent Venn diagrams illustrate overlapping genes in both mutants. (A, A') Genes that are expressed at higher/lower levels in *Cnp1* -/- and *Plp1* -/Y mutants at all time points; (B, B') genes that exhibit only expression changes at 3 months and (C, C') at 6 months time point.

Following our initial aim to identify differentially regulated genes in CPN in myelin mutant mice to uncover neuronal responses to loss of either Plp or Cnp

and based on the fact that we identified a rather modest number of differentially expressed genes in *Plp1* mutants in contrast to *Cnp1* mutants, we focused our subsequent analysis on samples derived from *Cnp1* mutants.

6.2.9 Gene Ontology annotation of co-clustered genes

The functional interpretation of microarray datasets still represents a time consuming and challenging task. In order to facilitate the annotation of microarray data we took advantage of the Gene Ontology (GO) consortium (Ashburner et al., 2000). GO provides a structured, controlled vocabulary for describing the function of given gene products in an organism. Three separate ontologies are provided:

- Biological process (BP) describes the biological objective to which the gene product contributes.

- Molecular function (MF) describes the biochemical activity of a gene product.

- Cellular component (CC) refers to the place in the cell in which a gene product exerts its activity.

To group the members of all clusters according their functional annotation, we extracted gene ontology categories shown for all six clusters employing the ID converter from Babelomics suite (Al-Shahrour et al., 2005; Al-Shahrour et al., 2006). GO terms were further analyzed and grouped according to their enrichment in each cluster using the "Blast 2 Go" application (Götz et al., 2008). A representation of enriched GO categories for each cluster is illustrated as pie charts in Appendix D, Appendix E and Appendix F.

6.2.10 Network integration and visualization

We used the Gene Ontology (GO) (http://www.geneontology.org/) and Kyoto Encyclopedia of Genes and Genomes KEGG (www.genome.jp/kegg.html) databases to functionally annotate the gene sets that were obtained by K-means clustering. We used the Visual Analysis Tool for Biological Networks

and Pathways (VISant, version 3.68) http://visant.bu.edu/) to integrate and visualize selected gene set clusters of CPNs from *Cnp1* null mice Fig. 21. We focussed on two clusters: (1st) those that were up- or downregulated in *Cnp1* null mutant CPNs at all time points which we refer to as the *Cnp1*-/- _CPN_CORE network (CCN) and (2nd) those that deviated at 3 months (referred to as the C3N) . We first uploaded the CORE probesets into VISant and visualized up- and downregulated gene products as red and blue circles (referred to as 'nodes'), respectively (Fig. 22). Next we used the VISant-database predictome of protein linked interactions to connect nodes based on published interactions (referred to as 'edges' and drawn as straight and undirected lines between respective nodes). We used the information available for the human protein collection (containing > 90.000 entries compared to the mouse collection with only roughly 6,000 entries) that has been extracted from several large-scale experimental and literature extracted databases (see http://visant.bu.edu/ for interaction statistics and methods selected). The inferred CORE network was arranged using the 'elegant relaxation' mode and subsequently re-arranged manually and extended using literature searches using iHOP (http://www.ihop-net.org/UniPub/iHOP/) and is depicted in Fig. 22. The CCN comprises 62 query (27 are upregulated and 26 downregulated genes) and 370 inferred nodes (in total 432). The number of edges is 424. The interaction network can be described as scale-free by an asymptotic function with $Y = 65,47 * X^{1,36}$ where Y is the number of nodes and X the number of edges.

We subgrouped nodes in so-called 'metanodes' both based on internal connectivity's and knowledge-driven with respect to putative entities relevant for axonal biology. The following metanodes of the CORE network were defined (see **Table 5** for annotations):

Table 5: Metanode annotation

'Filaments' structural proteins likely to be relevant for axonal stability

'Motors' motor proteins involved in anterograde and retrograde axonal transport

'Ribosome' ribsosomal or ribosome-associated proteins involved in translation

'Signaling' proteins with a presumptive function in cellular signalling processes

'Lipds' enzymes and proteins involved in lipid synthesis and homeostasis

'Apoptosis' proteins related to cell death control

'Ubiquitin' proteins involved in controlled protein degradation/stability

'Metabolism' enzymes involved in metabolic processes

Two transcription-related metanodes were subgroup based on internal connectivities and named by the corresponding 'hub' protein showing the highest connectivity:

'ID2' including the HLH factor ID2 and the MADS box protein MEF2C

'MED1' factors interconnected by TP53

A third transcription-related metanode was arbitrarily grouped:

'HBP1' proteins surrounding the HMG-Box factor HBP1
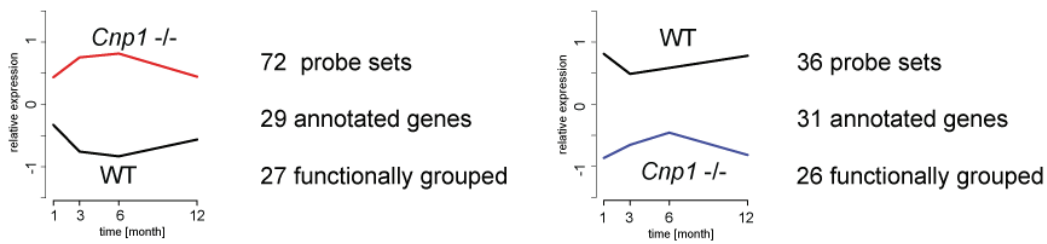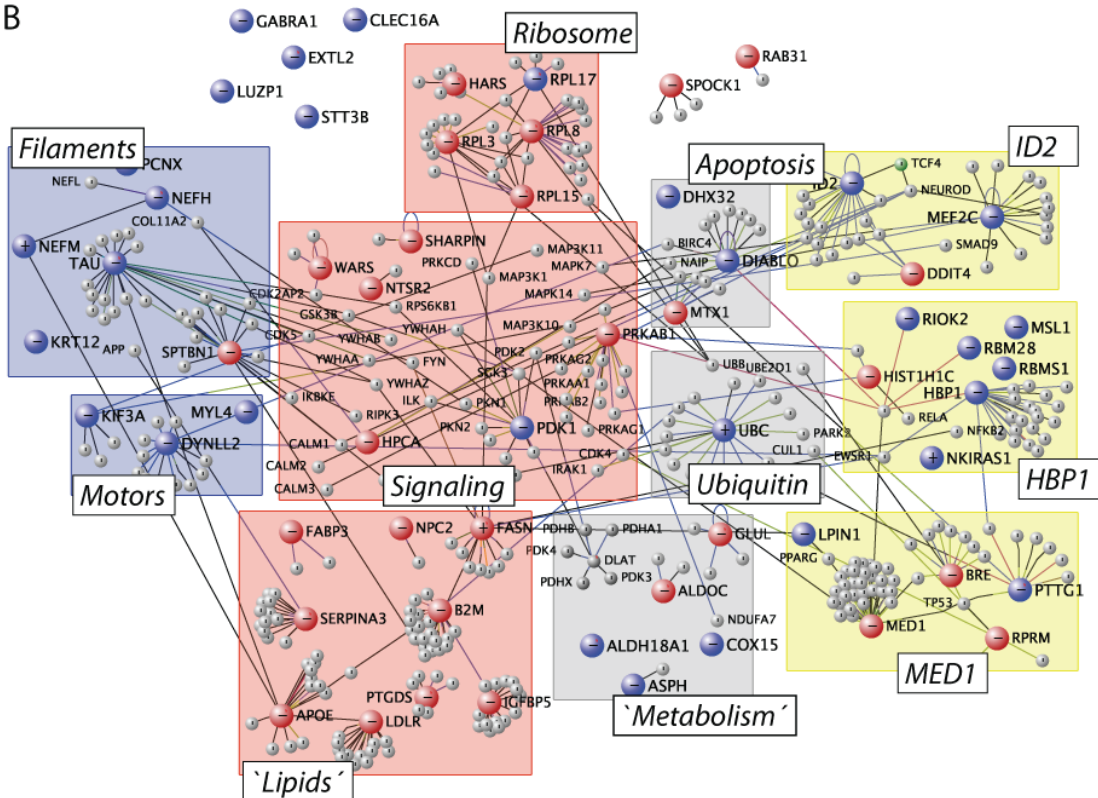
Fig. 22: Integrated 'core' network of genes regulated at all timepoints in CPNs of *Cnp1* null mutant mice (CCN).

(A) Gene-cluster that were either up- (left) or downregulated (right) in *Cnp1* null mutant CPNs were selected for network expansion and visualization. From 72/36 probe sets, 28/31 were annotated either with a GO or KEGG annotation and uploaded into VISant. 27/26 genes were subsequently subgrouped in functionally related subclusters. (B) Visualization of the CCN network comprised of up- and downregulated genes (nodes) depicted as blue and red circles, respectively. First level interactors are depicted as smaller circles in grey. Connections (edges) between nodes represent interactions either downloaded from the predictome database integrated in the VISant tool or from literature scans with iHOP or PubMed.

The CORE network was expanded with the GO/KEGG annotated gene symbols corresponding to the '3M cluster'. These additional nodes were not further extended by the predictome database to keep the core network dense. The

resulting combined network of genes regulated at 3 months was termed *Cnp1*-/-_**C**PN_**3**M **N**etwork (C3N). Nearly half of the genes additionally regulated at 3M could be grouped to the already existing metanodes defined for the CORE network (Fig. 23). The C3N comprises 101 query (75 are upregulated and 27 downregulated genes) and 360 inferred nodes (461 in total). The number of edges is 577. The interaction network can be described as scale-free by an asymptotic function with $Y = 160,7 * X^{1,57}$ where Y is the number of nodes and X the number of edges.

We observed that the complexity and internal connectivity of the C3N was higher as compared to the CCN. This was mainly due to a large increase in nodes and edges in the Signaling and Ubiquitine clusters, arguing for an enhanced demand of regulatory functions at 3 months in CPNs of *Cnp1* null mutant mice (Fig. 24).
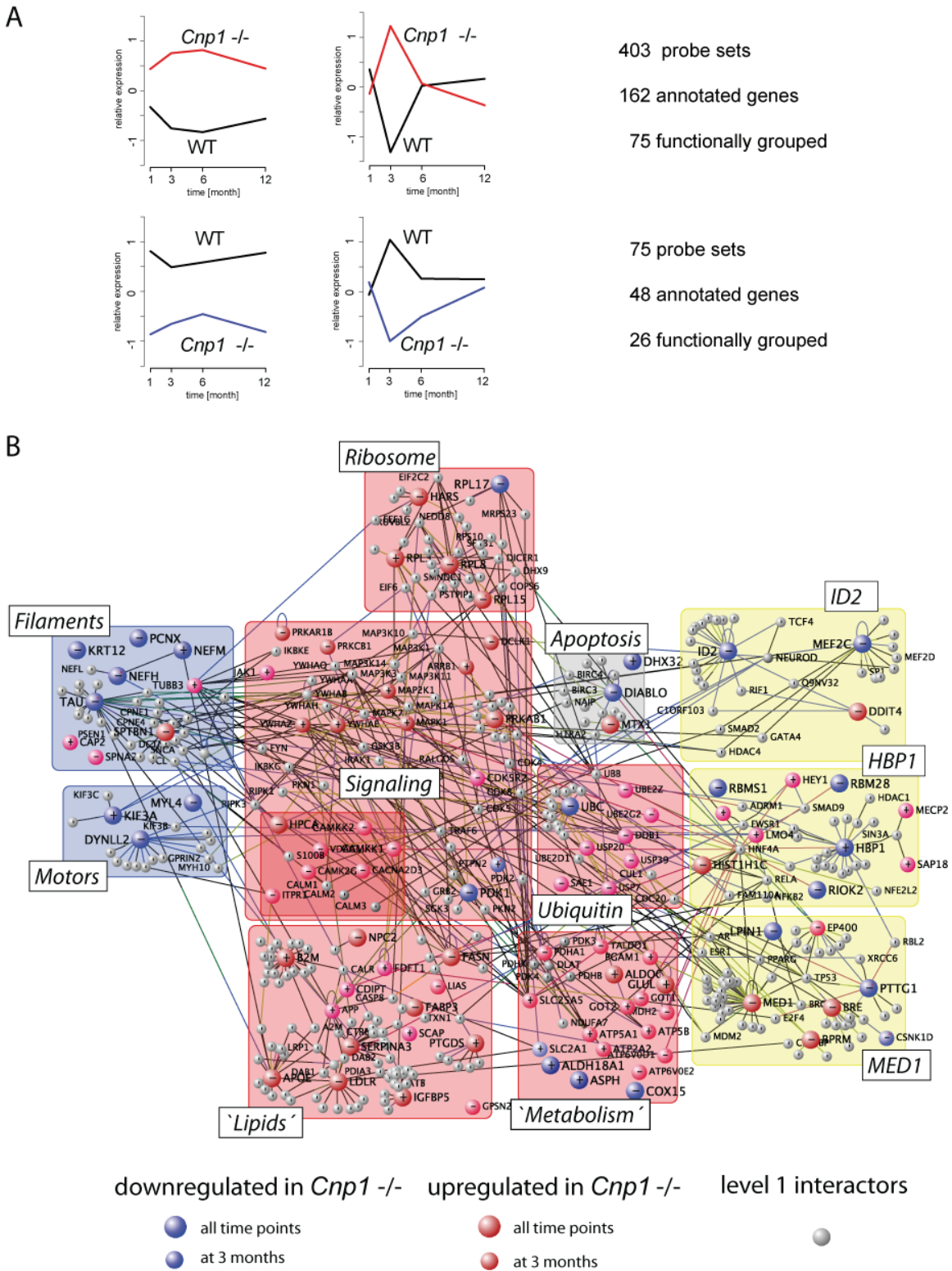
Fig. 23 Integrated 'core' network of genes regulated at all timepoints and at 3 months in CPNs of *Cnp1* null mutant mice (C3N).

(A) Gene-cluster that were either up- (left) or downregulated (right) in *Cnp1* null mutant CPNs at all timepoints and at 3 months were selected for network expansion and visualization. From 403/75 probe sets, 162/48 were annotated either with a GO or KEGG annotation and uploaded into VISant. 75/26 genes were subsequently subgrouped in functionally related subclusters. (B) Visualization of the C3N network comprised of up-

86

and downregulated genes (nodes) depicted as blue and red circles, respectively. Large circles correspond to genes regulated at all time points, whereas smaller circles depict genes found to be regulated at 3 months. First level interactors are depicted as smaller circles in grey. Connections (edges) between nodes represent interactions either downloaded from the predictome database integrated in the VISant tool or from literature scans with iHOP or PubMed.
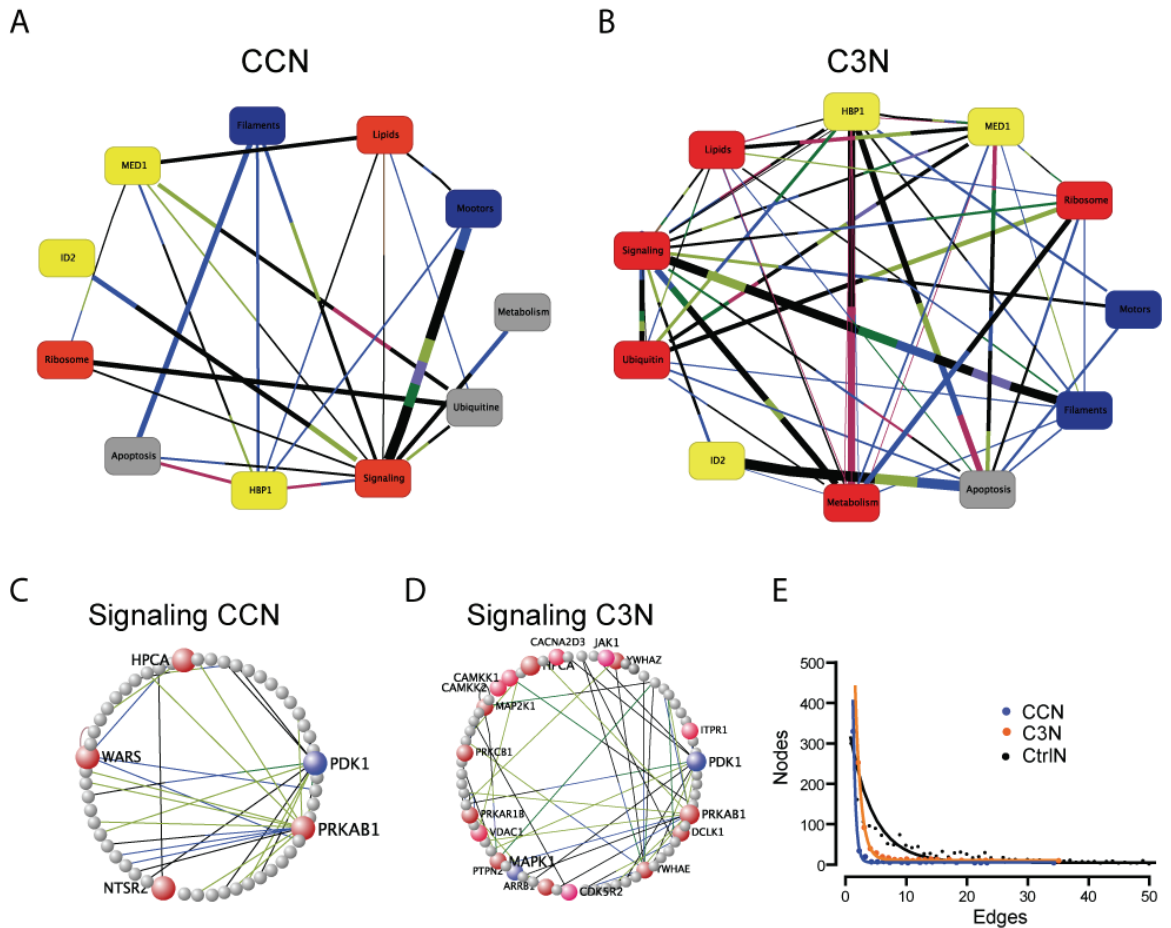
Fig. 24: CCN and C3N network properties.
(A) CCN and (B) C3N network visualization with all functional grouped nodes depicted as collapsed metanodes. Edges were weighted based on shared components, different colours represent different methods that identified interactions. Red metanodes represent grouped genes that are in average upregulated, blue downregulated and grey unregulated. Yellow metanodes refer to transcription related gene sets. (C) Signaling related metanode of the CPN and (D) C3N network. Note the change of query and level 1 interactors and the enormous increase in connectivity. (E) Number of CPN (blue) and C3N (red) nodes plotted as a function of connected edges. Depicted in black is part of a reference protein interaction network downloaded from VISant. Note. That both CPN and C3N curves are more steep indicating a high number of hubs (that I shighly connected nodes) within the respective networks.

In summary, the network level analysis revealed core sets of functionally grouped genes that are most likely relevant for the adaptation to the axonal stress caused by the lack of the CNP1 in oligodendrocytes. Among the most

interesting findings is the tight coupling of phosphor-signaling and structural components as well as the unexpected link towards an altered lipid homeostasis. Equally important with respect to current hypotheses regarding an trophic and/or metabolic support of axons by oligodendroglial cells are our findings of the coordinated downregulation of the pyruvate dehydrogenase kinase 1 (Pdk1) and up-regulation of key metabolic enzymes involved in the mitochondrial NADH shuttle, which seems to be required when lactate rather than glucose might be available as energy source.

6.2.11 Loss of *Cnp1* mediates transcriptional changes in CPN for genes involved in TP53 relevant pathways

Another focus of this study was to identify differentially expressed genes, which respond already at the 1 month time point to loss of major myelin proteins. These genes may reflect an early compensatory response of neurons to loss of glial support. We thus examined the CCN group (Fig. 21 A, A') to identify potentially promising candidate genes. Candidate genes were validated using QRT-PCR. One of the most interesting genes, which exhibited a highly significant constitutive up-regulation exclusively in *Cnp1* null mutants, is the mediator complex subunit 1 (Med1, p-value < 0,0001). The MED1 protein, interacts with nuclear receptors and transcription factors to form the mediator coactivator complex, which facilitates promoter recruitment and function of RNA polymerase II and associated general transcription factors. First identified as a part of a defined complex in yeast, *Med1* is evolutionarily conserved and belongs to a multi-protein complex that contains approximately 30 subunits. It is believed to connect transcriptional activators with the RNA polymerase II transcription machinery and appears to be essential for most, but not necessarily all, RNA polymerase II-mediated transcription. There are four different splice variants annotated for *Med1* in ENSEMBL. Variant 1, 3, and 4 code for transcripts ranging from 4900 bp to 5500 bp, whereas variant 2 is a shorter isoform lacking the 3'-end (2100 bp) shown in Fig. 25 A. The MOUSE430 A 2.0 microarray (Affymetrix) allows to distinguish between variant 2 and the longer variants 1, 3, and 4. In contrast to probesets coding for

variant 2 displaying no differential expression, probe sets for the variants 1, 3, and 4 revealed a strong up-regulation in *Cnp1* null mutants. Microarray expression profiles of *Med1* are shown in Fig. 25 B.
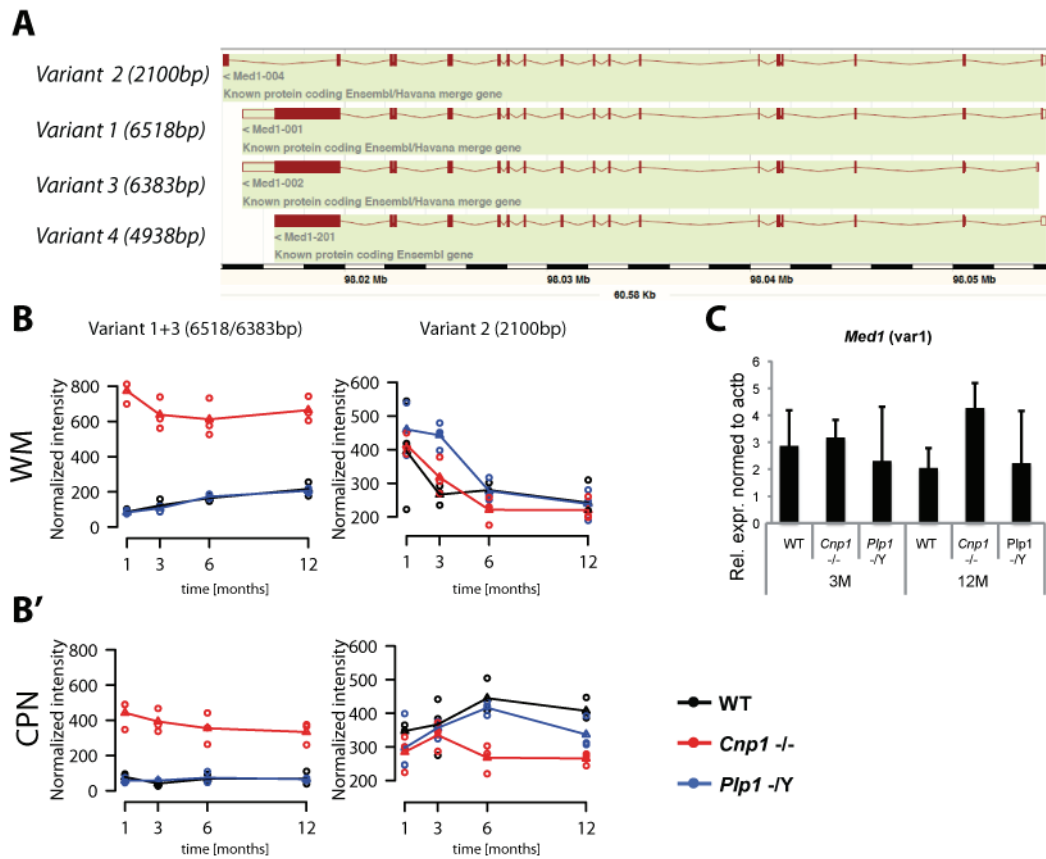
Fig. 25: Med1 mRNA expression is up-regulated in *Cnp1* null mutants.
(A) Four splice variants are annotated in Ensembl for Med1. (B) Time course expression profile of variant one and three shows constitutive higher expression in *Cnp1* mutant CPN compared to WT and *Plp1* mutant mice. Short variant 2 shows a similar expression profile for all groups over time. Plotted are normalized intensities; triangles represent mean values of three biological replicates; circles represent expression values for each biological replicate separately. (C) QRT-PCR results of whole cortex samples obtained from the same biological replicates used for microarrays (n=3). Significant up-regulation of Med1 at 12 months of age can be observed, changes at the 3 months time point were not significant. Error bars indicate standard error of the mean.

Using appropriately-sized spates we isolated total RNA from whole Cx at 3 and 12 months time points from the same brain samples, which were profiled by microarray analysis. Reverse transcribed cDNA was used for QRT-PCR. Relative quantification (ddCt-method) of *Med1* using specific hydrolysis probes revealed no difference at 3 months between WT, *Cnp1* and *Plp1* mutant samples, in contrast to the 12 months time point where we could observe a significant

higher expression in *Cnp1* mutants (Fig. 25 C). *Med1* in general was characterized by very low expression levels close to the detection limit (average Ct-values = 37, Beta actin (*Actb)* Ct = 23).

Genes, which were significantly down-regulated over all examined time points included cytokeratin 12 (*Krt12*) and human pituitary tumor transforming gene (*Pttg1*). *Krt12* showed a complete loss of transcripts in CPN of *Cnp1* mutants, shown in Fig. 26 A, which could be validated with QRT-PCR illustrated in Fig. 26 A''. On microarrays, no expression for both genes in WM samples was detected (Fig. 26 A'). The mRNA expression profiles obtained by microarrays of *Pttg1* revealed a down-regulation in CPN and WM of *Cnp1* mutants in all time points, depicted in Fig. 26 B, B'. Down-regulation of *Pttg1* could be validated by QRT-PCR in Cx samples for 12 months, but not for 3 months, where QRT-PCR indicated no significant difference in relative mRNA expression levels of *Pttg1*, as shown in Fig. 26 B''.
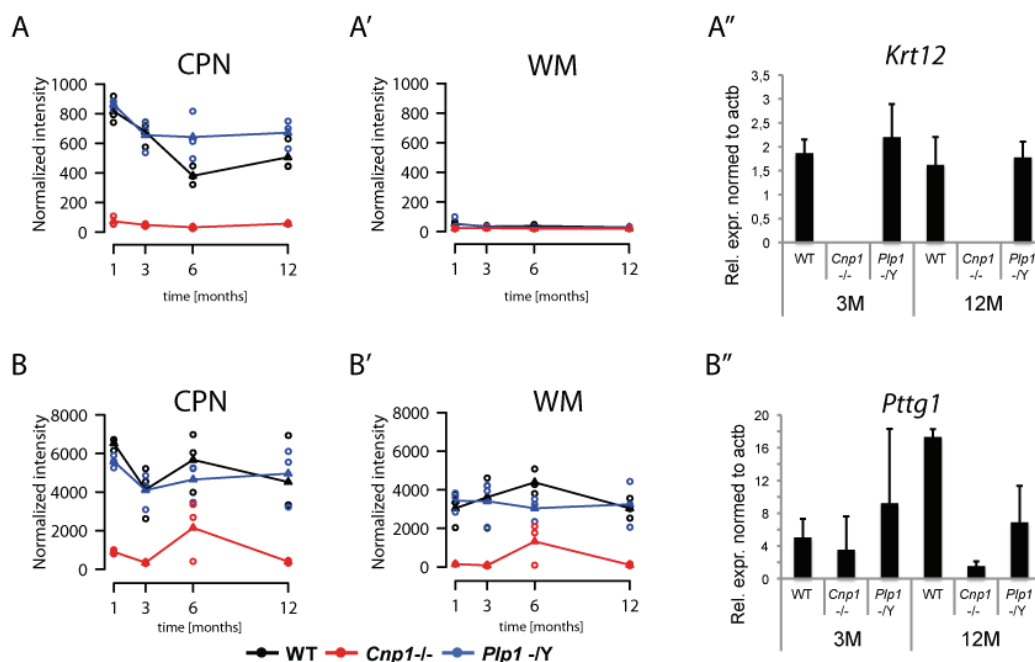
Fig. 26: mRNA expression profiles of *Krt12* and *Pttg1*
(A) Microarray profiles of *Krt12* mRNA showed complete loss of transcripts in *Cnp1* mutants at all time points. (A') *Krt12* could not be detected at the level of transcription in WM samples. Plotted are normalized intensities; triangles represent mean values of three biological replicates; circles represent expression values for each biological replicate (n = 3). (A'') QRT-PCR of three independent animals per genotype (n = 3) using cDNA derived from whole Cx validate findings from microarray data for *Krt12* (hydrolysis probe assay). Plotted are relative expression levels normalized to *Actb*. Error bars

represent SD. (B) Gene expression profiles of *Pttg1* showed decreased levels of transcription in *Cnp1* mutants over all time points. (B') Corresponding microarray profiles of WM samples showed the same tendency as in CPN. Plotted are normalized intensities; triangles represent mean values of three biological replicates; circles represent expression values for each biological replicate (n = 3). (B") QRT-PCR of three independent animals per genotype (n = 3) using cDNA derived from whole Cx validate findings from microarray data for *Pttg1* (hydrolysis probe assay) for the 12 month time point. Results for the three months time point exhibit a tendency towards down-regulation, but the differences are not significant. Plotted are relative expression levels normalized to *Actb*. Error bars represent SD.

92

7 Discussion

7.1 Cell purification techniques in the CNS

The cellular complexity in the CNS of mammals is enormous. The number of distinct neuronal cell types in the mammalian 'neurome' (10^3-10^4) is likely to be within an order of magnitude of the genes in the mammalian genome (2-3x 10^4). It seems very unlikely that single genes specify or can serve as markers for single cell types making the identification of distinct cell types extremely challenging. Most applications are limited by the lack of identifying single cell populations.

7.1.1 Identification methods

There are several approaches available to identify specific cell types. All of them have their benefits and limitations, which are briefly discussed here. The simplest method does not inlcude no labelling at all; cells are chosen randomly or based on position, morphology or electrophysiology. However, identification of cell types is *post-hoc*, so rare types can be missed and also the reproducibility is very difficult to assess. A similar approach involves unspecific cell labelling such as Nissl staining. An example is the dye thionin that intercalates in (predominantly ribosomal) nucleic acids, and labels therefore any cell on the slide. Nissl staining methods allow identification of cell types upon morphology (size, arborization), and position and, most importantly for our approach, are LCM compatible (Xinyu Zhao et al., 2001b; Hinkle et al., 2004a). Nissl staining becomes especially interesting for tissues where alternative methods are limited, as is the case for human brain samples.

Immunocytochemical labelling of cells with antibodies against known markers serves to distinguish between specific cell types. This approach allows the integration of several markers at the same time, which enables more precise selection of target cells due to several possible combinations. Antibody labelling can be performed on living cells for instance in combination with FACS or manual sorting. A limitation is the constriction to extracellular epitopes and the fact that samples are processed for several hours outside of their physiological environment, potentially mediating transcriptional changes in manipulated cells.

Antibody labelling can be also employed for LCM on unfixed cryosections requiring incubation in aqueous condition, which can compromise RNA integrity. However, Greene and colleagues used successfully an antibody against Tyrosine hydroxylase on cryosections to identify midbrain dopamine neurons for LCM (Greene et al., 2005).

Identifying cells with a tracer dye is another possibility to label specific types of neural cells. Hereby, cells are labelled by stereotaxic injection of fluorescent tracers into projection targets. Tracer dyes are absorbed by axons and are then retrogradely transported into the cell body. The internal restriction to this method is that only projection neurons are targeted, whereas multiple cell types can share projection targets. Transgenical labelling is one of the most consistent cell type identification approaches. During the last decade, hundreds of transgenic mice were generated, which express fluorescent proteins driven by cell type-specific promoters or enhancers to label for instance different neural cell populations. These mouse lines are compatible with FACS or manual sorting to isolate pure cell populations. A major drawback of these mice is its incompatibility with LCM. The fluorescent signal gets rapidly lost during section preparation. Therefore, we used a mouse line, which expressed a nuclear variant of EYFP under the control of the *Thy-1* promoter (Rossner et al., 2006). Nuclear localization of EYFP leads to cellular signal enhancement and is compatible with LCM. But generation of reliable reporter mice is laborious and cost-intensive, and limited availability of cell-type specific promoters further hampers the generation of these useful tools. In short, the choice of the appropriate labelling method depends strongly on the downstream analysis and funds.

As for labelling methods, many different approaches have emerged to isolate specific cell populations from brain. We discuss here briefly the most commonly applied methods in neuroscience.

7.1.2 Cell Isolation techniques in CNS

7.1.2.1 RNA-tagging

RNA tagging provides a way to purify mRNA from a genetically labeled cell population without the need to identify and isolate cells. A FLAG-tagged poly(A)-binding protein (PABP) is expressed in the population of interest, where it binds to polyadenylated mRNA. The tissue is fixed, to cross-link the PABP covalently to the mRNA, and then homogenized. mRNA from the cell population of interest is affinity-purified by anti-FLAG antibodies. The gene expression of ciliated sensory neurons in *C. elegans* was transcriptionally profiled used mRNA tagging (Kunitomo et al., 2005). In a different study polyadenylated RNAs from photoreceptors in *D. melanogaster* were enriched using this method (Z. Yang et al., 2005). Expression of known cell type markers validated in both cases reliability of this technical approach.

7.1.2.2 Single-cell aspiration

Following patch clamp recording, cytoplasmic contents can be aspirated. This approach enables the combination of electrophysiology and anatomy of transcriptomic or proteomic techniques in the same cell. Due to the tiny sample amounts obtained from single cells, which represent only a fraction of the corresponding population, high measurement noise and frequent false-negative results are a major drawback of this approach. These techniques were successfully employed by (J Eberwine et al., 1992), (Hinkle et al., 2004b), (Cauli et al., 2000) and (Toledo-Rodriguez et al., 2004).

7.1.2.3 Manual sorting

Manual sorting is the isolation of dissociated cells expressing a specific marker under a fluorescence microscope, using for instance a glass pipette for collection. This approach yields usually high purity of collected samples and it is applicable to isolate adult cells as well as dimly labeled cells. One of the pitfalls is the low RNA yield, which further requires RNA amplification for microarray analysis. A second drawback is the time-consuming procedure which may have an impact on transcriptional changes. However, transcriptome profiling of

twelve neuronal subpopulations could be performed employing manual sorting, where neurons of the forebrain were distinguished based on specific expression of fluorescent proteins (Sugino et al., 2006). RNA was successfully amplified and hybridized to microarrays. The authors could identify several novel cell type specific marker genes using this approach.

7.1.2.4 Fluorescence activated cell sorting

High purity of neuronal populations can be achieved using live-cell sorting because dissociated cells can be stripped completely bare of contaminating factors such as neuronal fibers, extracellular matrix and monocytes. In addition, such samples provide RNA in a pristine form because they are not subjected to freezing or fixation. Moreover, FACS can sort up to millions of cells depending on the source and can therefore be used for microarrays without additional amplification of RNA. On the other hand, there are also limitations inherited in this approach. Samples have to be handled for several hours to prepare them for FACS sorting, during which changes in gene expression can occur. In addition, cells have to be treated with proteases and are therefore removed from their cellular context, which represents a huge impact. Thus, during preparation, cells are exposed to enormous stress and it is likely that they react also on the level of transcription. Interpretation of microarray data obtained by this approach is therefore complicated because stress responses of isolated cells could mask relevant changes in gene expression. Neural cells, being in general highly fragile, can be FACS-sorted until P25 - P35, depending on the cell type of interest, restricting this technique to the analysis of embryonic and early postnatal stages. However, developmental questions such as cell type differentiation can be addressed using this technique in combination with numerous available reporter mice.

One of the first successful applications of FACS on neural samples provided insight into the transcriptome of touch receptors of *C. elegans*, which were labelled by GFP (Y. Zhang et al., 2002). Similar progress has been made in cell-type-specific expression profiling in the mammalian nervous system. GFP-expressing neural crest stem cells were FACS-sorted and profiled at several

developmental stages as they differentiate into Schwann cells, revealing hundreds of genes likely to be involved in this process (Buchstaller et al., 2004). Transcription profiles derived from specific neuronal subpopulations in the mammalian CNS were generated using live-cell sorting (Arlotta et al., 2005). In this study, the authors could detect several genes, which were only expressed by specific neuronal subpopulations, and therefore discovered new subpopulation specific markers, which could be further validated by immunohistochemstry (IHC) and *in-situ* hybridization (ISH).

In the present study, we applied FACS for highly purifying acutely-isolated specific glial cell types from developing mouse forebrain. We took advantage of three different mouse lines, which express fluorescent proteins driven by cell type-specific promoters to identify GPCs (hGFAP-EGFP), MG (*Cx3cr1*-EGFP), and OLs (*Plp1*-DsRed) (Fig. 5). We dissociated brains of these mice with papain, purified fluorescent cells on an automated FACS, and finally extracted mRNA for whole transcriptome microarray analysis.

The applied quality controls demonstrated high microarray performance and absence of major batch effects (Fig. 6). Global mRNA expression patterns of different glial cell types reflected nicely their affiliation to each other and further supported the reliability of the dataset. Expression profiles of several known marker genes validated the purity and identity of the isolated cell types (Fig. 7). We could detect a significant set of specifically expressed genes for every cell type under investigation (Fig. 7). Those genes represent potential new cell type-specific markers but need to be further validated with IHC or ISH.

The use of DNA microarray technology is very attractive for large-scale studies of alternative splicing. By measuring the relative amounts of distinct splice forms in a variety of tissues, microarrays could both test whether a novel splice form really constitutes an important fraction of the gene's transcripts in at least some cell types, and reveal its patterns of regulation across a large number of different tissues.

Taking full advantage of microarray technology to analyze alternative splicing poses many challenges for current methodologies. Traditional microarrays are designed to measure the total level of expression of a gene, without attempting to distinguish between different splice forms (for a review see (Butte, 2002)). For example, probe designs and labeling protocols used for microarray experiments tend to be biased towards the 3' end of the gene (G.K. Hu et al., 2001). As each gene is assumed to be expressed as a unit, this is not considered to be a problem. By contrast, for alternative splicing it is important to have probes throughout all regions of the gene - ideally covering all exons as well as splice junctions.

Alternative splicing also poses new challenges for microarray data analysis. The overall expression level of a gene can be represented by a single number and can be measured with reasonable accuracy by averaging the signals of many probes for the gene (Lipshutz et al., 1999). Individual probes that diverge significantly from the average profile are generally considered to be outliers and are excluded from the analysis (Li and Wong, 2001). But such 'inconsistent' results (in which a subset of probes show a large change in signal that is not seen in other probes for the gene) are exactly what alternative splicing will cause. Thus demonstrating that the probes considered by standard expression-data analysis to be 'noise' are actually reproducible signals, indicative of different patterns of regulation of multiple splice forms is highly challenging.

Despite these challenges, there is now broadly reproducible evidence that alternative splicing can be detected using microarrays. For example, (G.K. Hu et al., 2001) used standard Affymetrix array designs to search for evidence of alternative splicing in 1,600 rat genes, performing hybridizations with 10 normal tissue samples. They found that 268 genes (17%) showed signs of alternative splicing, and validation by QRT-PCR indicated that about half of these represented genuine alternative-splicing events. This work clearly demonstrates that microarrays can detect alternative splicing, but many types of alternative splicing have probably been missed in this study because of technical limitations

99

such as 3' labeling bias and the absence of probes designed to detect splice junctions.

Exon level analysis on our dataset revealed a large number of potential alternative splicing events between different cell types, which have to be further validated using QRT-PCR. The MOUSE Exon 1.0ST array used in this study provides expression levels for single exons but not for exon-exon junctions rendering transcript variant prediction difficult.

Our generated datasets may serve as a seed towards a transcriptome database housing genome-wide gene expression values for main glial cell types in the CNS. Our experimental approach can also be applied to study transcriptional changes occurring in specific cell types in pathological conditions such as neurodegeneration. The technique-inherited limitation to early postnatal stages does not allow analysis of more disease-relevant changes in the adult CNS. The generation of such datasets could offer resources to the neuroscience community to better understand functions of neural cell types in their physiological context. Databases of cell type-specific transcriptome data complement existing online available resources, which contain regional gene expression patterns like the Allen brain atlas (www.brain-map.org) and GENSAT (www.gensat.org). These *in situ* tools correlated to a high degree with our expression data (data not shown) and therefore served as an invaluable resource for cross-validation. The genome-wide coverage of microarrays enables us to quantitatively detect much more cell type specific differential expressed genes. In particular the usage of whole transcriptome microarrays, designed for analysis of alternative spicing events, provides powerful tools to look into cell type-specific changes which can hardly be detected using standard techniques like IHC or ISH.

7.1.3 Laser capture microdissection

Laser-capture microdissection (LCM) is a method to procure subpopulations of tissue cells under direct microscopic visualization. LCM technology can harvest the cells of interest directly or can isolate specific cells by cutting away

unwanted cells to give histologically pure enriched cell populations. LCM is most commonly performed on cryo sections, which are subsequently dehydrated to prevent RNA degradation. Cryo section can also be subjected to several staining protocols (see section 7.1.1). To obtain CNS tissue, brains are removed from the skull and directly frozen on dry ice; therefore cell status is captured immediately after death. To perform FACS, manual sorting or single cell aspiration the cells are exposed to enormous stress for up to several hours after displacement from their physiological environment. Expression of immediate early genes for instance is induced after 10 min in a stress paradigm (Honkaniemi et al., 1994; Burmeister et al., 2008), demonstrating that cells change rapidly their pattern of transcription to adapt to new stress situations. Physiological relevant differences in vivo could be masked by stress-induced changes in gene transcription ex vivo. LCM method provides a snap shot of the transcriptome taken at the time when animal was sacrificed.

LCM was successfully applied in several studies to purify specific cell types fom the CNS. Midbrain dopaminergic neurons have been a favored target for such investigations, both because of their clinical importance in neurodegenerative disorders such as Parkinson's disease and because they are readily labeled by antibodies to tyrosine hydroxylase (TH), the enzyme responsible for the production of dopamine. Two groups (Chung et al., 2005), (Greene et al., 2005) compared dopaminergic neurons from neighboring midbrain regions, the ventral tegmental area (VTA) and the substantia nigra, to identify genes that might contribute to the higher susceptibility of the latter population to neurodegeneration in Parkinson's disease. Both studies identified numerous genes that had statistically significant differential expression. (Yao et al., 2005) compared VTA dopaminergic neurons with corticostriatal pyramidal cells retrogradely labeled by striatal injection of fluorogold. Several dozen genes were identified as differentially expressed using very rigid criteria. Several genes enriched in corticostriatal neurons match those found in this cell type by other investigators using cell-type-specific expression analysis (Arlotta et al., 2005; Sugino et al., 2006). Altogether, these studies demonstrate that LCM achieves sufficient purity and RNA integrity, and thus serve as a useful

complement to the cell-sorting approaches outlined in the previous section, especially because it can be more readily applied to the study of human tissue. We could in a different study successfully capture transcription profiles of human hippocampal CA4 neurons of schizophrenic patients and healthy controls (Wichert et al. manuscript in preparation).

7.2 Gene expression changes in CNS cell subpopulations in *Cnp1* and *Plp1* deficient mice over time

The central aim of the presented thesis was to determine gene expression profiles (i) of white matter and (ii) of cortical projection neurons in wild-type and two genetically modified mouse lines that lack functional *Plp1* and *Cnp1* genes, respectively. The corresponding proteins, PLP and CNP, are major constituents of CNS myelin sheaths, which engulf axons to enable rapid saltatory signal propagation. Somewhat surprisingly, however, *Cnp1* and *Plp1* null mice display first signs of axonal damage at around 3 months of age before structural myelin alterations, signs of demyelination or behavioral phenotypes become apparent (Klugmann et al., 1997; Lappe-Siefke et al., 2003). This observation led to the hypothesis that a still unknown glial support mechanism (or mechanisms) may be missing in the respective mutant mice causing local axonal stress and damage (Klugmann et al., 1997; Lappe-Siefke et al., 2003). Axonal loss is a central but still underappreciated mechanism that is part of the phenotypes observed most likely in all neurodegenerative diseases. The processes that underlie axonal degeneration and eventually secondary neuronal loss are not very well understood. The causes of human neurodegenerative diseases are often genetically highly complex and display many individual and local differences. The investigation of the mechanisms leading (or protecting from) axonal damage in patients suffering from Multiple Sclerosis (MS) and in corresponding mouse models is further complicated by inflammatory processes that likely contribute to the disease severity (De Vos, 2000; Stagi et al., 2005; Stagi et al., 2006). Axonal damage can be observed upon acute ischemic lesions, however, corresponding animal models display a high experimentally variability rendering precise molecular investigations difficult. For several

reasons, the genetic mouse models and experimental strategy we employed to study axonal degeneration offered several advantages and opportunities:

(i)   By introducing a transgenic and microdissection-compatible label (a nuclear expressed GFP variant), we were able to isolate cell bodies and the corresponding RNAs of cortical projection neurons at high purity whose axons were most likely evenly affected by the glial defect.

(ii)   Axonal damage occurs physiologically in a progressive manner, ranging from 'normal' to pathological conditions that is characterized by enhanced debris clearance by activated microglia and is accompanied by a 'stress-response' of astroglial cells particularly in white matter tracts. Both our time-course, as well as the investigated cell types, take this into account

(iii) Age-, sex-matched and cell-type-enriched analyses reduced the experimental variability and -most likely- improved the specificity of the results.

(iv)   We hypothesize that the corresponding neuronal gene expression profiles reflect direct markers of the disease mechanisms eventually detectable before histological or behavioral phenotypes.

7.2.1   QC controls see

Expression profiling from LCM derived samples inherits several challenges including limited RNA amount/quality and purity of sample isolation (contamination). We isolated RNA from 700 - 800 CPN yielding in minute amounts of total RNA (<1 ng), therefore RNA quality as well as quantity could not be evaluated. Isolated RNA was subjected to 2-round T7-RNA polymerase-mediated linear amplification, yielding in up to 10µg amplified RNA. From previous observations, we know that RNA integrity is compromised during cryo-section preparation, dehydration-, and LCM-procedure (data not shown) but is still suitable for reliable microarray analysis. In order to draw valid conclusions from microarray data, analysis quality control (QC) parameters have to be evaluated critically. Standard QC parameters showed typical values. RNA quality

was comparable in all samples under investigation supported by homogeneous RNA degradation slopes between the samples, which is a crucial feature. Reliability of the dataset was further supported by high correlation of biological replicates. Our microarray data met stringent QC criteria and indicate therefore high microarray performances. Moreover, results for the cell type specific marker gene expression showed high purity of the LCM procedure.

7.2.2 Correlation of histological parameters with marker gene expression

Although the activation of astrocytes and microglia has been reported in previous studies in *Cnp1* and *Plp1* null mutant mice (Klugmann et al., 1997; Lappe-Siefke et al., 2003; Edgar et al., 2009), we performed quantitative analyses of immunohistochemical stainings to allow a precise kinetic comparison of marker gene expression and protein detection for all time points investigated. However, only selected time points were analyzed. Oligodendrocytes were stained for nuclear APC (using the CC1 antibody) and revealed neither dramatic changes between genotypes nor at different time points in the CC. A slight increase in the number of CC1 positive cells was observed from 1 month to 12 months old animals. This finding may indicate a slightly increased number in oligodendrocytes or could reflect an improved detection/higher expression level of APC with the CC1 antibody. Since probably not all oligodendrocytes in white matter tracts stain positive for CC1 (M. Rossner, unpublished observation), the latter scenario appears to be more likely. This finding is, however, in agreement with previous findings (Klugmann et al., 1997; Lappe-Siefke et al., 2003) and (Burzyńska, 2007) showing normally sized white matter structures in and *Plp1 null* mice. In the cortex, the number of CC1^{+} cells likely reflecting oligodendrocytes remained also constant from 1-6 months. At 12 months, the antibody detected not only small nuclei but also large cell bodies of -most likely- pyramidal neurons rendering an unambiguous interpretation difficult. That the number of oligodendrocytes most probably did not change over time in the CC was corroborated by the expression of oligodendrocyte specific genes. Although *Plp1* mRNA was reduced

to app. 50% of the expression level seen at 1 month, *Cnp1* expression (as well as other myelin markers such as *Mobp* or *Mbp*, data not shown) remained constant. The *Plp1* and *Cnp1* messages were not detected in the corresponding null mutants. The gradual down regulation of the *Plp1* mRNA with age represents itself a novel finding and appears to be a marker for aged white matter/oligodendrocytes that has not been appreciated before.

We also employed histological staining and transgenic labeling to assess the number of all cortical neurons, of cortical projection neurons and Purkinje cell in WT, *Cnp1* and *Plp1* mutant mice. In accordance with published data (Klugmann et al., 1997; Lappe-Siefke et al., 2003) and (Burzyńska, 2007) we could not detect substantially altered numbers of neuronal cells in the cortex as assessed by the pan-neuronal nuclear marker NeuN. Likewise, the analysis of the transgenically introduced *in vivo* label of cortical projection neurons did not reveal altered cell numbers. In contrast, the numbers of cerebellar purkinje cells (PCs) were highly reduced in *Cnp1* null mutants at one year of age likely explaining the severe motor phenotype at this age. This cell-type specific susceptibility is a typical phenomenon of several neurodegenerative diseases including Parkinsons disease (Chung et al., 2005; Greene et al., 2005), Niemann Pick Type C disease, a neurodegenerative lysosomal storage disorder (Ko et al., 2005), Alzheimer (Capetillo-Zarate et al., 2006), and myelinopathies such as Pelizaeus-Märzbacher. We particularly focused in this study on the cell death 'resistant' CPNs since corresponding gene expression profiles of PCs would have been strongly biased by cell death effects rather than serving as indicators of axonal stress.

Immunhistochemical identification of astrocytes was performed with staining directed against GFAP, which serves as a reliable marker for a subpopulation of activated astroglial cells (Ghandour et al., 1983). Quantitative analyses of stained sections revealed an elevated level of GFAP in CC of *Cnp1* null mutants and a time dependent increase in *Plp1 null* mutants. At the level of gene expression, *Gfap* mRNA remained constant in WT CC over time but was substantially elevated both in *Plp1* and *Cnp1* mutants with age. Gene

expression of another astrocytic marker, S100b, was similarly increasing with age in all genotypes. These findings indicate that astrocytes are molecularly activated in both myelin mutants but the cell number may remain constant (assuming that S100b expression represents a reliable indicator of astrocyte cell numbers). The discrepancy of immunohistochemical detection and gene expression of *Gfap* may be explained by different half-lives of protein versus mRNA in CC astrocytes. In the Cx, we observed a several fold increase in *Gfap* positive cells in *Cnp1* mutants with age peaking at 6 months. Interestingly, this peak of astrocyte activation coincides with the peak of axonal swellings and collagen deposition in the CC (Burzyńska, 2007), see below. The expression of the 'astroglial' marker *S100b* in CPNs was corroborated by inspection of the Allen brain atlas (www.brain-map.org), *Gfap* was not detected in the CPN samples.

Microglia activation was assessed with immunostainings directed against MAC-2 and IBA1, showing an age dependent increase in *Plp1* and *Cnp1* mutants. The corresponding gene expression profiles depicted the gradual increase of microglia markers in CC in a more sensitive and reliable fashion. Particularly, *Mac-2* expression was robustly detected in both mutant CC samples already at 3 months further increasing in the 6 and 12 months time points. The *Mac-2* and *Iba1* mRNA profiles correlate well with observations made independently at the level of immunostainings (Burzyńska, 2007).

In summary, marker gene expression profiles very well reflected observations made with immunohistochemical analyses such as genotype- and time-dependent astroglial and microglial activation with constant numbers of oligodendrocyte markers in cortical white matter. In general, marker gene expression profiles were more sensitive in reflecting the increased disease severity seen in *Cnp1* mutants compared to *Plp1* null mice, further supported by total number of deregulated genes at each time point **Fig. 19**. In CPN the pattern of total deregulated gene numbers showed high correlation with disease time course suggesting that our expression profiles reflect neuronal adaptations to oligodendrocyte dysfunction. In contrast reflect the observed

massive transcriptional changes in WM samples more likely the activation of astroglia and microglia in cortical white matte tracts than changes occurring in deficient oligodendrocytes, rendering the dissection of disease relevant gene expression changes rather difficult.

Therefore we addressed our analysis more to the question how neurons react upon loss off glial support on the level of transcription. Due to the fact that we detected a broader response in CPN of *Cnp1* mutants we focused further analysis on this particular mutant. K-mean clustering served as a method to build subgroups of genes, which exhibit similar time course profiles. We were mainly interested in genes, which respond already at the early time points (1 and 3 month) when primary changes in transcription are not masked by secondary effects. Investigation of genes, which showed up/down regulation at all time points, revealed core sets of functionally grouped genes that are most likely relevant for the adaptation to the axonal stress caused by the lack of CNP in oligodendrocytes. Among the most interesting findings is the tight coupling of phospho-signaling and structural components as well as the unexpected link towards an altered lipid homeostasis. That changes in lipid regulation cause mitochondrial dysfunction were previously shown in several studies (Y Huang et al., 2001; F.M. Harris et al., 2003; Chang, 2005; T. Nakamura et al., 2009). Contribution of lipid deregulation to development of neurodegenerative diseases has been proven by several mouse models reviewed by (Adibhatla and Hatcher, 2008). Equally important with respect to current hypotheses regarding an trophic and/or metabolic support of axons by oligodendroglial cells are our findings of the coordinated downregulation of the pyruvate dehydrogenase kinase 1 (*Pdk1*) and up-regulation of key metabolic enzymes involved in the mitochondrial NADH shuttle, which seems to be required when lactate rather than glucose might be available as energy source (Rossner et al., 2006). Network analysis formed a cluster of proteins, which are interacting with TP53 and are deregulated at all time points such as Brain and reproductive organ-expressed protein (*Bre*), Reprimo (*Rprm*), Mediator complex 1 (*Med1*) and Pituitary transforming gene 1 (*Pttg1*) (Tang et al., 2006; Vanlandingham et al., 2005; Frade et al., 2000; Bernal et al., 2002). It was recently demonstrated

that TP53 not only protects neurons from transformation and DNA damage (Jacobs et al., 2006; Helton and X. Chen, 2007) but is also involved in axon outgrowth and regeneration (Tedeschi and Di Giovanni, 2009). *Med1* (constitutively higher expressed in CPN of *Cnp1* mutants), as one of the most significant candidates interacts with nuclear receptors and transcription factors. The Mediator coactivator complex, in contrast to chromatin modifying factors, acts more directly to facilitate promoter recruitment and function of RNA polymerase II and cognate general transcription factors. Another interesting candidate, which interacts with TP53 is PTTG1 (*Pttg1* is constitutively lower expressed in CPN of *Cnp1* mutants) since it was found to be down-regulated in the wallerian degeneration slow (WldS) mouse model and is presently be considered as a candidate for downstream mediation of neuroprotective phenotype in Wlds (Gillingwater et al., 2006). Although *Pttg1* as well as *Med1* also exhibited the same trend in WM micro-regions and appear therefore not to be a neuron specific program but rather a general response of a variety of cell to the loss of *Cnp1*. A third interesting candidate for follow-up investigations is cytokeratin 12 (*Krt12*), which is highly expressed in CPN of WT and *Plp1 null* mutants but absent in *Cnp1* null mutants. Krt12 is the unit of a polymeric protein complex which forms 10 nm intermediate filaments in epithelial cells (Lane, 1993). So far *Krt12* has been described as exclusively expressed in corneal epithelia and mutations of *Krt12* cause Meesmann corneal dystrophy (Corden et al., 2000; Sullivan et al., 2007; Seto et al., 2008). In situ data derived from Allen-brain-atlas (www.brain-map.org) revealed high signal of *Krt12* in cortical layer V neurons, which further corroborated our microarray data. The function of *Krt12* in neurons is so far unknown and will be further characterized in a follow up study.

In summary, we have shown the feasibility to "snapshot" gene expression profiles of genetically defined neuronal subtypes *in vivo* and to compare morphologically similar neurons at a given time in pathological conditions. We followed gene expression changes starting from early disease states until stages of severe pathological signs, focusing on cells known to be susceptible to a genetic predisposition. Our analysis revealed several known and novel

candidate genes and mechanisms that likely play a role in the early adaptive responses of neurons to cope with axonal stress.

8 References

Adibhatla, R.M., and Hatcher, J.F., 2008, Altered lipid metabolism in brain injury and disorders: Sub-Cellular Biochemistry, v. 49, p. 241-268.

Aloisi, F., 2001, Immune function of microglia: Glia, v. 36, no. 2, p. 165-179.

Al-Shahrour, F., Minguez, P., Tárraga, J., Montaner, D., Alloza, E., Vaquerizas, J.M., Conde, L., Blaschke, C., Vera, J., and Dopazo, J., 2006, BABELOMICS: a systems biology perspective in the functional annotation of genome-scale experiments: Nucleic Acids Research, v. 34, no. Web Server issue, p. W472-476.

Al-Shahrour, F., Minguez, P., Vaquerizas, J.M., Conde, L., and Dopazo, J., 2005, BABELOMICS: a suite of web tools for functional annotation and analysis of groups of genes in high-throughput experiments: Nucleic Acids Research, v. 33, no. Web Server issue, p. W460-464.

Arlotta, P., Molyneaux, B.J., Chen, J., Inoue, J., Kominami, R., and Macklis, J.D., 2005, Neuronal Subtype-Specific Genes that Control Corticospinal Motor Neuron Development In Vivo: Neuron, v. 45, no. 2, p. 207-221.

Ashburner, M., Ball, C.A., Blake, J.A., Botstein, D., Butler, H., Cherry, J.M., Davis, A.P., Dolinski, K., Dwight, S.S., Eppig, J.T., Harris, M.A., Hill, D.P., Issel-Tarver, L., Kasarskis, A., Lewis, S., et al., 2000, Gene ontology: tool for the unification of biology. The Gene Ontology Consortium: Nature Genetics, v. 25, no. 1, p. 25-29.

B\ö, L., M\örk, S., Kong, P.A., Nyland, H., Pardo, C.A., and Trapp, B.D., 1994, Detection of MHC class II-antigens on macrophages and microglia, but not on astrocytes and endothelia in active multiple sclerosis lesions.: Journal of neuroimmunology, v. 51, no. 2, p. 135.

Banati, R.B., Gehrmann, J., Czech, C., Mönning, U., Jones, L.L., König, G., Beyreuther, K., and Kreutzberg, G.W., 1993, Early and rapid de novo synthesis of Alzheimer beta A4-amyloid precursor protein (APP) in activated microglia: Glia, v. 9, no. 3, p. 199-210.

Barres, B.A., Hart, I.K., Coles, H.S., Burne, J.F., Voyvodic, J.T., Richardson, W.D., and Raff, M.C., 1992, Cell death in the oligodendrocyte lineage: Journal of Neurobiology, v. 23, no. 9, p. 1221-1230.

Barron, K.D., 1995, The microglial cell. A historical review: Journal of the neurological sciences, v. 134, p. 57–68.

Bartsch, S., Bartsch, U., Dorries, U., Faissner, A., Weller, A., Ekblom, P., and Schachner, M., 1992, Expression of tenascin in the developing and adult cerebellar cortex: J. Neurosci., v. 12, no. 3, p. 736-749.

Bernal, J.A., Luna, R., Espina, A., Lázaro, I., Ramos-Morales, F., Romero, F., Arias, C., Silva, A., Tortolero, M., and Pintor-Toro, J.A., 2002, Human securin interacts with p53 and modulates p53-mediated transcriptional activity and apoptosis: Nature Genetics, v. 32, no. 2, p. 306-311.

Bernard, R., Kerman, I.A., Meng, F., Evans, S.J., Amrein, I., Jones, E.G., Bunney, W.E., Akil, H., Watson, S.J., and Thompson, R.C., 2009, Gene expression profiling of neurochemically defined regions of the human brain by in situ hybridization-guided laser capture microdissection: Journal of Neuroscience Methods, v. 178, no. 1, p. 46-54.

Bhat, R.V., Axt, K.J., Fosnaugh, J.S., Smith, K.J., Johnson, K.A., Hill, D.E., Kinzler, K.W., and Baraban, J.M., 1996, Expression of the APC tumor suppressor protein in oligodendroglia: Glia, v. 17, no. 2, p. 169-174.

Bifulco, M., Laezza, C., Stingo, S., and Wolff, J., 2002, 2',3'-Cyclic nucleotide 3'-phosphodiesterase: a membrane-bound, microtubule-associated protein and membrane anchor for tubulin: Proceedings of the National Academy of Sciences of the United States of America, v. 99, no. 4, p. 1807-1812.

Boison, D., Büssow, H., D'Urso, D., Müller, H.W., and Stoffel, W., 1995, Adhesive properties of proteolipid protein are responsible for the compaction of CNS myelin sheaths: The Journal of Neuroscience: The Official Journal of the Society for Neuroscience, v. 15, no. 8, p. 5502-5513.

Bossy-Wetzel, E., Schwarzenbacher, R., and Lipton, S.A., 2004, Molecular pathways to neurodegeneration: Nature Medicine, v. 10 Suppl, p. S2-9.

Braun, P.E., Sandillon, F., Edwards, A., Matthieu, J.M., and Privat, A., 1988, Immunocytochemical localization by electron microscopy of 2'3'-cyclic nucleotide 3'-phosphodiesterase in developing oligodendrocytes of normal and mutant brain: The Journal of Neuroscience: The Official Journal of the Society for Neuroscience, v. 8, no. 8, p. 3057-3066.

Braun, P.E., 1984, Molecular Organization of myelin, *in* InMyelin, Morell, P. (Ed.) Plenum, NY, p. 97-116.

Buchstaller, J., Sommer, L., Bodmer, M., Hoffmann, R., Suter, U., and Mantei, N., 2004, Efficient Isolation and Gene Expression Profiling of Small Numbers of Neural Crest Stem Cells and Developing Schwann Cells: J. Neurosci., v. 24, no. 10, p. 2357-2365.

Burmeister, S.S., Mangiamele, L.A., and Lebonville, C.L., 2008, Acoustic modulation of immediate early gene expression in the auditory midbrain of female túngara frogs: Brain Research, v. 1190, p. 105-114.

Burzyńska, A., 2007, White matter microstructure in CNS of mouse models of neurodegeneration – a correlation of MRI and histopathology:

Butte, A., 2002, The use and analysis of microarray data: Nature Reviews. Drug Discovery, v. 1, no. 12, p. 951-960.

Cahoy, J.D., Emery, B., Kaushal, A., Foo, L.C., Zamanian, J.L., Christopherson, K.S., Xing, Y., Lubischer, J.L., Krieg, P.A., Krupenko, S.A., Thompson, W.J., and Barres, B.A., 2008, A transcriptome database for astrocytes, neurons, and oligodendrocytes: a new resource for understanding brain development and function: The Journal of Neuroscience: The Official Journal of the Society for Neuroscience, v. 28, no. 1, p. 264-278.

Capetillo-Zarate, E., Staufenbiel, M., Abramowski, D., Haass, C., Escher, A., Stadelmann, C., Yamaguchi, H., Wiestler, O.D., and Thal, D.R., 2006, Selective vulnerability of different types of commissural neurons for amyloid {beta}-protein-induced neurodegeneration in APP23 mice correlates with dendritic tree morphology: Brain, v. 129, no. 11, p. 2992-3005.

Caroni, P., 1997, Overexpression of growth-associated proteins in the neurons of adult transgenic mice: Journal of Neuroscience Methods, v. 71, no. 1, p. 3-9.

Cauli, B., Porter, J.T., Tsuzuki, K., Lambolez, B., Rossier, J., Quenet, B., and Audinat, E., 2000, Classification of fusiform neocortical interneurons based on unsupervised clustering: Proceedings of the National Academy of Sciences of the United States of America, v. 97, no. 11, p. 6144-6149.

Chan, W.Y., Kohsaka, S., and Rezaie, P., 2007, The origin and cell lineage of microglia: new concepts: Brain Research Reviews, v. 53, no. 2, p. 344-354.

Chang, S., 2005, Lipid- and receptor-binding regions of apolipoprotein E4 fragments act in concert to cause mitochondrial dysfunction and neurotoxicity: Proceedings of the National Academy of Sciences, v. 102, no. 51, p. 18694-18699.

Chung, C.Y., Seo, H., Sonntag, K.C., Brooks, A., Lin, L., and Isacson, O., 2005, Cell type-specific gene expression of midbrain dopaminergic neurons reveals molecules involved in their vulnerability and protection: Human Molecular Genetics, v. 14, no. 13, p. 1709-1725.

Colosimo, M.E., Brown, A., Mukhopadhyay, S., Gabel, C., Lanjuin, A.E., Samuel, A.D.T., and Sengupta, P., 2004, Identification of thermosensory and olfactory neuron-specific genes via expression profiling of single neuron types: Current Biology: CB, v. 14, no. 24, p. 2245-2251.

Colton, C.A., and Gilbert, D.L., 1987, Production of superoxide anions by a CNS macrophage, the microglia: FEBS Letters, v. 223, no. 2, p. 284-288.

Corden, L.D., Swensson, O., Swensson, B., Smith, F.J., Rochels, R., Uitto, J., and McLEAN, W.H., 2000, Molecular genetics of Meesmann's corneal dystrophy: ancestral and novel mutations in keratin 12 (K12) and complete sequence of the human KRT12 gene: Experimental Eye Research, v. 70, no. 1, p. 41-49.

Curtis, R., Cohen, J., Fok-Seang, J., Hanley, M.R., Gregson, N.A., Reynolds, R., and Wilkin, G.P., 1988, Development of macroglial cells in rat cerebellum. I. Use of antibodies to follow early in vivo development and migration of oligodendrocytes: Journal of Neurocytology, v. 17, no. 1, p. 43-54.

Dautigny, A., Mattei, M.G., Morello, D., Alliel, P.M., Pham-Dinh, D., Amar, L., Arnaud, D., Simon, D., Mattei, J.F., and Guenet, J.L., 1986, The structural gene coding for myelin-associated proteolipid protein is mutated in jimpy mice: Nature, v. 321, no. 6073, p. 867-869.

Davalos, D., Grutzendler, J., Yang, G., Kim, J.V., Zuo, Y., Jung, S., Littman, D.R., Dustin, M.L., and Gan, W., 2005, ATP mediates rapid microglial response to local brain injury in vivo: Nature Neuroscience, v. 8, no. 6, p. 752-758.

De Vos, K., 2000, Tumor Necrosis Factor Induces Hyperphosphorylation of Kinesin Light Chain and Inhibits Kinesin-Mediated Transport of Mitochondria:

Deiters, O., 1865, Untersuchungen \über Gehirn und R\ückenmark des Menschen und der S\äugethiere. 1865: Braunschweig: Vieweg,

Dickson, D.W., Mattiace, L.A., Kure, K., Hutchins, K., Lyman, W.D., and Brosnan, C.F., 1991, Microglia in human disease, with an emphasis on acquired immune deficiency syndrome.: Laboratory investigation; a journal of technical methods and pathology, v. 64, no. 2, p. 135.

Dong, Y., and Benveniste, E.N., 2001, Immune function of astrocytes: Glia, v. 36, no. 2, p. 180-190.

Dreyfus, C.F., Dai, X., Lercher, L.D., Racey, B.R., Friedman, W.J., and Black, I.B., 1999, Expression of neurotrophins in the adult spinal cord in vivo: Journal of neuroscience research, v. 56, no. 1, p. 1–7.

Dugas, J.C., Tai, Y.C., Speed, T.P., Ngai, J., and Barres, B.A., 2006, Functional Genomic Analysis of Oligodendrocyte Differentiation: J. Neurosci., v. 26, no. 43, p. 10967-10983.

Eberwine, J., Yeh, H., Miyashiro, K., Cao, Y., Nair, S., Finnell, R., Zettel, M., and Coleman, P., 1992, Analysis of gene expression in single live neurons: Proceedings of the National Academy of Sciences of the United States of America, v. 89, no. 7, p. 3010-3014.

Edgar, J.M., McLaughlin, M., Werner, H.B., McCulloch, M.C., Barrie, J.A., Brown, A., Faichney, A.B., Snaidero, N., Nave, K., and Griffiths, I.R., 2009, Early ultrastructural defects of axons and axon-glia junctions in mice lacking expression of Cnp1: Glia, v. 57, no. 16, p. 1815-1824.

Edgar, J.M., McLaughlin, M., Yool, D., Zhang, S., Fowler, J.H., Montague, P., Barrie, J.A., McCulloch, M.C., Duncan, I.D., Garbern, J., Nave, K.A., and Griffiths, I.R., 2004, Oligodendroglial modulation of fast axonal transport in a mouse model of hereditary spastic paraplegia: J. Cell Biol., v. 166, no. 1, p. 121-131.

Endo, A., Nagai, N., Urano, T., Takada, Y., Hashimoto, K., and Takada, A., 1999, Proteolysis of neuronal cell adhesion molecule by the tissue plasminogen activator-plasmin system after kainate injection in the mouse hippocampus: Neuroscience Research, v. 33, no. 1, p. 1-8.

Fitch, M.T., and Silver, J., 2008, CNS injury, glial scars, and inflammation: Inhibitory extracellular matrices and regeneration failure: Experimental Neurology, v. 209, no. 2, p. 294-301.

Frade, R., Balbo, M., and Barel, M., 2000, RB18A, Whose Gene Is Localized on Chromosome 17q12-q21.1, Regulates in Vivo p53 Transactivating Activity: Cancer Res, v. 60, no. 23, p. 6585-6589.

Gao, H., and Hong, J., 2008, Why neurodegenerative diseases are progressive: uncontrolled inflammation drives disease progression: Trends in Immunology, v. 29, no. 8, p. 357-365.

Gehrmann, J., Matsumoto, Y., and Kreutzberg, G.W., 1995, Microglia: intrinsic immuneffector cell of the brain: Brain Research Reviews, v. 20, no. 3, p. 269–287.

Gelman, B.B., 1993, Diffuse microgliosis associated with cerebral atrophy in the acquired immunodeficiency syndrome: Annals of neurology, v. 34, no. 1, p. 65–70.

Geren, B.B., 1954, The formation from the schwann cell surfaceof myelin in the peripheral nerves of chick embryos: Experimental Cell Research, v. 7, no. 2, p. 558-562.

Ghandour, M., Langley, O., and Clos, J., 1983, Immunohistochemical and biochemical approaches to the development of neuroglia in the CNS, with special reference to cerebellum: International Journal of Developmental Neuroscience, v. 1, no. 6, p. 411-425.

Gillingwater, T.H., Wishart, T.M., Chen, P.E., Haley, J.E., Robertson, K., MacDonald, S.H., Middleton, S., Wawrowski, K., Shipston, M.J., Melmed, S., Wyllie, D.J.A., Skehel, P.A., Coleman, M.P., and Ribchester, R.R., 2006, The neuroprotective WldS gene regulates expression of PTTG1 and erythroid differentiation regulator 1-like gene in mice and human cells: Human Molecular Genetics, v. 15, no. 4, p. 625-635.

Giulian, D., and Baker, T.J., 1986, Characterization of ameboid microglia isolated from developing mammalian brain: The Journal of Neuroscience: The Official Journal of the Society for Neuroscience, v. 6, no. 8, p. 2163-2178.

Giulian, D., and Moore, S., 1980, Identification of 2':3'-cyclic nucleotide 3'-phosphodiesterase in the vertebrate retina: The Journal of Biological Chemistry, v. 255, no. 13, p. 5993-5995.

Golgi, C., 1874, Opera Omnia, Vol. I: Istologia Normale:

Gonzalez-Scarano, F., and Baltuch, G., 1999, Microglia as mediators of inflammatory and degenerative diseases: Annual review of neuroscience, v. 22, no. 1, p. 219–240.

115

Götz, S., García-Gómez, J.M., Terol, J., Williams, T.D., Nagaraj, S.H., Nueda, M.J., Robles, M., Talón, M., Dopazo, J., and Conesa, A., 2008, High-throughput functional annotation and data mining with the Blast2GO suite: Nucleic Acids Research, v. 36, no. 10, p. 3420-3435.

Greene, J.G., Dingledine, R., and Greenamyre, J.T., 2005, Gene expression profiling of rat midbrain dopamine neurons: implications for selective vulnerability in parkinsonism: Neurobiology of Disease, v. 18, no. 1, p. 19-31.

Griffiths, I., Klugmann, M., Anderson, T., Thomson, C., Vouyiouklis, D., and Nave, K.A., 1998, Current concepts of PLP and its role in the nervous system: Microscopy Research and Technique, v. 41, no. 5, p. 344-358.

Griffiths, I., Klugmann, M., Anderson, T., Yool, D., Thomson, C., Schwab, M.H., Schneider, A., Zimmermann, F., McCulloch, M., Nadon, N., and Nave, K.A., 1998, Axonal swellings and degeneration in mice lacking the major proteolipid of myelin: Science (New York, N.Y.), v. 280, no. 5369, p. 1610-1613.

Hanisch, U.K., and Kettenmann, H., 2007, Microglia: active sensor and versatile effector cells in the normal and pathologic brain: Nature neuroscience, v. 10, no. 11, p. 1387–1394.

Hardy, R., and Reynolds, R., 1991, Proliferation and differentiation potential of rat forebrain oligodendroglial progenitors both in vitro and in vivo: Development (Cambridge, England), v. 111, no. 4, p. 1061-1080.

Harris, F.M., Brecht, W.J., Xu, Q., Tesseur, I., Kekonius, L., Wyss-Coray, T., Fish, J.D., Masliah, E., Hopkins, P.C., Scearce-Levie, K., Weisgraber, K.H., Mucke, L., Mahley, R.W., and Huang, Y., 2003, Carboxyl-terminal-truncated apolipoprotein E4 causes Alzheimer's disease-like neurodegeneration and behavioral deficits in transgenic mice: Proceedings of the National Academy of Sciences of the United States of America, v. 100, no. 19, p. 10966-10971.

He, F., and Sun, Y.E., 2007, Glial cells more than support cells?: International Journal of Biochemistry and Cell Biology, v. 39, no. 4, p. 661–665.

Heaton, P.A., and Eckstein, F., 1996, Diastereomeric specificity of 2',3'-cyclic nucleotide 3'-phosphodiesterase: Nucleic Acids Research, v. 24, no. 5, p. 850-853.

Hellemans, J., Mortier, G., De Paepe, A., Speleman, F., and Vandesompele, J., 2007, qBase relative quantification framework and software for management and automated analysis of real-time quantitative PCR data: Genome Biology, v. 8, no. 2, p. R19.

Helton, E.S., and Chen, X., 2007, p53 modulation of the DNA damage response: Journal of Cellular Biochemistry, v. 100, no. 4, p. 883-896.

Henle, J., and Merkel, F., 1869, \Über die sogenannte Bindesubstanz der Centralorgane des Nervensystems: Z. rat. Med, v. 34, p. 48–82.

Hinkle, D., Glanzer, J., Sarabi, A., Pajunen, T., Zielinski, J., Belt, B., Miyashiro, K., McIntosh, T., and Eberwine, J., 2004a, Single neurons as experimental systems in molecular biology: Progress in Neurobiology, v. 72, no. 2, p. 129-142.

Hinkle, D., Glanzer, J., Sarabi, A., Pajunen, T., Zielinski, J., Belt, B., Miyashiro, K., McIntosh, T., and Eberwine, J., 2004b, Single neurons as experimental systems in molecular biology: Progress in Neurobiology, v. 72, no. 2, p. 129-142.

Hirrlinger, P.G., Scheller, A., Braun, C., Quintela-Schneider, M., Fuss, B., Hirrlinger, J., and Kirchhoff, F., 2005, Expression of reef coral fluorescent proteins in the central nervous system of transgenic mice: Molecular and Cellular Neurosciences, v. 30, no. 3, p. 291-303.

Honkaniemi, J., Kononen, J., Kainu, T., Pyykönen, I., and Pelto-Huikko, M., 1994, Induction of multiple immediate early genes in rat hypothalamic paraventricular nucleus after stress: Molecular Brain Research, v. 25, no. 3-4, p. 234-241.

Horner, P.J., and Palmer, T.D., 2003, New roles for astrocytes: The nightlife of an 'astrocyte'. La vida loca!: TRENDS in Neurosciences, v. 26, no. 11, p. 597–603.

Hu, G.K., Madore, S.J., Moldover, B., Jatkoe, T., Balaban, D., Thomas, J., and Wang, Y., 2001, Predicting splice variant from DNA chip expression data: Genome Research, v. 11, no. 7, p. 1237-1245.

Huang, Y., Liu, X.Q., Wyss-Coray, T., Brecht, W.J., Sanan, D.A., and Mahley, R.W., 2001, Apolipoprotein E fragments present in Alzheimer's disease brains induce neurofibrillary tangle-like intracellular inclusions in neurons: Proceedings of the National Academy of Sciences of the United States of America, v. 98, no. 15, p. 8838-8843.

Jacobs, W.B., Kaplan, D.R., and Miller, F.D., 2006, The p53 family in nervous system development and disease: Journal of Neurochemistry, v. 97, no. 6, p. 1571-1584.

Jung, S., Aliberti, J., Graemmel, P., Sunshine, M.J., Kreutzberg, G.W., Sher, A., and Littman, D.R., 2000, Analysis of Fractalkine Receptor CX3CR1 Function by Targeted Deletion and Green Fluorescent Protein Reporter Gene Insertion: Mol. Cell. Biol., v. 20, no. 11, p. 4106-4114.

Kanehisa, M., Araki, M., Goto, S., Hattori, M., Hirakawa, M., Itoh, M., Katayama, T., Kawashima, S., Okuda, S., Tokimatsu, T., and Yamanishi, Y., 2008, KEGG for linking genomes to life and the environment: Nucleic Acids Research, v. 36, no. Database issue, p. D480-484.

Klugmann, M., Schwab, M.H., Pühlhofer, A., Schneider, A., Zimmermann, F., Griffiths, I.R., and Nave, K.A., 1997, Assembly of CNS myelin in the absence of proteolipid protein: Neuron, v. 18, no. 1, p. 59-70.

Ko, D.C., Milenkovic, L., Beier, S.M., Manuel, H., Buchanan, J., and Scott, M.P., 2005, Cell-autonomous death of cerebellar purkinje neurons with autophagy in Niemann-Pick type C disease: PLoS Genetics, v. 1, no. 1, p. 81-95.

Kreutzberg, G.W., 1996, Microglia: a sensor for pathological events in the CNS: Trends in Neurosciences, v. 19, no. 8, p. 312-318.

Kunitomo, H., Uesugi, H., Kohara, Y., and Iino, Y., 2005, Identification of ciliated sensory neuron-expressed genes in Caenorhabditis elegans using targeted pull-down of poly(A) tails: Genome Biology, v. 6, no. 2, p. R17.

Kurihara, T., and Tsukada, Y., 1967, The regional and subcellular distribution of 2',3'-cyclic nucleotide 3'-phosphohydrolase in the central nervous system: Journal of Neurochemistry, v. 14, no. 12, p. 1167-1174.

Laezza, C., Wolff, J., and Bifulco, M., 1997, Identification of a 48-kDa prenylated protein that associates with microtubules as 2',3'-cyclic nucleotide 3'-phosphodiesterase in FRTL-5 cells: FEBS Letters, v. 413, no. 2, p. 260-264.

Lane, E.B., 1993, Keratins: Connective Tissue and its Heritable Disorders. Molecular, Genetic and Medical Aspects,, p. 237–247.

Lappe-Siefke, C., Goebbels, S., Gravel, M., Nicksch, E., Lee, J., Braun, P.E., Griffiths, I.R., and Nave, K., 2003, Disruption of Cnp1 uncouples oligodendroglial functions in axonal support and myelination: Nature Genetics, v. 33, no. 3, p. 366-374.

Lassmann, H., 2008, Models of multiple sclerosis: new insights into pathophysiology and repair: Current Opinion in Neurology, v. 21, no. 3, p. 242-247.

Lees MB, and Brostoff SW, 1984, Proteins in myelin, *in* Morell (ed) Myelin, lenum Press, New York and London, p. 197-224.

Lenhossék, M., 1895, Der feinere Bau des Nervensystems im Lichte neuester Forschungen: eine allgemeine Betrachtung der Strukturprinzipien des Nervensystems, nebst einer Darstellung des feineren Baues des R\ückenmarkes: Fischer.

Levine, J.M., Stincone, F., and Lee, Y.S., 1993, Development and differentiation of glial precursor cells in the rat cerebellum: Glia, v. 7, no. 4, p. 307-321.

LeVine, S.M., and Goldman, J.E., 1988, Ultrastructural characteristics of GD3 ganglioside-positive immature glia in rat forebrain white matter: The Journal of Comparative Neurology, v. 277, no. 3, p. 456-464.

Levison, S.W., and Goldman, J.E., 1993, Both oligodendrocytes and astrocytes develop from progenitors in the subventricular zone of postnatal rat forebrain: Neuron, v. 10, no. 2, p. 201-212.

Li, C., and Wong, W.H., 2001, Model-based analysis of oligonucleotide arrays: expression index computation and outlier detection: Proceedings of the National Academy of Sciences of the United States of America, v. 98, no. 1, p. 31-36.

Lipshutz, R.J., Fodor, S.P., Gingeras, T.R., and Lockhart, D.J., 1999, High density synthetic oligonucleotide arrays: Nature Genetics, v. 21, no. 1 Suppl, p. 20-24.

Lobo, M.K., Karsten, S.L., Gray, M., Geschwind, D.H., and Yang, X.W., 2006, FACS-array profiling of striatal projection neuron subtypes in juvenile and adult mouse brains: Nature Neuroscience, v. 9, no. 3, p. 443-452.

LOWRY, O.H., ROSEBROUGH, N.J., FARR, A.L., and RANDALL, R.J., 1951, Protein measurement with the Folin phenol reagent: The Journal of Biological Chemistry, v. 193, no. 1, p. 265-275.

Lu, L., Neff, F., Dun, Z., Hemmer, B., Oertel, W.H., Schlegel, J., and Hartmann, A., 2004, Gene expression profiles derived from single cells in human postmortem brain: Brain Research Protocols, v. 13, no. 1, p. 18-25.

Markram, H., Toledo-Rodriguez, M., Wang, Y., Gupta, A., Silberberg, G., and Wu, C., 2004, Interneurons of the neocortical inhibitory system: Nat Rev Neurosci, v. 5, no. 10, p. 793-807.

Martin, C.B., Ingersoll, S.A., and Martin, B.K., 2007, Transcriptional control of the C3a receptor gene in glial cells: Dependence upon AP-1 but not Ets: Molecular Immunology, v. 44, no. 5, p. 703-712.

Mattson, M.P., and Magnus, T., 2006, Ageing and neuronal vulnerability: Nature Reviews. Neuroscience, v. 7, no. 4, p. 278-294.

McFerran, B., and Burgoyne, R., 1997, 2',3'-Cyclic nucleotide 3'-phosphodiesterase is associated with mitochondria in diverse adrenal cell types: Journal of Cell Science, v. 110 (Pt 23), p. 2979-2985.

McGeer, P.L., Kawamata, T., Walker, D.G., Akiyama, H., Tooyama, I., and McGeer, E.G., 1993, Microglia in degenerative neurological disease: Glia, v. 7, no. 1, p. 84-92.

McGeer, P.L., and McGeer, E.G., 1995, The inflammatory response system of brain: implications for therapy of Alzheimer and other neurodegenerative diseases: Brain Research Reviews, v. 21, no. 2, p. 195–218.

Mirnics, K., Middleton, F.A., Marquez, A., Lewis, D.A., and Levitt, P., 2000, Molecular Characterization of Schizophrenia Viewed by Microarray Analysis of Gene Expression in Prefrontal Cortex: Neuron, v. 28, no. 1, p. 53-67.

Mohri, I., Kadoyama, K., Kanekiyo, T., Sato, Y., Kagitani-Shimono, K., Saito, Y., Suzuki, K., Kudo, T., Takeda, M., Urade, Y., Murayama, S., and Taniike, M., 2007, Hematopoietic prostaglandin D synthase and DP1 receptor are selectively upregulated in microglia and astrocytes within senile plaques from human patients and in a mouse model of Alzheimer disease: Journal of Neuropathology and Experimental Neurology, v. 66, no. 6, p. 469-480.

Mootha, V.K., Lindgren, C.M., Eriksson, K., Subramanian, A., Sihag, S., Lehar, J., Puigserver, P., Carlsson, E., Ridderstrale, M., Laurila, E., Houstis, N., Daly, M.J., Patterson, N., Mesirov, J.P., Golub, T.R., et al., 2003, PGC-1[alpha]-responsive genes involved in oxidative phosphorylation are coordinately downregulated in human diabetes: Nat Genet, v. 34, no. 3, p. 267-273.

Morfini, G., Szebenyi, G., Richards, B., and Brady, S.T., 2001, Regulation of kinesin: implications for neuronal development: Developmental Neuroscience, v. 23, no. 4-5, p. 364-376.

Morfini, G., Szebenyi, G., Brown, H., Pant, H.C., Pigino, G., DeBoer, S., Beffert, U., and Brady, S.T., 2004, A novel CDK5-dependent pathway for regulating GSK3 activity and kinesin-driven motility in neurons: The EMBO Journal, v. 23, no. 11, p. 2235-2245.

Morfini, G., Szebenyi, G., Elluru, R., Ratner, N., and Brady, S.T., 2002, Glycogen synthase kinase 3 phosphorylates kinesin light chains and negatively regulates kinesin-based motility: The EMBO Journal, v. 21, no. 3, p. 281-293.

Morfini, G.A., Burns, M., Binder, L.I., Kanaan, N.M., LaPointe, N., Bosco, D.A., Brown, R.H., Brown, H., Tiwari, A., Hayward, L., Edgar, J., Nave, K., Garberrn, J., Atagi, Y., Song, Y., et al., 2009, Axonal Transport Defects in Neurodegenerative Diseases: J. Neurosci., v. 29, no. 41, p. 12776-12786.

Mott, D.D., and Dingledine, R., 2003, Interneuron Diversity series: Interneuron research--challenges and strategies: Trends in Neurosciences, v. 26, no. 9, p. 484-488.

Myer, D.J., Gurkoff, G.G., Lee, S.M., Hovda, D.A., and Sofroniew, M.V., 2006, Essential protective roles of reactive astrocytes in traumatic brain injury: Brain: A Journal of Neurology, v. 129, no. Pt 10, p. 2761-2772.

Nair, A., Frederick, T.J., and Miller, S.D., 2008, Astrocytes in multiple sclerosis: a product of their environment: Cellular and Molecular Life Sciences, v. 65, no. 17, p. 2702–2720.

Nakamura, T., Watanabe, A., Fujino, T., Hosono, T., and Michikawa, M., 2009, Apolipoprotein E4 (1-272) fragment is associated with mitochondrial proteins and affects mitochondrial function in neuronal cells: Molecular Neurodegeneration, v. 4, p. 35.

Nave, K.A., Lai, C., Bloom, F.E., and Milner, R.J., 1986, Jimpy mutant mouse: a 74-base deletion in the mRNA for myelin proteolipid protein and evidence for a primary defect in RNA splicing: Proceedings of the National Academy of Sciences of the United States of America, v. 83, no. 23, p. 9264-9268.

Nedergaard, M., Ransom, B., and Goldman, S.A., 2003, New roles for astrocytes: redefining the functional architecture of the brain: TRENDS in Neurosciences, v. 26, no. 10, p. 523–530.

Nielsen, J.A., Maric, D., Lau, P., Barker, J.L., and Hudson, L.D., 2006, Identification of a Novel Oligodendrocyte Cell Adhesion Protein Using Gene Expression Profiling: J. Neurosci., v. 26, no. 39, p. 9881-9891.

Nimmerjahn, A., Kirchhoff, F., and Helmchen, F., 2005, Resting microglial cells are highly dynamic surveillants of brain parenchyma in vivo: Science (New York, N.Y.), v. 308, no. 5726, p. 1314-1318.

Nishizawa, Y., Kurihara, T., Masuda, T., and Takahashi, Y., 1985, Immunohistochemical localization of 2',3'-cyclic nucleotide 3'-phosphodiesterase in adult bovine cerebrum and cerebellum: Neurochemical Research, v. 10, no. 8, p. 1107-1118.

Nolte, C., Matyash, M., Pivneva, T., Schipke, C.G., Ohlemeyer, C., Hanisch, U.K., Kirchhoff, F., and Kettenmann, H., 2001, GFAP promoter-controlled EGFP-expressing transgenic mice: a tool to visualize astrocytes and astrogliosis in living brain tissue: Glia, v. 33, no. 1, p. 72-86.

Okoniewski, M.J., Yates, T., Dibben, S., and Miller, C.J., 2007, An annotation infrastructure for the analysis and interpretation of Affymetrix exon array data: Genome Biology, v. 8, no. 5, p. R79.

Paxinos, G., and Franklin, K.B., 2004, The mouse brain in stereotaxic coordinates: Academic Press.

Perry, V.H., and Gordon, S., 1988, Macrophages and microglia in the nervous system: Trends in Neurosciences, v. 11, no. 6, p. 273-277.

Pfaffl, M.W., 2001, A new mathematical model for relative quantification in real-time RT-PCR: Nucl. Acids Res., v. 29, no. 9, p. e45.

Pollard, J.W., 1997, Role of colony-stimulating factor-1 in reproduction and development: Molecular Reproduction and Development, v. 46, no. 1, p. 54-60; discussion 60-61.

Pringle, N.P., Mudhar, H.S., Collarini, E.J., and Richardson, W.D., 1992, PDGF receptors in the rat CNS: during late neurogenesis, PDGF alpha-receptor expression appears to be restricted to glial cells of the oligodendrocyte lineage: Development (Cambridge, England), v. 115, no. 2, p. 535-551.

Ramon y Cajal, S., 1952, Structure and connections of neurons: Bulletin of the Los Angeles Neurological Society, v. 17, no. 1-2, p. 5-46.

Ramon y Cajal, S.R., 1911, Histology of the nervous system of man and vertebrates: Reprinted by Consejo Superior de Investigaciones Cientificas.

Rasband, M.N., Tayler, J., Kaga, Y., Yang, Y., Lappe-Siefke, C., Nave, K., and Bansal, R., 2005, CNP is required for maintenance of axon-glia interactions at nodes of Ranvier in the CNS: Glia, v. 50, no. 1, p. 86-90.

Retzius, G., 1894, Die neuroglia des Gehirns beim Menschen und bei Saeugethieren: Gustav Fischer.

del Rio-Hortega, P., 1919, El tercer elemento de los centros nerviosos: Biol Soc Espan Biol, v. 9, p. 68–83.

Rock, R.B., Gekker, G., Hu, S., Sheng, W.S., Cheeran, M., Lokensgard, J.R., and Peterson, P.K., 2004, Role of microglia in central nervous system infections: Clinical Microbiology Reviews, v. 17, no. 4, p. 942-964, table of contents.

Rosenbluth, J., Stoffel, W., and Schiff, R., 1996, Myelin structure in proteolipid protein (PLP)-null mouse spinal cord: The Journal of Comparative Neurology, v. 371, no. 2, p. 336-344.

Rossner, M.J., Hirrlinger, J., Wichert, S.P., Boehm, C., Newrzella, D., Hiemisch, H., Eisenhardt, G., Stuenkel, C., von Ahsen, O., and Nave, K., 2006, Global transcriptome analysis of genetically identified neurons in the adult cortex: The Journal of Neuroscience: The Official Journal of the Society for Neuroscience, v. 26, no. 39, p. 9956-9966.

van Rossum, D., and Hanisch, U., 2004, Microglia: Metabolic Brain Disease, v. 19, no. 3-4, p. 393-411.

Sandberg, R., Yasuda, R., Pankratz, D.G., Carter, T.A., Del Rio, J.A., Wodicka, L., Mayford, M., Lockhart, D.J., and Barlow, C., 2000, Regional and strain-specific gene expression mapping in the adult mouse brain: Proceedings of the National Academy of Sciences of the United States of America, v. 97, no. 20, p. 11038-11043.

Scherer, S.S., Braun, P.E., Grinspan, J., Collarini, E., Wang, D.Y., and Kamholz, J., 1994, Differential regulation of the 2',3'-cyclic nucleotide 3'-phosphodiesterase gene during oligodendrocyte development: Neuron, v. 12, no. 6, p. 1363-1375.

Schneider, A., Montague, P., Griffiths, I., Fanarraga, M., Kennedy, P., Brophy, P., and Nave, K.A., 1992, Uncoupling of hypomyelination and glial cell death by a mutation in the proteolipid protein gene: Nature, v. 358, no. 6389, p. 758-761.

Seto, T., Fujiki, K., Kishishita, H., Fujimaki, T., Murakami, A., and Kanai, A., 2008, A novel mutation in the cornea-specific keratin 12 gene in Meesmann corneal dystrophy: Japanese Journal of Ophthalmology, v. 52, no. 3, p. 224-226.

Skoff, R.P., Saluja, I., Bessert, D., and Yang, X., 2004, Analyses of proteolipid protein mutants show levels of proteolipid protein regulate oligodendrocyte number and cell death in vitro and in vivo: Neurochemical Research, v. 29, no. 11, p. 2095-2103.

Sousa, A.D., Berg, J.S., Robertson, B.W., Meeker, R.B., and Cheney, R.E., 2006, Myo10 in brain: developmental regulation, identification of a headless isoform and dynamics in neurons: J Cell Sci, v. 119, no. 1, p. 184-194.

Sprinkle, T.J., 1989, 2',3'-cyclic nucleotide 3'-phosphodiesterase, an oligodendrocyte-Schwann cell and myelin-associated enzyme of the nervous system: Critical Reviews in Neurobiology, v. 4, no. 3, p. 235-301.

Sprinkle, T.J., McMorris, F.A., Yoshino, J., and DeVries, G.H., 1985, Differential expression of 2':3'-cyclic nucleotide 3'-phosphodiesterase in cultured central, peripheral, and extraneural cells: Neurochemical Research, v. 10, no. 7, p. 919-931.

Sprinkle, T.J., Zaruba, M.E., and McKhann, G.M., 1978, Radioactive measurement of 2',3'-cyclic nucleotide 3'-phosphodiesterase activity in the central and peripheral nervous system and in extraneural tissue: Analytical Biochemistry, v. 88, no. 2, p. 449-456.

Stagi, M., Dittrich, P.S., Frank, N., Iliev, A.I., Schwille, P., and Neumann, H., 2005, Breakdown of Axonal Synaptic Vesicle Precursor Transport by Microglial Nitric Oxide: J. Neurosci., v. 25, no. 2, p. 352-362.

Stagi, M., Gorlovoy, P., Larionov, S., Takahashi, K., and Neumann, H., 2006, Unloading kinesin transported cargoes from the tubulin track via the inflammatory c-Jun N-terminal kinase pathway: FASEB J., v. 20, no. 14, p. 2573-2575.

Streit, W.J., Graeber, M.B., and Kreutzberg, G.W., 1988, Functional plasticity of microglia: a review: Glia, v. 1, no. 5, p. 301–307.

Subramanian, A., Tamayo, P., Mootha, V.K., Mukherjee, S., Ebert, B.L., Gillette, M.A., Paulovich, A., Pomeroy, S.L., Golub, T.R., Lander, E.S., and Mesirov, J.P., 2005, Gene set enrichment analysis: A knowledge-based approach for interpreting genome-wide expression profiles: Proceedings of the National Academy of Sciences of the United States of America, v. 102, no. 43, p. 15545-15550.

Sugino, K., Hempel, C.M., Miller, M.N., Hattox, A.M., Shapiro, P., Wu, C., Huang, Z.J., and Nelson, S.B., 2006, Molecular taxonomy of major neuronal classes in the adult mouse forebrain: Nat Neurosci, v. 9, no. 1, p. 99-107.

Sullivan, L.S., Baylin, E.B., Font, R., Daiger, S.P., Pepose, J.S., Clinch, T.E., Nakamura, H., Zhao, X.C., and Yee, R.W., 2007, A novel mutation of the Keratin 12 gene responsible for a severe phenotype of Meesmann's corneal dystrophy: Molecular Vision, v. 13, p. 975-980.

Suzumura, A., Marunouchi, T., and Yamamoto, H., 1991, Morphological transformation of microglia in vitro: Brain Res, v. 545, no. 1-2, p. 301–306.

Tang, M.K., Wang, C.M., Shan, S.W., Chui, Y.L., Ching, A.K.K., Chow, P.H., Grotewold, L., Chan, J.Y.H., and Lee, K.K.H., 2006, Comparative proteomic analysis reveals a function of the novel death receptor-associated protein BRE in the regulation of prohibitin and p53 expression and proliferation: Proteomics, v. 6, no. 8, p. 2376-2385.

Tedeschi, A., and Di Giovanni, S., 2009, The non-apoptotic role of p53 in neuronal biology: enlightening the dark side of the moon: EMBO Rep, v. 10, no. 6, p. 576-583.

Toledo-Rodriguez, M., Blumenfeld, B., Wu, C., Luo, J., Attali, B., Goodman, P., and Markram, H., 2004, Correlation Maps Allow Neuronal Electrical Properties to be Predicted from Single-cell Gene Expression Profiles in Rat Neocortex: Cereb. Cortex, v. 14, no. 12, p. 1310-1327.

Towbin, H., Staehelin, T., and Gordon, J., 1979, Electrophoretic transfer of proteins from polyacrylamide gels to nitrocellulose sheets: procedure and some applications: Proceedings of the National Academy of Sciences of the United States of America, v. 76, no. 9, p. 4350-4354.

Vanlandingham, J.W., Tassabehji, N.M., Somers, R.C., and Levenson, C.W., 2005, Expression profiling of p53-target genes in copper-mediated neuronal apoptosis: Neuromolecular Medicine, v. 7, no. 4, p. 311-324.

Virchow, R., 1856, Gesammelte Abbildung zur wissenschaftlichen Medizin: Verlag von Meidinger Sohn & Comp,

Werner, H.B., Kuhlmann, K., Shen, S., Uecker, M., Schardt, A., Dimova, K., Orfaniotou, F., Dhaunchak, A., Brinkmann, B.G., Möbius, W., Guarente, L., Casaccia-Bonnefil, P., Jahn, O., and Nave, K., 2007, Proteolipid protein is required for transport of sirtuin 2 into CNS myelin: The Journal of Neuroscience: The Official Journal of the Society for Neuroscience, v. 27, no. 29, p. 7717-7730.

Williams, A., Piaton, G., and Lubetzki, C., 2007, Astrocytes--friends or foes in multiple sclerosis?: Glia, v. 55, no. 13, p. 1300-1312.

Witt, A., and Brady, S.T., 2000, Unwrapping new layers of complexity in axon/glial relationships: Glia, v. 29, no. 2, p. 112-117.

Wren, D., Wolswijk, G., and Noble, M., 1992, In vitro analysis of the origin and maintenance of O-2Aadult progenitor cells: The Journal of Cell Biology, v. 116, no. 1, p. 167-176.

Yamamoto, Y., Mizuno, R., Nishimura, T., Ogawa, Y., Yoshikawa, H., Fujimura, H., Adachi, E., Kishimoto, T., Yanagihara, T., and Sakoda, S., 1994, Cloning and expression of myelin-associated oligodendrocytic basic protein: J Biol Chem, v. 269, p. 31725–31730.

Yang, Z., Edenberg, H.J., and Davis, R.L., 2005, Isolation of mRNA from specific tissues of Drosophila by mRNA tagging: Nucl. Acids Res., v. 33, no. 17, p. e148.

Yao, F., Yu, F., Gong, L., Taube, D., Rao, D.D., and MacKenzie, R.G., 2005, Microarray analysis of fluoro-gold labeled rat dopamine neurons harvested by laser capture microdissection: Journal of Neuroscience Methods, v. 143, no. 2, p. 95-106.

Yuasa, S., 2001, Development of astrocytes in the mouse hippocampus as tracked by tenascin-C gene expression: Archives of Histology and Cytology, v. 64, no. 2, p. 149-158.

Zhang, Y., Ma, C., Delohery, T., Nasipak, B., Foat, B.C., Bounoutas, A., Bussemaker, H.J., Kim, S.K., and Chalfie, M., 2002, Identification of genes expressed in C. elegans touch receptor neurons: Nature, v. 418, no. 6895, p. 331-335.

Zhao, X., Lein, E.S., He, A., Smith, S.C., Aston, C., and Gage, F.H., 2001a, Transcriptional profiling reveals strict boundaries between hippocampal subregions: The Journal of Comparative Neurology, v. 441, no. 3, p. 187-196.

Zhao, X., Lein, E.S., He, A., Smith, S.C., Aston, C., and Gage, F.H., 2001b, Transcriptional profiling reveals strict boundaries between hippocampal subregions: The Journal of Comparative Neurology, v. 441, no. 3, p. 187-196.

Zirlinger, M., and Anderson, D., 2003, Molecular dissection of the amygdala and its relevance to autism: Genes, Brain & Behavior, v. 2, no. 5, p. 282-294.

9 Appendices

Appendix A: Genes comprising cluster of Cnp1-/-_Core_Network (CCN)

Symbol	Description	1M	3M	6M	12M
Regulation of transcription					
Med1	mediator complex subunit 1	2,54	3,33	2,41	2,38
Hbp1	high mobility group box transcription factor	-0,24	-1,05	-1,1	-1,04
Id2	inhibitor of DNA binding 2	-0,82	0,17	-0,6	-0,92
Mef2c	myocyte enhancer factor 2	-1,36	-0,01	-0,15	-0,65
Riok2	RIO kinase 2	-0,21	-0,6	-0,47	-0,64
Pttg1	pituitary tumor-transforming 1	-4,34	-5,43	-2,63	-4,89
Cytoskeleton					
Spnb2	spectrin beta 2	0,03	0,2	0,49	1,32
Nefm	neurofilament, medium polypeptide	-0,48	-0,04	-0,07	-0,67
Nefh	neurofilament, heavy polypeptide	-0,46	-0,06	-0,23	-0,7
Mapt	microtubule-associated protein tau	-0,78	0,02	-0,15	-0,14
Lpin1	lipin 1	-0,57	-0,8	0,32	-0,38
Krt12	keratin 12	-3,55	-3,81	-3,56	-3,13
Dynll2	dynein light chain LC8-type 2	-0,32	-0,37	-0,23	-0,23
Kif3a	kinesin family member 3A	-0,17	-0,56	0,28	-0,66
Myl4	myosin, light polypeptide 4	-0,77	-0,5	-0,4	-0,45
Cholesterol / Lipid					
Ldlr	low density lipoprotein receptor	0,32	0,55	1,65	0,32
Npc2	Niemann Pick type C2	0,2	0,38	0,66	0,22
Prkab1	protein kinase, AMP-activated, beta 1 non-catalytic subunit	0,46	0,31	1,07	0,01
Fabp3	fatty acid binding protein 3, muscle and heart	0,26	0,27	0,17	0,17
Apoe	apolipoprotein E	0,38	0,5	0,69	1,03
Ptgds	prostaglandin D2 synthase (brain)	0,55	1,05	1,08	2,18
Fasn	fatty acid synthase	-0,01	0,26	0,56	0,11
Signaling					
Rprm	reprimo, TP53 dependent G2 arrest mediator candidate	-0,07	1,26	0,73	1,19
Ubc	ubiquitin C	-0,49	-0,12	-0,37	-0,35
Pdk1	pyruvate dehydrogenase kinase, isoenzyme 1	-0,66	-0,03	0,08	-0,3
Apoptosis					
Bre	brain and reproductive organ-expressed protein	0,4	0,62	0,88	0,12
Ddit4	DNA-damage-inducible transcript 4	-0,09	0,54	0,56	0,72
Diablo	diablo homolog	-0,6	-0,24	-0,4	-1,22
Others					
Aldoc	aldolase C, fructose-bisphosphate	0,05	0,82	0,38	0,25
B2m	beta-2 microglobulin	0,22	0,66	0,44	0,54
Glul	glutamate-ammonia ligase (glutamine synthetase)	0,24	0,12	0,45	0,23
Hars	histidyl-tRNA synthetase	-0,01	1,3	1,15	0,86
Hebp1	heme binding protein 1	0,52	0,54	0,32	0,45
Hist1h1c	histone cluster 1, H1c	0,49	1,24	0,93	0,48
Hpca	hippocalcin	0	0,83	0,56	0,3
Igfbp5	insulin-like growth factor binding protein 5	0,02	0,53	1,42	0,33
Igh-6	immunoglobulin heavy chain 6 (heavy chain of IgM)	0,54	1,07	1,81	0,66
Mag	myelin-associated glycoprotein	0,54	0,46	0,29	0,48
Mtx1	metaxin 1	0,16	0,35	0,71	-0,07
Ntsr2	neurotensin receptor 2	0,31	0,28	0,93	0,64
Rab31	RAB31, member RAS oncogene family	0,14	0,52	0,69	0,73
Rpl15	ribosomal protein L15	0,76	0,51	0,6	0,49
Rpl3	ribosomal protein L3	0,15	0,27	0,24	0,14
Rpl8	ribosomal protein L8	0,13	0,36	0,21	0,14
Serpina3n	serine (or cysteine) peptidase inhibitor, clade A, member 3N	1,68	1,54	1,62	1,47
Sharpin	SHANK-associated RH domain interacting protein	0,21	0,57	0,56	-0,13

Appendix B: Genes comprising cluster of *Cnp1-/-*_CPN_3M Network (C3N)

Symbol	Description	1M	3M	6M	12M
Transcription					
Polr2h	polymerase (RNA) II (DNA directed) polypeptide H	0,04	0,64	-0,14	-0,53
Ddx54	DEAD (Asp-Glu-Ala-Asp) box polypeptide 54	-0,2	0,5	0,55	-0,13
Mecp2	methyl CpG binding protein 2	-0,34	0,56	0	-0,07
Ndn	necdin	-0,5	0,71	0,18	-0,2
Sf1	splicing factor 1	-0,16	0,53	-0,14	-0,26
Sap18	Sin3-associated polypeptide 18	0,02	0,72	0,38	-0,12
Lmo4	LIM domain only 4	-0,15	1,21	0,23	-0,27
Tcf25	transcription factor 25 (basic helix-loop-helix)	-0,06	0,61	0,1	-0,01
Sirt3	sirtuin 3	0,03	0,68	-0,12	-0,02
Chmp1a	chromatin modifying protein 1A	-0,02	1,15	0,01	-0,17
Elp3	elongation protein 3 homolog (S, cerevisiae)	-0,2	0,73	0,42	-0,15
Fhl2	four and a half LIM domains 2	-0,31	0,55	0,29	-0,46
Foxp1	forkhead box P1	-0,07	0,55	0,6	-0,7
Habp4	hyaluronic acid binding protein 4	-0,15	0,66	0,05	-0,09
Hdgf	hepatoma-derived growth factor	0,1	0,74	0,15	0,16
Hey1	hairy/enhancer-of-split related with YRPW motif 1	-0,94	0,3	-0,18	-0,16
Lass2	LAG1 homolog, ceramide synthase 2	0,5	0,57	-0,1	0,07
Ldoc1l	leucine zipper, down-regulated in cancer 1-like	-0,16	0,59	0,36	-0,22
Lrrc14	leucine rich repeat containing 14	-0,33	0,73	0,19	-0,27
Lrrc20	leucine rich repeat containing 20	-0,29	1,12	0,47	0
Lrrc59	leucine rich repeat containing 59	0,12	0,77	0,09	-0,12
Phb2	prohibitin 2	-0,28	0,85	0,21	-0,08
Rnf14	ring finger protein 14	-0,32	0,45	-0,22	-0,38
Sqstm1	sequestosome 1	-0,2	0,95	0,3	-0,18
Ssbp3	single-stranded DNA binding protein 3	0,11	0,62	0,05	-0,23
Tox4	TOX high mobility group box family member 4	-0,16	0,69	-0,14	-0,3
Bcl6	B-cell leukemia/lymphoma 6	-0,2	-0,81	-0,77	0,08
Ddx5	DEAD (Asp-Glu-Ala-Asp) box polypeptide 5	0,05	-0,61	0,02	0,16
Hoxc6	homeo box C6	0,31	-0,44	-0,72	0,33
Cytoskeleton					
Pak1	p21 (CDKN1A)-activated kinase 1	-0,35	1,27	0,13	-0,09
Baiap2	brain-specific angiogenesis inhibitor 1-associated protein 2	-0,06	0,76	-0,22	-0,02
Spna2	spectrin alpha 2	-0,19	0,57	-0,15	-0,08
Tubb3	tubulin, beta 3	-0,33	0,38	0,01	-0,42
Jak1	Janus kinase 1	-0,46	0,85	0,11	0,09
Cap2	CAP, adenylate cyclase-associated protein, 2 (yeast)	-0,27	0,56	-0,36	-0,31
Lasp1	LIM and SH3 protein 1	-0,4	0,68	-0,45	-0,43
Maea	macrophage erythroblast attacher	-0,31	0,5	-0,29	-0,34
Sirpa	signal-regulatory protein alpha	-0,31	0,67	-0,11	-0,26
Kalrn	kalirin, RhoGEF kinase	-0,03	0,45	0,2	-0,03
Elmo1	engulfment and cell motility 1, ced-12 homolog (C, elegans)	-0,33	0,97	-0,18	-0,22
Csrp1	cysteine and glycine-rich protein 1	0,16	1,13	0,51	0,21
Capn10	calpain 10	-0,28	0,82	0,22	0,2
Cdk2ap1	CDK2 (cyclin-dependent kinase 2)-associated protein 1	-0,11	0,55	0,28	-0,28
Elmo2	engulfment and cell motility 2, ced-12 homolog (C, elegans)	-0,2	0,65	0,01	-0,22
Enc1	ectodermal-neural cortex 1	-0,26	0,25	-0,23	-0,14
Epb4,9	erythrocyte protein band 4,9	-0,01	0,89	0,07	-0,04
Cholesterol / Lipid					
Fdft1	farnesyl diphosphate farnesyl transferase 1	-0,16	0,57	0,31	0,07
Atp5a1	ATP synthase, H+ transporting, mitochondrial F1 complex, alpha subunit, isoform 1	-0,18	0,96	-0,11	-0,22

Atp5b	*ATP synthase, H+ transporting mitochondrial F1 complex, beta subunit*	-0,16	0,64	-0,05	-0,15
Got2	*glutamate oxaloacetate transaminase 2, mitochondrial*	-0,53	0,91	0,38	-0,04
Cdipt	*CDP-diacylglycerol--inositol 3-phosphatidyltransferase*	-0,1	0,62	-0,08	-0,08
Gpsn2	*glycoprotein, synaptic 2*	-0,32	1,69	0,13	0,18
Vamp2	*vesicle-associated membrane protein 2*	-0,28	0,46	0,09	-0,11
Stard3	*START domain containing 3*	-0,01	0,72	-0,04	-0,08
Rab15	*RAB15, member RAS oncogene family*	-0,04	0,87	0,12	0,04
Scap	*SREBF chaperone*	-0,05	0,61	-0,19	0,11
Paqr7	*progestin and adipoQ receptor family member VII*	-0,01	0,63	0,31	-0,34
Pitpna	*phosphatidylinositol transfer protein, alpha*	-0,08	0,83	-0,13	-0,26
Psap	*prosaposin*	-0,25	0,98	0,06	0,07
Akr1b3	*aldo-keto reductase family 1, member B3 (aldose reductase)*	0,13	-2,42	-0,07	-0,86
Csnk1d	*casein kinase 1, delta*	0,2	-0,27	-0,3	0,56

<u>Signaling</u>

Arrb1	*arrestin, beta 1*	-0,02	1,02	0,44	-0,12
Cacna2d3	*calcium channel, voltage-dependent, alpha2/delta subunit 3*	-0,42	0,14	0	-0,38
Prkcb	*protein kinase C, beta*	-0,18	0,59	0,13	0,06
Mapk1	*mitogen-activated protein kinase 1*	-0,44	0,84	0,11	-0,37
Map2k1	*mitogen-activated protein kinase kinase 1*	-0,28	0,91	0,01	0,06
Camk2g	*calcium/calmodulin-dependent protein kinase II gamma*	-0,04	0,65	0,27	0,06
Atp2a2	*ATPase, Ca++ transporting, cardiac muscle, slow twitch 2*	-0,22	0,2	-0,12	-0,13
Slc25a5	*solute carrier family 25, member 5*	-0,23	0,31	-0,22	-0,22
Gabrg2	*gamma-aminobutyric acid (GABA-A) receptor, subunit gamma 2*	-0,53	0,8	-0,2	-0,25
Eif4b	*eukaryotic translation initiation factor 4B*	-0,19	0,94	0,21	-0,13
Aph1a	*anterior pharynx defective 1a homolog (C, elegans)*	0,01	0,92	0,39	-0,04
Ngef	*neuronal guanine nucleotide exchange factor*	-0,08	1,44	0,39	0,04
Asb8	*ankyrin repeat and SOCS box-containing 8*	-0,47	0,74	0,01	-0,21
D0H4S114	*DNA segment, human D4S114*	0,23	1,37	0,74	-0,21
Dclk1	*doublecortin-like kinase 1*	-0,29	0,61	-0,26	-0,09
Gnb5	*guanine nucleotide binding protein (G protein), beta 5*	0,06	0,54	-0,36	-0,13
Slc2a1	*solute carrier family 2 (facilitated glucose transporter), member 1*	0,1	-0,91	-0,39	0,41
Ptpn2	*protein tyrosine phosphatase, non-receptor type 2*	0,36	-1,01	0,48	-0,1
Pdcd5	*programmed cell death 5*	0,19	-0,57	-0,06	0,09

<u>Apoptosis</u>

App	*amyloid beta (A4) precursor protein*	0,04	1,19	-0,18	-0,05
Vdac1	*voltage-dependent anion channel 1*	-0,25	0,57	-0,08	-0,31
Ube2z	*ubiquitin-conjugating enzyme E2Z (putative)*	0,09	0,58	-0,39	0,01
Prkar1b	*protein kinase, cAMP dependent regulatory, type I beta*	-0,06	1,34	0,16	0,05
Prdx2	*peroxiredoxin 2*	0,16	0,58	-0,08	-0,38
Bcl2l2	*BCL2-like 2*	-0,18	0,79	0,35	0,15
Fem1b	*feminization 1 homolog b (C, elegans)*	-0,27	0,59	-0,33	-0,29
Rnf34	*ring finger protein 34*	-0,04	0,54	-0,33	-0,21
Tegt	*testis enhanced gene transcript*	0,06	0,36	-0,14	0,28
Pgam1	*phosphoglycerate mutase 1*	-0,18	0,55	-0,11	-0,14
Thoc1	*THO complex 1*	0,34	-1,12	0,25	-0,3
Akr1b3	*aldo-keto reductase family 1, member B3 (aldose reductase)*	0,27	-2,55	-0,18	-1,05

128

Appendix C: Genes comprising cluster of *Cnp1*-/-_CPN_6M Network (C6N)

Symbol	Description	1M	3M	6M	12M
Transcription					
Gtf2h2	general transcription factor II H, polypeptide 2	-0,02	0,42	0,64	-0,87
Jun	Jun oncogene	0,07	0,22	1,22	0,97
Nr3c1	nuclear receptor subfamily 3, group C, member 1	-0,42	0,46	0,38	-0,3
Mitf	microphthalmia-associated transcription factor	-0,35	-0,27	2,06	-0,29
Med8	mediator of RNA polymerase II transcription, subunit 8 homolog (yeast)	-0,2	0,5	1,03	-0,45
Tcf12	transcription factor 12	0,08	0	1,37	-0,22
Med22	mediator complex subunit 22	0,21	0,59	0,3	-0,31
Xab2	XPA binding protein 2	0,15	-0,5	0,56	0,28
Hmgb3	high mobility group box 3	0	1,11	1,17	-0,36
Mbtps1	membrane-bound transcription factor peptidase, site 1	-0,2	0,5	0,59	-0,24
Mll1	myeloid/lymphoid or mixed-lineage leukemia 1	-0,11	-0,21	0,75	0,24
Pqbp1	polyglutamine binding protein 1	0,12	-0,19	0,51	0,09
Purb	purine rich element binding protein B	0,23	-0,58	0,99	-0,6
Rcor1	REST corepressor 1	-0,32	-0,17	0,45	-0,71
Gtf2e2	general transcription factor II E, polypeptide 2 (beta subunit)	-0,4	0,12	-1,26	-0,52
Nfatc2	nuclear factor of activated T-cells, cytoplasmic, calcineurin-dependent 2	-0,05	0,11	-1,05	0,23
Med1 (short)	mediator complex subunit 1	-0,3	-0,11	-0,74	-0,62
Bzw1	basic leucine zipper and W2 domains 1	-0,11	-0,06	-0,55	-0,65
Dmtf1	cyclin D binding myb-like transcription factor 1	-0,32	0,23	-1,25	-0,85
Klf10	Kruppel-like factor 10	0,03	-0,2	-0,98	-0,46
Tsc22d3	TSC22 domain family, member 3	-0,28	-0,12	-0,4	-0,77
Sfpq	splicing factor proline/glutamine rich	-0,56	0,09	-1,16	-0,52
Cytoskeleton					
Cfl2	cofilin 2, muscle	-0,58	0,08	1,1	-0,76
Fhod3	formin homology 2 domain containing 3	-0,18	0,45	0,5	-0,22
Rock2	Rho-associated coiled-coil containing protein kinase 2	-0,11	-0,27	-1,1	-0,81
Cholesterol / Lipid					
Nsdhl	NAD(P) dependent steroid dehydrogenase-like	-0,03	0,68	0,76	-0,08
Tm7sf2	transmembrane 7 superfamily member 2	0,11	0,51	0,97	-0,22
Hexb	hexosaminidase B	0,5	-0,74	0,54	0,65
Dbi	diazepam binding inhibitor	-0,11	-0,07	0,75	0,24
Scp2	sterol carrier protein 2, liver	-0,07	0,46	0,34	-0,2
0610007P14Rik	RIKEN cDNA 0610007P14 gene	0,15	0,51	0,52	-0,37
Asah2	N-acylsphingosine amidohydrolase 2	-0,04	-0,37	0,43	-0,21
Erlin1	**ER lipid raft associated 1**	0,02	-0,22	0,99	-0,18
Hsd17b11	hydroxysteroid (17-beta) dehydrogenase 11	-0,11	-0,02	0,71	0,29
Pgrmc2	progesterone receptor membrane component 2	-0,1	0,25	0,5	-0,15
Sqle	squalene epoxidase	0,09	0,41	1,03	-0,22
Prkag2	protein kinase, AMP-activated, gamma 2 non-catalytic subunit	1,14	0,28	-0,43	-0,85
Rgs19	regulator of G-protein signaling 19	0,25	0,04	-0,79	-0,4
Signaling					
Dbi	diazepam binding inhibitor	0,12	-0,34	0,5	0,39
Dusp8	dual specificity phosphatase 8	-0,1	0,03	0,68	0,21
Map4k4	mitogen-activated protein kinase kinase kinase kinase 4	0,11	-0,11	0,77	-0,28
Phka2	phosphorylase kinase alpha 2	0,07	-0,45	1,2	0,2
Ifnar2	interferon (alpha and beta) receptor 2	-0,13	0,33	0,85	-0,51
Npy	neuropeptide Y	1	-1,12	1,62	1,15
Sel1l	sel-1 suppressor of lin-12-like (C, elegans)	-0,16	0,02	0,61	-0,43
Il11ra1	interleukin 11 receptor, alpha chain 1	0,11	0,29	-0,33	-0,81
Rfwd2	ring finger and WD repeat domain 2	-0,41	0,05	-0,39	-0,28

Adcyap1	*adenylate cyclase activating polypeptide 1*	-0,35	0,22	-0,94	-0,59
Adam19	*a disintegrin and metallopeptidase domain 19 (meltrin beta)*	0,09	-0,13	-1,27	-0,49

Apoptosis

Syvn1	*synovial apoptosis inhibitor 1, synoviolin*	-0,09	0,59	0,57	-0,15
Cdc2l1	*cell division cycle 2-like 1*	0,39	0,3	0,32	-0,2
Acat2	*acetyl-Coenzyme A acetyltransferase 2*	0,21	-0,21	0,56	0,64
Polb	*polymerase (DNA directed), beta*	-0,06	-0,14	-1,01	-0,29
Bdnf	*brain derived neurotrophic factor*	-0,03	-0,51	-1,2	-0,81
Pdcd2	*programmed cell death 2*	-0,22	-0,11	-0,61	-0,55
Cs	*citrate synthase*	-0,3	-0,17	-0,69	0,01

Appendix D:

Gene Ontology (GO) annotations enriched in CCN (Fig. 21 A, A').

GO annotation is separated into three onto-logies: biological process (BP), molecular function (MF) and cellular component (CC). (A) GO terms of genes, which are up-regulated in CPN in *Cnp1* mutants at all time points. (B) GO terms of genes, which are down-regulated in CPN in *Cnp1* mutants at all time points.

A

relative expression — time [month] — 1 3 6 12 — 72 probe sets — WT — *Cnp1 -/-*

BP

neurological system process (6) · carboxylic acid metabolic process (5) · regulation of cellular metabolic process (7) · RNA metabolic process (7) · regulation of cellular component organization (5) · intracellular transport (5) · response to stress (6) · regulation of gene expression (5) · translation (5)

nervous system development (5) · regulation of developmental process (5) · cell proliferation (5) · organelle organization (5) · chemical homeostasis (5) · protein modification process (5) · cellular developmental process (5) · cell surface receptor linked signal transduction (5) · cell-cell signaling (5) · immune system process (5) · cellular lipid metabolic process (6)

MF

kinase activity (4) · nucleoside-triphosphatase activity (3) · substrate-specific transmembrane transporter activity (3) · ATP binding (5) · structural constituent of ribosome (3) · actin binding (3) · channel activity (3) · structural constituent of myelin sheath (3) · receptor binding (3)

transmembrane receptor activity (3) · GTP binding (3) · ligase activity (3) · lipid binding (4) · zinc ion binding (4) · transcription regulator activity (3) · enzyme regulator activity (3) · DNA binding (4) · calcium ion binding (5)

CC

kinase activity (3) · ATP binding (4) · transcription regulator activity (3) · structural constituent of cytoskeleton (3) · protein binding (7)

transition metal ion binding (3) · DNA binding (4) · oxidoreductase activity (3) · motor activity (3)

B

relative expression — time [month] — 1 3 6 12 — 36 probe sets — WT — *Cnp1 -/-*

positive regulation of cellular process (3) · transport (4) · peptidyl-amino acid modification (3) · cytoskeleton organization (5) · cellular component assembly (3) · regulation of transcription, DNA-dependent (3) · organ development (3)

neurological system process (3) · signal transduction (4) · microtubule-based process (3) · regulation of cell differentiation (3) · post-translational protein modification (3) · cell cycle (3) · carbohydrate metabolic process (3) · nervous system development (3)

cytoskeleton (3) · extracellular space (13) · nucleus (10) · membrane fraction (5) · protein complex (6) · ribosome (3) · mitochondrion (5) · intracellular organelle part (5) · integral to plasma membrane (7)

extracellular space (3) · nucleus (10) · axon (3) · microtubule (3) · intermediate filament (3) · organelle membrane (3) · endoplasmic reticulum (3) · microtubule associated complex (3) · integral to membrane (6) · mitochondrion (5)

131

Appendix E:

GO annotations enriched in C3N (Fig. 21 B, B').

The GO annotation is separated into three biological ontologies: biological process (BP), molecular function (MF) and cellular component (CC). (A) GO terms of genes, which are up-regulated in CPN in *Cnp1* mutants at the three months time point. (B) GO terms of genes, which are down-regulated in CPN in *Cnp1* mutants at the three months time point.

# Appendix F:

**GO annotations enriched in C6N (Fig. 21 C, C').**

The GO annotation is separated into three ontologies: biological process (BP), molecular function (MF) and cellular component (CC). (A) GO terms of genes, which are up-regulated in CPN in Cnp1 mutants at the six months time point. (B) GO terms of genes, which are down-regulated in CPN in Cnp1 mutants at the 6 months time point.

Appendix G: Abbreviations

°C	Degrees Celsius (centigrades)
µg	Microgram
µl	Microliter
µm	Micrometer
Amg	Amygdala
AONDs	Adult-onset neurodegenerative diseases
APC	Adenomatous polyposis coli
APP	Amyloid precursor protein
APS	Ammonium persulfate
AS	Astrocytes
BP	Biological process
bp	Base pairs
Bre	Brain and reproductive organ-expressed protein
BSA	Bovine serum albumin
C3ar1	Complement component 3a receptor 1
CC	Cellular component
Ccl3	Chemokine (C-C motif) ligand 3
CCN	Cnp1-/-_Core_Network
C3N	Cnp1-/-_3M_Network
C6N	Cnp1-/-_6M_Network
Chrna3	Cholinergic receptor, nicotinic, alpha polypeptide 3
Chrna5	Cholinergic receptor, nicotinic, alpha polypeptide 5
CNP / *Cnp1*	2', 3'-cyclic nucleotide 3'-phosphodiesterase
CNS	Central nervous system
CPN	Callosal projection neurons
Csf1r	Colony stimulating factor 1 receptor
Cspg4	Chondroitin sulfate proteoglycan 4
Cx	Cortex
DAB	3,3'- Diaminobenzidine
Dcx	Doublecortin
ddH2O	Double distilled (or miliQ) water
DMSO	Dimethylsulfoxide
EB I	Elution buffer I
EB II	Elution buffer II
EDTA	Ethylened acid
EGFP	Enhanced green fluorescent protein
Egfr	Epidermal growth factor receptor
Eno2	Enolase 2
Enpp2	Extracellular lysophospholipase D
EYFP	Enhanced yellow fluorescent protein
EYFPnuc	Nuclear-targeted EYFP
f.c.	Final concentration
FACS	Fluorescent-activated cell sorting
FC	Fold change
gcos	Gene chip operating software
GO	Gene Ontology
GPC	Glial precursors cells
Grin1	Glutamate receptor, ionotropic, NMDA1
GSEA	Gene set enrichment analysis
HE	Haematoxylin-Eosin
HE	Haematoxylin-Eosin staining
hGFAP	Human glial fibrillary acidic protein

HS	Horse serum
Iba1	Ionized Ca2+-binding adaptor 1
IHC	Immunohistochemstry
IP	Immunoprecipitation
ISH	*in-situ hybridization*
Kb	Kilobases
kDa	Kilodalton
ko	Knock-out (null mutant)
Krt12	Cytokeratin 12
LB	Luria-Bertani broth
LCM	Laser capture microdissection
LV	Lateral ventricle
M	Molar
mA	MilliAmpere
Mal	Myelin and lymphocyte protein
Med1	Mediator complex 1 (
MF	Molecular function
MG	Microglia
MGB	Modified Gitschier buffer
min	Minutes
ml	Milliliter
mM	Millimolar
mo	Month
Mobp	Myelin-associated oligodendrocyte basic protein
Mog	Myelin oligodendrocyte glycoprotein
MS	Multiple Sclerosis
MSigDB	Molecular Signature Database
Myo10	Myosin 10
NB	Neutralization buffer
Ncam1	Neural cell adhesion molecule 1
Nefm	Neurofilament, medium polypeptide
ng	Nanogram
nm	Nanometer
Npas1	Neural PAS domain protein 1
OL	Oligodendrocytes
ON	Overnight
OPC	Oligodendrocyte progenitor cell
P	Postnatal day
PABP	Poly(A)-binding protein
PAGE	Polyacrylamide gel electrophoresis
PBS	Phosphate buffered saline
PC	Purkinje cells
PCA	Principal component analysis
PCR	Polymerase chain reaction
Pdgfra	Platelet derived growth factor receptor, alpha
Pdk1	Pyruvate dehydrogenase kinase 1
PFA	Paraformaldehyde
Pfkm	Phosphofructokinase-1
PI	Propidium iodide
Plat	Plasminogen activator, tissue
PLP /*Plp1*	Proteolipid protein
PMD	Pelizaeus-Merzbacher disease
PMSF	Phenylmethanesulphon
PNS	Peripheral nervous system
Polr3h	Polymerase (RNA) III (DNA directed) polypeptide H

Ptgds2	Prostaglandin D2 synthase 2,
Pttg1	Pituitary transforming gene 1
QC	Quality control
QRT-PCR	Quantitative real-time PCR
RMA	Robust Multichip Average
Rprm	Reprimo
RQ	Relative qunatity
RT	Room temperature
SC	Schwann cell
SD	Standard deviation
SDS	Sodium dodecyl sulfate
sec	Seconds
SEM	Standard error mean
Sir2	Sirtuin-2
SN	Substantia nigra
SNR	Signal-to-Noise ratio
Sox10	SRY-box containing gene 10
SPG2	Spastic paraplegia 2
ssDNA	Single stranded DNA
TBE	Tris-Borat-EDTA
TBS	Tris buffered salin
TBST	TBS with Tween
TH	Tyrosine hydroxylase
Thy1	Thymus cell antigen 1
Tnc	Tenascin-C
Tris-HCl	Tris-(hydroxymethyl)-amin
Ttll1	Tubulin tyrosine ligase-like 1
U	Unit, (for enzyme activities)
V	Volt
VTA	Ventral tegmental area
WB	Western blotting
WB I	Wash buffer I
WB II	Wash buffer II
WldS	Wallerian degeneration slow
WM	White matter
WT	Whole transcript
wt	Wildtype (control)

Appendix H: **Curriculum Vitae**

Personal Data

Name	Sven Peter Wichert
Date of birth	September 30th, 1977
Place of birth	Forchheim, Germany
Nationality	german
Marital status	single
Address business	Max-Planck-Institute for Experimental Medicine
	Department Neurogenetics
	Hermann-Rein-Str. 3
	37075 Göttingen
Phone business	+49-(0)551 3899-785
Mobile phone	+49-(0)179 2257126
Fax	+49-(0)551 3899-758
E-Mail	wichert@em.mpg.de
Address private	Weender Str. 93
	37073 Göttingen

Scientific education:

1998 – 2000   Basic studies in Biology, Friedrich-Alexander-University Erlangen

2000 – 2004   Advance studies in Biology, Ruprecht-Karls-   University Heidelberg

Degree: Diploma

Main focus: Molecular Biology, Biochemistry,   Cellbiology

May 2005 - present Dissertation at Max Planck Institute for experimental Medicine, Göttingen

137

Department Neurogenetics

Subject: "Transcriptomic approaches in the brain with cell-type resolution: Analysis of neuron-glia interactions in PLP and CNP null-mutant mice"

Language

German – mother tongue

Englisch – fluent

Spanish - basic

Courses and Stipends

2004   Laser microdissection course at PALM, Starnberg, Germany

2005   "Courses in practical DNA Microarray Analysis", MPI for Bioinformatics, Saarbruecken, Germany

2006   "Workshop on good statistical practice", MPI for Genetics, Berlin, Germany

2006   "Transcriptome Data Analysis", Exon-Array workshop, EMBL, Heidelberg, Germany

2007   "Integrated data analysis for high throughput biology" Cold Spring Harbor Labor, New York, USA

2008   ESF Exchange Grant, Frontiers of Functional Genomics

Project: A transcriptome database for astrocytes, neurons, and oligodendrocytes: a new resource for understanding brain development and function, Centro de Investigacion Principe Felipe (CIPF), Valencia, Spain

Presentations at Conferences

2008   "Expression profiling of cortical projection neurons and white matter in PLP1 and CNP1 null mutant mice", Wichert SP, Nave K-A, Rossner MJ, 6th FENS forum of European neuroscience, Geneva, Switzerland

2008   "Genomics of axonal degeneration   in myelin mutant mice", Wichert SP, Nave K-A, Rossner MJ, Neuropromise meeting, Toulouse, France

Publications

Moritz J. Rossner, Johannes Hirrlinger, Wichert SP, Christine Boehm, Dieter Newrzella, Holger Hiemisch, Gisela Eisenhardt, Carolin Stuenkel, Oliver von Ahsen, and Klaus-Armin Nave (2006), Global Transcriptome Analysis of Genetically Identified Neurons in the Adult Cortex. J. Neurosci. 26 (39) 9956-9966

Pankratov Y, Wichert SP, Rossner MJ, North RA, Kirchhoff F, Verkhratsky A. (2008), P2X1 and P2X5 subunits form the functional P2X receptor in mouse cortical astrocytes. J Neurosci. 28(21):5473-80.

Lalo U, Rossner MJ, Oster H, Wichert SP, Reinecke L, Wehr MC, Johannes Reinecke, Gregor Eichele, Reshma Taneja, Klaus-Armin Nave (2008), Disturbed Clockwork Resetting in Sharp-1 and Sharp-2 Single and Double Mutant Mice. PLoS ONE 3(7): e2762 doi:10.1371

Begemann M, Sargin D, Rossner MJ, Bartels C, Theis F, Wichert SP, Stender N, Fischer B, Sperling S, Stawicki S, Wiedl A, Falkai P, Nave KA, Ehrenreich H. (2008), Episode-specific differential gene expression of peripheral blood mononuclear cells in rapid cycling supports novel treatment approaches. Mol Med. 14(9-10):546-52.

Anna Botvinnik, Sven P. Wichert, Tobias M. Fischer and Moritz J. Rossner,Integrated analysis of ERBB receptor activation and downstream signaling with EXTassays.(Nature Methods. Accepted).

Magdalena M. Brzózka, Konstantin Radyushkin, Sven P. Wichert, Hannelore Ehrenreich and Moritz J. Rossner, Cognitive and sensorimotor impairments in transgenic mice overexpressing the schizophrenia-susceptible gene Tcf4 in the forebrain. (Submitted).

Wichert SP, Nave K-A, Rossner MJ. Expression profiling of neuronal and glial cell types in PLP and CNP null mutant mice. (Manuscript in preparation).